personal buildup for

Force Motors Limited Library

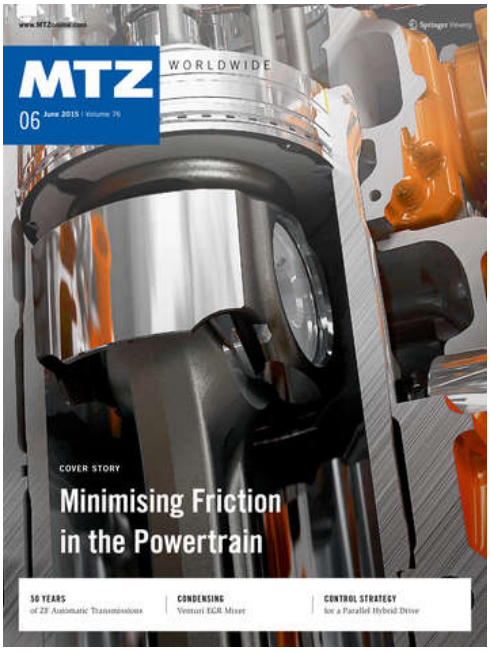

mtzw 6/2015, as epaper released on 06.05.2015
http://http:www.mtz-worldwide.com

content:

www.MTZonline.com

Springer Vieweg

MTZ WORLDWIDE

06 June 2015 | Volume 76

COVER STORY

Minimising Friction in the Powertrain

50 YEARS
of ZF Automatic Transmissions

CONDENSING
Venturi EGR Mixer

CONTROL STRATEGY
for a Parallel Hybrid Drive

CONTENTS

COVER STORY

Minimising Friction in the Powertrain

Lowering friction levels is an ongoing aspect of CO_2 reduction. In addition to the engine and its auxiliaries, it is important to focus on the entire powertrain in order to fully exploit the potential for reducing friction. This is because the savings achieved in the engine, gearbox and final drive right through to the wheels represent the individual components that add up to a low-friction powertrain.

COVER FIGURE © Scania
FIGURE ABOVE © Schaeffler

Business Case

Dear Reader,

the long-term future of the combustion engine will depend on the growing availability of sustainable energy sources. The use of carbon-neutral energy is fully in line with EU policy, which is aiming for a gradual reduction in greenhouse gas emissions of 80 to 95 % by 2050. As far as fuels are concerned, it is obvious that the challenges presented by renewable fuels which circulate CO_2 can be resolved. A carbon-neutral solution can be achieved by using the CO_2 produced in industrial processes (in particular steel and cement production) and in electricity generation as a raw material for the fuels. The recovery of CO_2 from the air is also technically possible using low temperature heat. Sustainable electricity generated from wind or solar energy can be used to produce hydrogen by means of electrolysis or for endothermic processes (such as methane or methanol splitting or dry reforming). The hydrogen can reduce the CO_2 created during the production of methanol and this can then be processed further.

However, the process engineering presents a much more serious problem. Obviously, the incentives needed to enlarge the production systems from a laboratory scale to an industrial scale are lacking. The obstacles referred to in this context include in particular the investment of several hundred million euros required and the lack of security in the planning process. In this respect, politicians could set an important example by making a clear commitment to this technology. But to focus only on this area would be too short-sighted. What is lacking is a clear business case which will allow the large amounts of money to be raised for investments that will only bring a return in the long term. Against the background of impending CO_2 taxes, some car manufacturers are currently considering developing a business model based on carbon-neutral fuels. This could give the technology the long-awaited momentum necessary for large-scale implementation. Let's hope this happens.

Best regards,

Richard Backhaus

Richard Backhaus
Vice-Editor in Chief
Wiesbaden, 27 March 2015

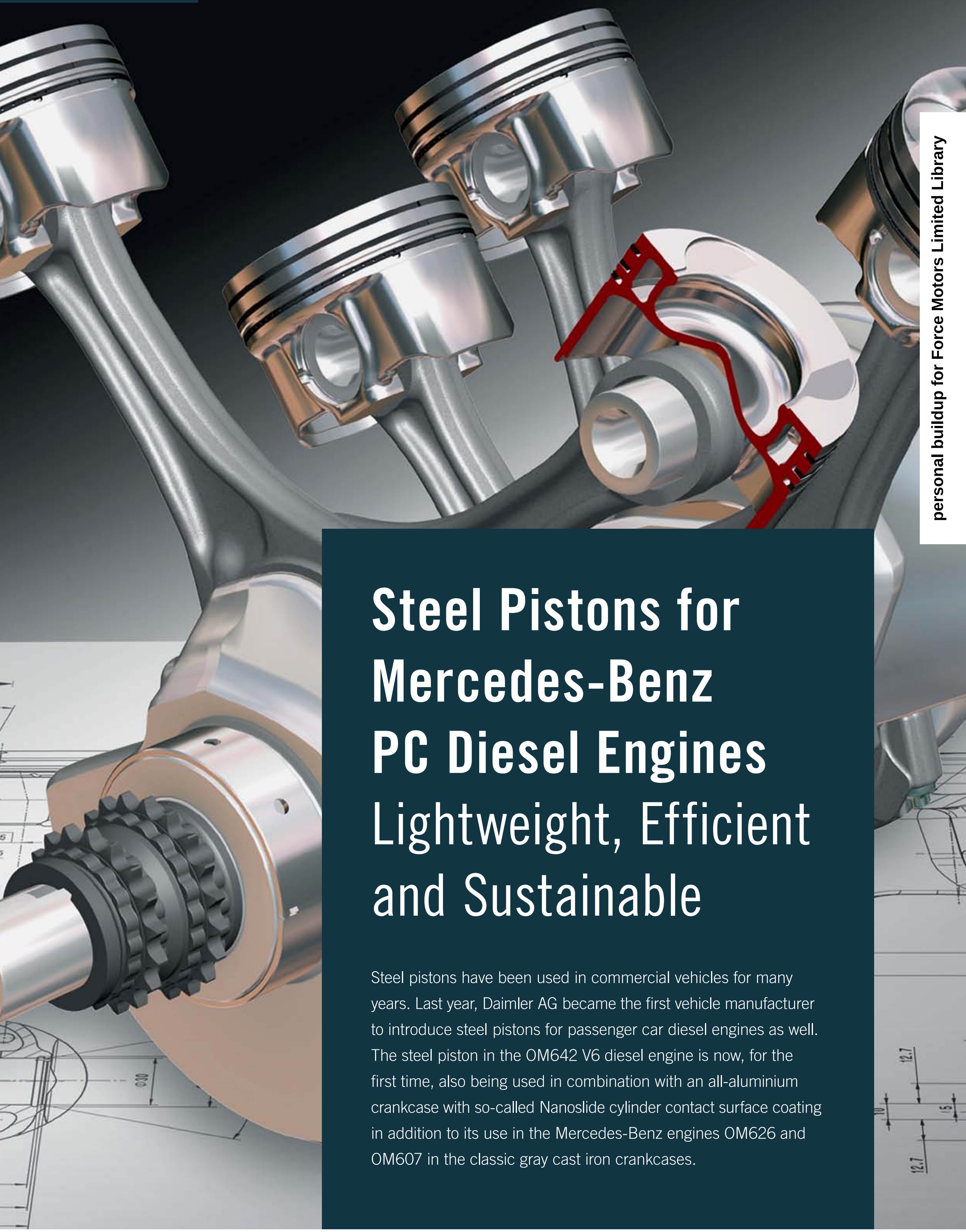

Steel Pistons for Mercedes-Benz PC Diesel Engines

Lightweight, Efficient and Sustainable

Steel pistons have been used in commercial vehicles for many years. Last year, Daimler AG became the first vehicle manufacturer to introduce steel pistons for passenger car diesel engines as well. The steel piston in the OM642 V6 diesel engine is now, for the first time, also being used in combination with an all-aluminium crankcase with so-called Nanoslide cylinder contact surface coating in addition to its use in the Mercedes-Benz engines OM626 and OM607 in the classic gray cast iron crankcases.

AUTHORS

Dr.-Ing. Joachim Schommers
was Head of CoC Engine Development at the Daimler AG in Stuttgart (Germany).

Dr.-Ing. Volker Lagemann
is Head of CAE, Design and Calculation at the Daimler AG in Ulm (Germany).

Jens Böhm
is Head of Mechanical System Development and Concepts at the Daimler AG in Stuttgart (Germany).

Simon Binder
is Test/Measuring Technology Engineer for Indication, Thermodynamic Analyses and Combustion Diagnostics at the Daimler AG in Stuttgart (Germany).

FOCUS ON FURTHER EFFICIENCY INCREASE

Combustion-engine-related drive systems dominate the market, increasing their efficiency further via thermodynamic and mechanical measures is thus of crucial importance for achieving the fleet targets in the different international markets. An interesting factor in this context is the reduction of in-engine friction losses [1, 2]. New or high-strength materials for highly stressed subsystems also offer new design potentials for weight reduction and improved efficiency together with a long service life. Due to the high peak pressures, diesel engines have significantly more solid piston designs and thus a higher friction reduction potential. One alternative here is the use of steel pistons. In commercial vehicle engines [3], steel pistons are already used in addition to aluminium pistons, but have yet to be series-manufactured for passenger car engines.

HIGH FRICTION RATE DUE TO PISTON ASSEMBLY

The piston assembly is responsible for the highest individual share of mechanical losses in the basic engine friction and has therefore been the focus of optimisations for years. In addition to the classic approaches, such as improving the piston ring geometry and piston ring prestress, significant progress has been achieved in recent years in particular in the area of the cylinder contact surface via precision honing and extra-fine honing as well as the newly developed so-called Nanoslide cylinder contact surface coating technology. As part of close cooperation between Mechanical System Development, the internal Simulation Department, Daimler Research and the respective piston supplier, the piston clearances and profiles of the aluminium pistons used have also been optimised with regard to the respective cylinder contact surface system. A significant reduction in the piston skirt friction was achieved in the 2.1-l four-cylinder diesel engine (aluminium piston in gray cast iron crankcase), for example [4, 5, 6]. Thanks to the above measures, key potential has already been leveraged and implemented in series production. This article focuses on the further potential of steel pistons in diesel engines.

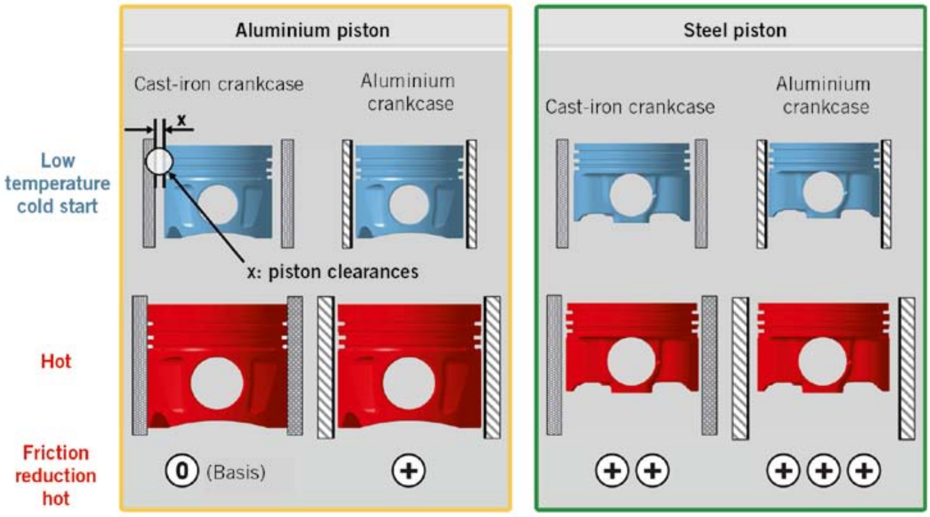

FIGURE 1 Schematic illustration of piston clearance situation in combination with different crankcases for cold start (-25 °C) and in hot condition (aluminium crankcase in each case with Nanoslide coating)

COMBINATIONS OF PISTON AND CRANKCASE MATERIALS

In case of aluminium pistons, a large piston clearance leads to rattling noises during a cold start, particularly in the case of gray cast iron crankcases. Classic designs with acoustic optimisation for the cold start thus usually lead to very tight clearances when the engine is warm; this in turn has an unfavourable impact on the friction. Due to the inhomogeneous temperature distribution and contact between different materials, the clearance situation at warm conditions play a decisive role for the functionally optimised piston design. Different piston and crankcase material pairings result in different clearances as shown schematically in **FIGURE 1**. An optimal solution from a friction perspective arises if the piston changes from being guided on both sides to being guided on one side only. This prevents the piston skirt from undergoing greater deformation as a result of the ensuing hydrodynamic pressure, which in addition leads to an increase in the friction power losses. Particularly suitable prerequisites are offered here by the steel piston with its lower expansion coefficient in comparison to the aluminium piston. This applies in particular for the combination involving a steel piston in an aluminium crankcase, which leads to the smallest cold clearance and the largest warm clearance with a particularly positive impact on friction losses at high piston temperatures.

STEEL PISTON DESIGN

Steel and aluminium pistons for passenger car diesel engines basically differ in their compression height. The differences between both piston variants are illustrated in **FIGURE 2**. The shown steel piston is a single-piece forged part made from 42CrMo4. The advantage of the high heat resistance offered by 42CrMo4 is offset by its greater density compared to aluminium. With a density of 7.7 g/cm³, 42CrMo4 is more than twice as heavy as the same volume of aluminium, which has a density of 2.8 g/cm³. The steel piston has been produced in an almost weight-neutral manner thanks to a design that is as thin-walled as possible as well as a reduction in the piston height and piston pin length. The tight weight tolerances of the aluminium piston also had to be fulfilled in order to obtain optimal vibration comfort. A new, extremely high level of precision was developed for the forging processes as a result.

ALUMINIUM AND STEEL PISTON TEMPERATURE PROFILES

At 236 W/(m·K), the thermal conductivity of aluminium is more than five times

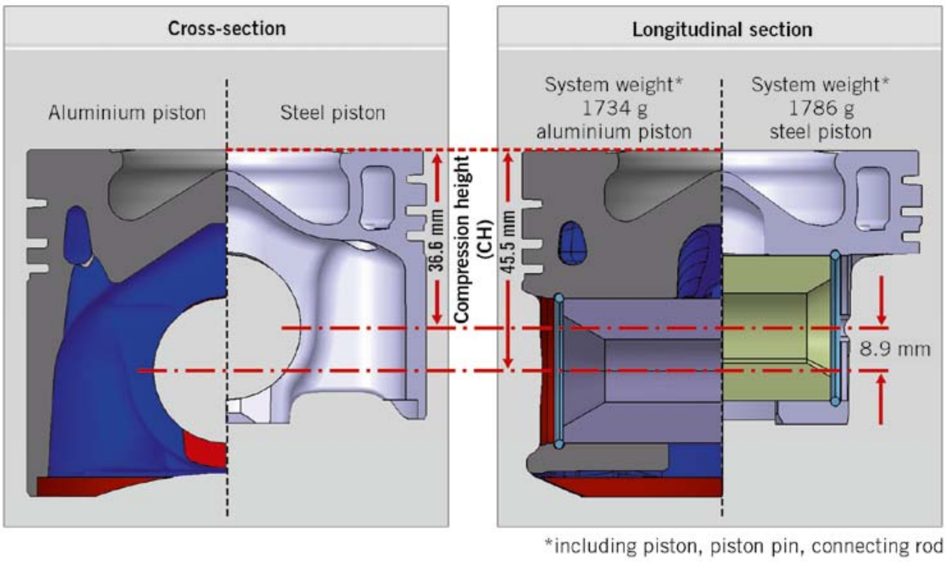

FIGURE 2 Comparison of aluminium and steel piston cross-sections (OM642)

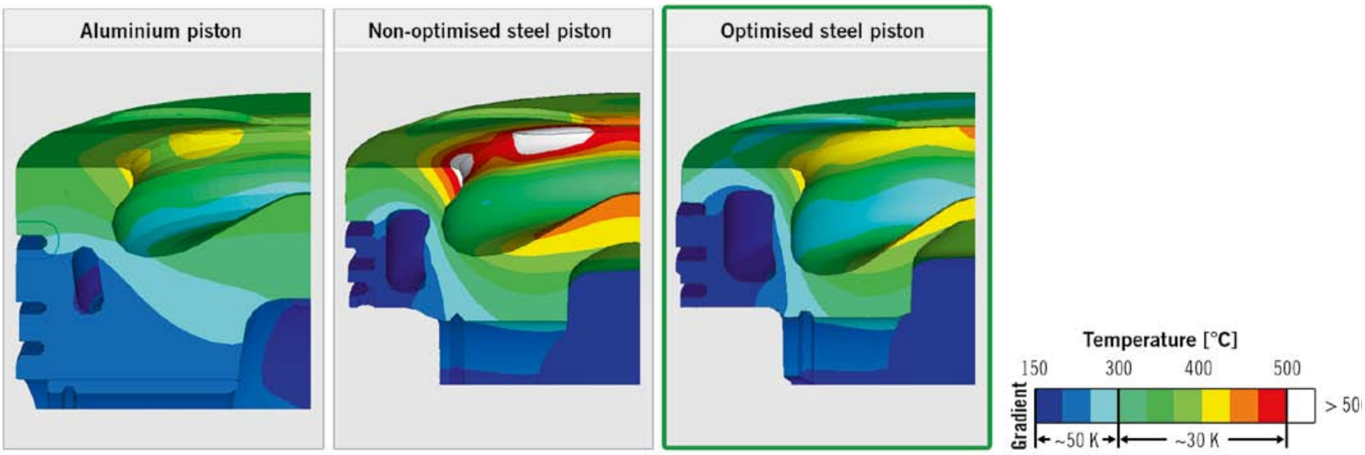

FIGURE 3 Temperature profile between the piston bowl rim and the cooling gallery – comparison of aluminium piston (left) and steel piston in the initial state (middle) and after optimisation (right), in each case at full load

greater than that of 42CrMo4, which has a thermal conductivity of 42 W/(m·K). The steel piston thus becomes hotter at the same combustion temperature. In **FIGURE 3**, it can see that a major challenge of the steel piston is targeted heat dissipation, in particular from the area of the piston bowl rim. Failure to achieve this will lead to the formation of surface scaling, followed by crack formation in the mechanically and thermally highly stressed areas as well as damage to the engine oil together with carbon deposits in the area of the piston cooling gallery. CAD was used to optimise the position and shape of the cooling gallery. By means of computer-aided sensitivity studies in comparison with measurements, it was calculated that a potential of about 70 K could be achieved through optimising the wall thickness and about 20 K through recess shape variation of the piston designs. The oil cooling was improved by removing the friction welding flash in the cooling gallery due to changing the piston design and welding process and the additional optimisation of the oil spray geometry. Therefore it is possible to cool the steel piston in the V6 diesel engine without increasing the oil pump efficiency, i.e. with the same oil supply volume as for the current series-production engines.

STEEL PISTON INTEGRATION IN THE BASIC ENGINE

Due to the reduced compression hight of the steel piston in comparison to the aluminium piston, additional weight and installation space potential can in principle be exploited for future engine generations by reduced crankcase height. This provides advantages, for example, in the vehicle package and for passive safety (optimised pedestrian protection). This was not implemented in the OM642 V6 diesel engine due to its integration in an already existing basic engine.

The increased clearance of the steel piston in the aluminium crankcase and the increased piston skirt rigidity lead to a slightly higher mechanical excitation of the cylinder wall. One challenge therefore was to achieve a trade-off between friction loss, function during heat and extreme cold, and noise comfort. For this purpose, advanced simulation methods were used in close collaboration with the piston manufacturers to derive optimisation measures for the steel piston. The vibration velocity of the cylinder wall were calculated for the virtual evaluation of the structure-borne noise excitation, **FIGURE 4** (left).

The measures derived for the reduction of the structure-borne noise excitation for the OM642 steel piston are based on the rotation profile, skirt rigidity, piston pin axial offset and an improved

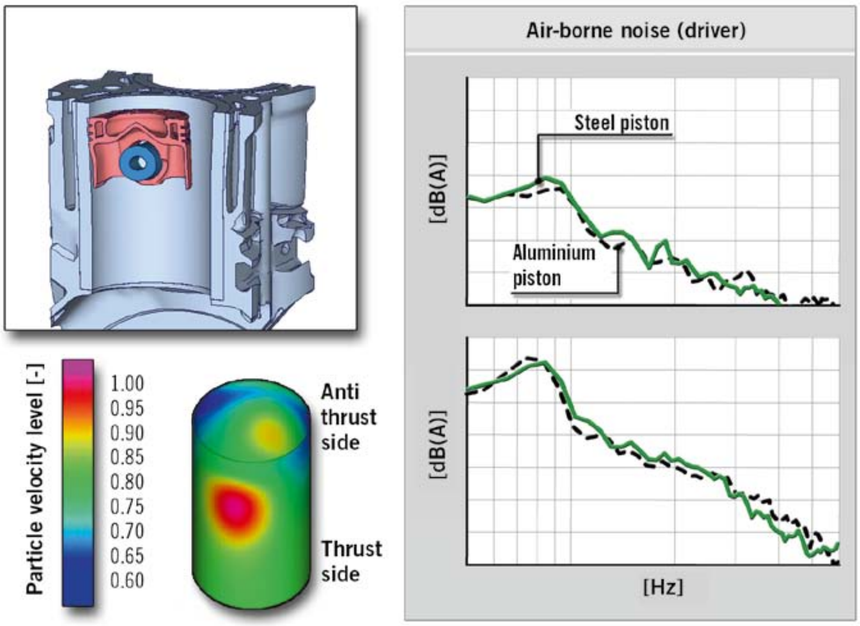

FIGURE 4 Virtual structure-borne noise optimisation and acoustic evaluation via the airborne noise measurement of the optimised steel piston in comparison to the aluminium piston (partially schematic)

crankcase material quality. The omission of the gray cast iron cylinder liners allowed a significant increase in the ductility of the gravity-cast material AlSi8Cu3 before the Nanoslide cylinder contact surface was applied via heat treatment.

The acoustic behaviour was investigated via airborne and structure-borne sound measurements on test benches and in vehicles. **FIGURE 4** (right) shows sample airborne sound measurements on a vehicle test stand in which engines with aluminium and steel pistons were compared. The excitation spectra show both advantages and disadvantages for individual frequency ranges. Differences in noise of a mechanical origin can barely be perceived from a subjective perspective. The only difference that can be observed is a stronger, deeper sound pattern, which can largely be attributed to the more rapid combustion process.

STEEL PISTON IN ALUMINIUM CRANKCASE WITH FRICTION ADVANTAGES

The piston friction is determined by virtual test runs that take into account elastohydrodynamic friction models including mixed friction contact. Whereas the aluminium piston in the V6 diesel engine at hot conditions is mainly guided on both sides, the steel piston with its larger clearance benefits from the one-sided piston guidance shows improved skirt friction. A reduction in the piston skirt friction losses of 35 and 47 % respectively can be seen in **FIGURE 5** at the two load points shown. In conventional, motored friction loss analyses, however, these advantages cannot be validated through measurements as temperature fields do not match fired conditions. Engine-operating performance map investigations by means of high-precision indicating and torque measurements are required here.

THERMODYNAMIC ADVANTAGES OF STEEL IN COMPARISON TO ALUMINIUM PISTON

The differential performance map in **FIGURE 6** (top) shows the improvement in the effective efficiency, which includes the overall advantages resulting from friction and thermodynamics. The purely thermodynamic advantages are apparent in the differential performance map for the indicated high-pressure consumption, **FIGURE 6** (bottom). The thermodynamic differences arise in this connection from the higher surface temperature on the piston crown of the steel piston. The heat accumulates due to the lower thermal conductivity and the higher heat capacity of the steel.

The typical but unfavourable burn-out for diesel engines only makes a minor contribution to the work on the crankshaft. The fuel should ideally be fully combusted at the ignition TDC. This leads to a high degree of constant volume and significantly influences the efficiency of the high-pressure process. In the case of steel pistons, the fuel is more quickly converted and the duration of combustion is thus reduced.

The high piston temperature is responsible for the more rapid rate of conversion. This causes the cylinder charge to heat up during the intake and compression phases, which in turn reduces the ignition delay. For this reason, the process temperatures and pressure in the steel piston are higher.

The hotter surface raises the temperature level. This favors the vaporisation of the fuel close to the nozzle and leads to a slightly earlier ignition. Furthermore, the increased temperature level in the early phase of main combustion leads to greater reactivity (Arrhenius), which entails a higher flame temperature and steeper rise in pressure.

The higher gas temperature usually leads to similar wall heat losses for the steel piston and the aluminium piston, as the underlying gas/wall temperature gradient is approximately the same. The piston is warmer, but so is the gas; the wall heat losses can thus even increase depending on the operating point. The heat-transfer coefficients only change negligibly due to the higher process temperature and higher cylinder pressure. The lower thermal conductivity of the steel piston leads in transient operation and during the heating phase to an even higher surface temperature. This quicker heat-up behaviour is another advantage, e.g. in exhaust gas tests, in comparison to the steady-state performance maps shown here.

SUMMARY AND OUTLOOK

The introduction of the steel piston started in September 2014 in the Mercedes-Benz E 350 BlueTEC. The as-yet-unused combination of a steel piston with an all-aluminium crankcase with Nanoslide cylinder contact surface coating is to be highlighted here. Together with additional consumption-related measures, fuel-economy figures of 133 g CO_2/km (5.0 l/100 km) are achieved.

At the same time as its application in the OM642 V6 diesel engine with alu-

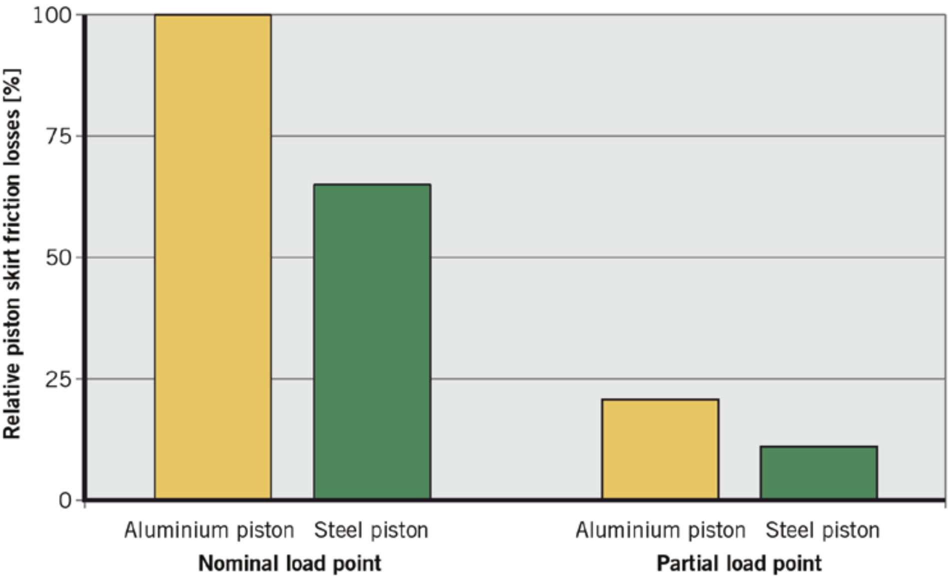

FIGURE 5 Calculated friction loss advantages of steel piston in OM642 at rated output (4000 rpm) and partial load (1600 rpm)

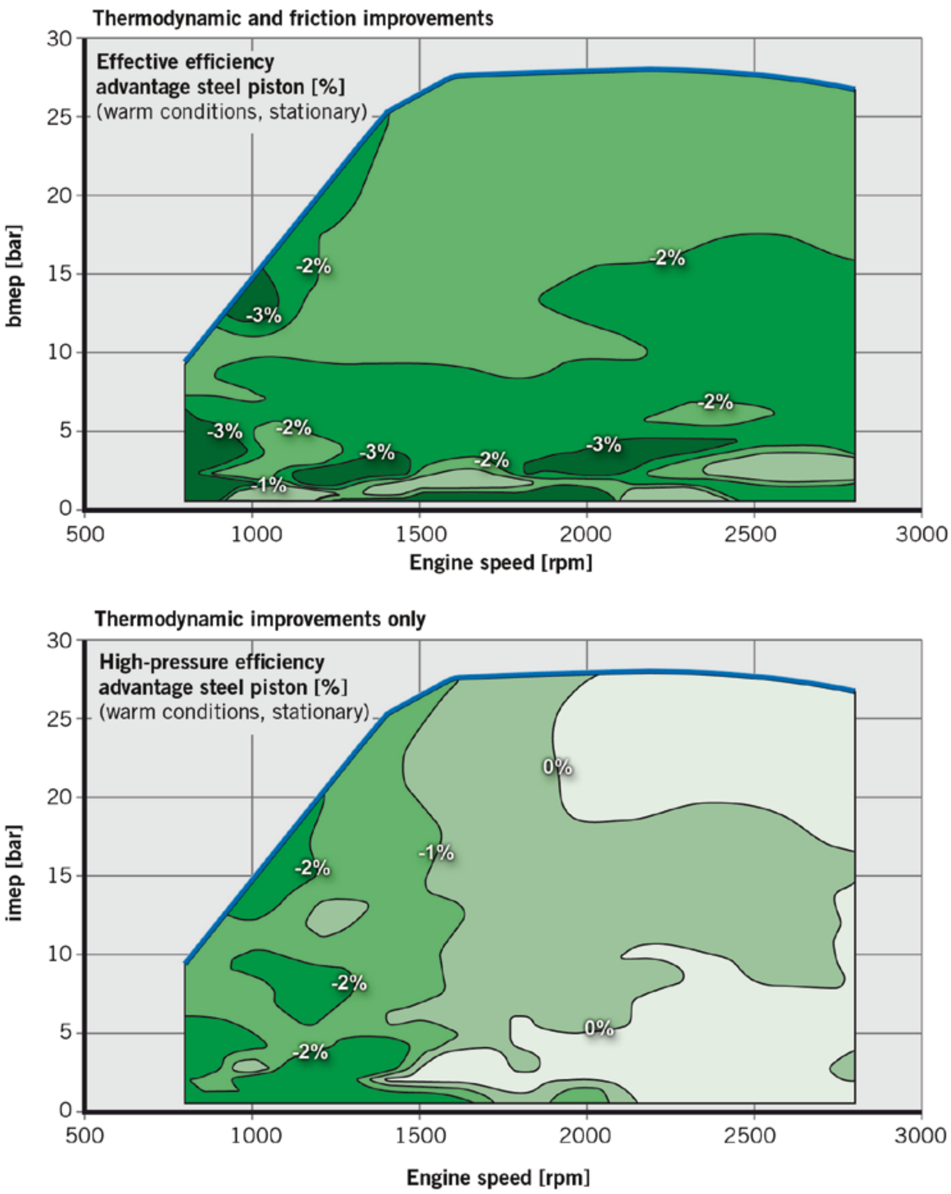

FIGURE 6 Advantages due to use of steel piston in warm performance map

minium crankcase, the steel piston has been introduced in two four-cylinder entry-level diesel engines, the OM626 [7] and OM607, with gray cast iron crankcases in collaboration with the cooperation partner Renault. The steel piston is establishing itself as the standard for Mercedes-Benz passenger car diesel engines and will thus also form the basis for future engines with ever-increasing specific engine output.

REFERENCES

[1] Schommers, J.; Doll, G.; Weller, R.; Behr, T.; Scheib, H.; Löffler, M.; Böhm, J.; Hartweg, M.; Bosler, A.: Reibleistungsoptimierung – Basis für die Zukunftsfähigkeit der Verbrennungsmotoren [Friction Loss Optimization – Basis for Sustainability in Combustion Engines]. 33rd International Vienna Motor Symposium, 2012

[2] Scheib, H.; Hartweg, M.; Heyd, M.; Tomaschko, S.; Lagemann, V.; Doll, G.; Behr, T.; Schommers, J.: Konsequente Reibleistungs- und Verbrauchsreduktion am Beispiel der neuen Mercedes-Benz V6- und V8-Ottomotoren. 2nd ATZlive conference "Reibungsminimierung im Antriebsstrang", Esslingen, 2011

[3] Kreso, A.; Behr, T.; Maier, S.; Hartweg, M.; Lagemann, V.; Nowotni, D.; Rubi, J.: Friction Optimization Heavy Duty Truck Engines. 13th International Stuttgart Symposium, 2013

[4] Lagemann, V.; Bosler, A.; Mueller, F.; Rösch, H.; Ruoff, A.; Ströer, M.: Optimierung der Kolbenreibung durch konsequenten Einsatz virtueller Prüfläufe in der Motorenentwicklung [Optimization of Piston Friction via the Consistent Use of Virtual Test Runs in Engine Development]. 3rd ATZlive conference "Reibungsminimierung im Antriebsstrang", Esslingen, 2013

[5] Schommers, J.; Scheib, H.; Hartweg, M.; Bosler, A.: Reibungsminimierung bei Verbrennungsmotoren [Friction Minimization in Combustion Engines]. In: MTZ 74 (2013), No. 7-8

[6] Lückert, P.; Busenthür, D.; Arndt, S.; Sass, H.: The Mercedes-Benz OM 651 Four-Cylinder Diesel Engine for Worldwide Use. 22nd Aachen Colloquium Vehicle and Engine Technology, 2013

[7] Andres, C.; Ebelsheiser, O.; Gödecke, T.; Hawig, P.; Hanselmann, J.: Vier gewinnt. In: ATZextra "Die neue C-Klasse von Mercedes-Benz", 2014, pp. 48-55

[8] Schommers, J.; Eder, T.; Behr, T.; Lagemann, V.; Weller, R.; Böhm, J.; Schnüpke, H.; Binder, S.; Dietz, W.: Steel Piston for Diesel Passenger Car Engines – Efficient, Sustainable and Light. 23rd Aachen Colloquium Vehicle and Engine Technology, 2014

THANKS

Particular thanks to Wolfgang Dietz, Dr. Thomas Behr, Dr. Ralph Weller, Dr. Martin Hartweg, Frank Mueller, Dr. Stefan Kienzle and Udo Grimmer, all Daimler AG, for their cooperation in the compilation of this article.

Real Time Characterisation of Wear Behaviour

In the development of combustion engines lightweight design and friction reduction still play an important role. More and more composite materials, partly using brand new components, are utilised. For the optimisation of new composite materials, part geometries and lubricants online-methods for the characterisation of wear on component- and full fired engine testbeds are absolutely necessary. Within the APL Group the Radionuclide Wear Measurement Technology (RTM) is successfully in use since many years. Furthermore an online characterisation tool based on ICP-OES technique (Inductively Coupled Plasma – Optical Emission Spectroscopy) is under development.

AUTHORS

Prof. Dr.-Ing. Jens Hadler
is Managing Director of the APL GmbH in Landau (Germany).

Dr. Gunther Müller
is Head of Oils and Fuels Analytical Laboratory at the APL GmbH in Landau (Germany).

Dipl.-Ing. (FH) Daniel Stern
is Manager of Oils and Fuels Analytical Laboratory at the APL GmbH in Landau (Germany).

Dr. Peter Berlet
is Manager Engine Development at the IAVF Antriebstechnik GmbH in Karlsruhe (Germany).

HIGHER SPECIFIC PART STRESS

To optimise the future emission the request of increasing specific power in combination with lightweight concepts leads to higher specific part stress in the powertrain aggregates [1]. So, optimisation and new development of combinations of materials, part geometries and last but not least the used lubricants, which are often taylor-made as system components for specific requirements, will be necessary [2]. Therefor it is necessary to characterise the wear behaviour in dynamic drive cycles to enable an estimate of the lifetime of parts.

Since many years, the Radionuclide Wear Measurement Technology (RTM) is successfully in use to investigate the wear behaviour of combustion engines [3]. For that purpose the tribologically stressed area of the surface can be precisely irradiated. The increase of wear particles of the selected parts can be measured continuously and with a high resolution, for example on an engine testbed in the engine oil and the oil filter. The wear behaviour can be correlated with the actual driving conditions and single parameters like temperatures or pressures in the engine.

To analyse the additive- and wear elements in lubricating oils the ICP-OES is in use since many years [4]. The main target of this investigation within this project was to check, whether this laboratory method is also suitable for the realtime-investigation of wear behaviour on component and full engine testbeds.

MEASURING PRINCIPLE AND STRUCTURE OF THE TECHNIQUE

At the ICP-OES, **FIGURE 1**, an oil sample will be transported after dilution with white oil by a peristaltic pump into a nebuliser chamber. The oil droplets generated in this nebuliser are selected according to their size and the small droplets transferred into a plasma. The plasma of the ICP-torch is generated with Argon in an alternating high frequency field and has a temperature of approximately 8000 K. Under those conditions the outer electrons of the additive- and wear elements like Fe, Cu, Ca, Mg and S will be thermally stimulated and pushed on a higher energetic level. Falling back into the original energy status the energy

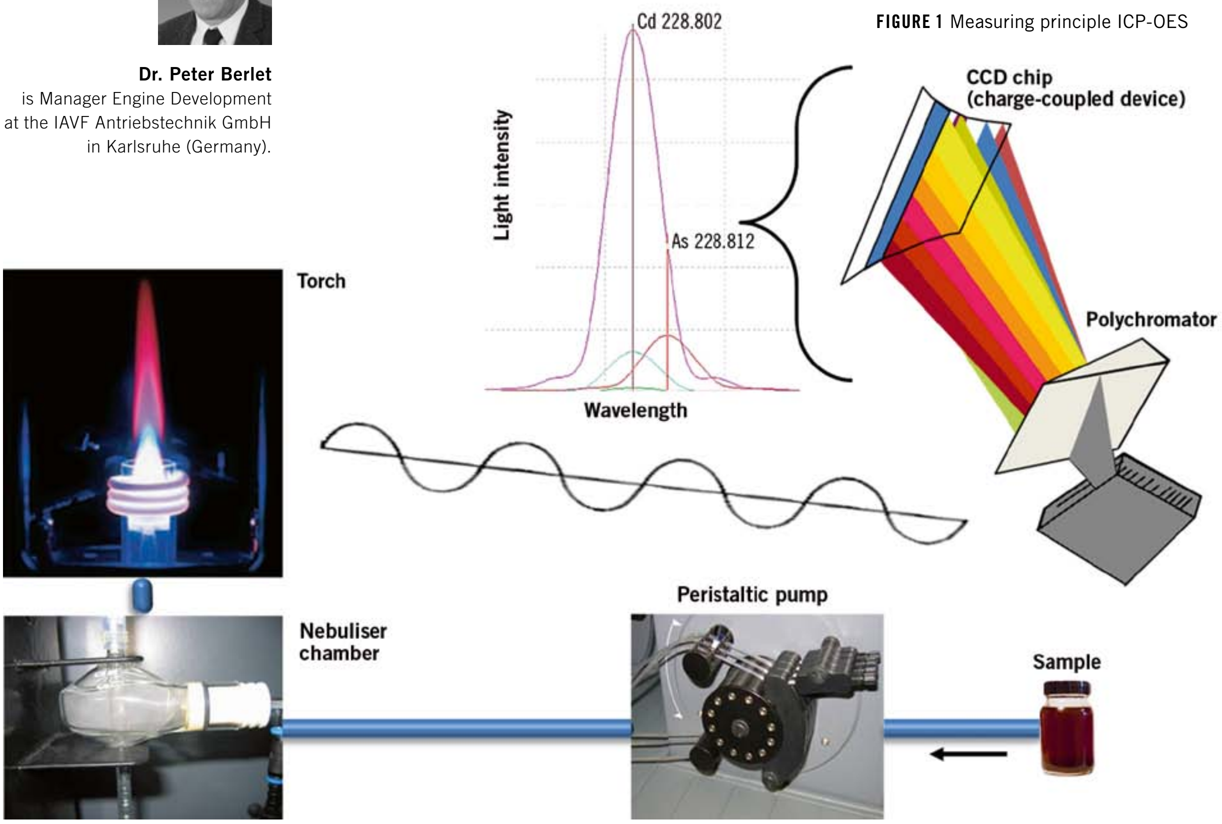

FIGURE 1 Measuring principle ICP-OES

difference will be given back in the form of light emission. The wavelength of this light emission allows a qualitative statement about elements being contained in the oil. By splitting the wavelengths via dichromator normally up to 21 elements per measurement can be detected. The wavelength specific intensity of the light emission gives the quantitative information, evaluated by the use of a calibration line. Depending on the specific elements a concentration can be determined in the range of µg/kg with this technique.

The structure of the ICP-online technique – for example on an engine testbed – is schematically shown in **FIGURE 2**. An external oil circuit has to be installed: By an additional bore in the oil sump for the sampling of the actual oil quality and a feedback pipe into the oil filler neck a ring circuit has to be implemented. With a micro gear pump a constant oil volume is pumped through this circuit. After a mixing chamber to homogenise the oil sample a portion of the oil flow is taken out of the circuit and guided to the ICP. As the droplet formation in the nebuliser is influenced by the physical properties of the sample like viscosity, the sample is temperature conditioned in a heating pipe before the nebulising, so even at different oil temperatures in the engine constant characteristics can be ensured. During the following investigation a sampling interval of 30 s was used. The oil consumption of the sampling for the ICP is 2 ml/h only.

BASIC INVESTIGATION ON A COMPONENT TESTRIG

In a first step the ICP online technique was tested on an FZG testrig (Forschungsstelle für Zahnräder und Getriebebau der TU München). In this test the relative scuffing load capacity of lubricants, mainly gear oils, is investigated. The test procedure which was used corresponds to CEC L-84-02. In this test, the friction partners, a pair of gear wheels (driving wheel and driven wheel) in a box filled with test oil are mechanically stressed. In at most ten stages with increasing Hertzian Stress (206 N/mm² up to 2175 N/mm²) the gear wheels are tribologically stressed for 7.5 min/stage at a speed of 2910 rpm (equivalent to 21825 total revolutions). The test box was modified with two bores for the inlet and the outlet of the ring circuit. One ICP-measurement per 35 s was performed. The development of the Iron concentration across the stages/running time is shown in **FIGURE 3**.

The development of the Iron concentration across the test stages in **FIGURE 3** shows a significant step to the beginning of each new stage (higher pressure stress). Up to stage 7 this is only visible with rather high magnification. This effect is caused by the run in of the friction partners in the new stage with higher surface pressure. The test runs on the FZG testrig show a very good reproducibility and very constant results, even at very low ranges of concentration. This can also be led back to the fact, that the test conditions do not change significantly the physical properties of the lubricant. Compared to an engine oil, running in a fired engine, oil aging is mainly limited to a variation of the wear elements. Aging processes, as can be find in a fired combustion engine, like input of fuel, water and soot are not relevant in this test.

WEAR CHARACTERISATION IN THE ENGINE

The investigations have been performed in a direct injecting, turbocharged, four-cylinder gasoline engine. The influence of the oil pressure on the wear behaviour should be characterised. The oil pressure level of the running engine

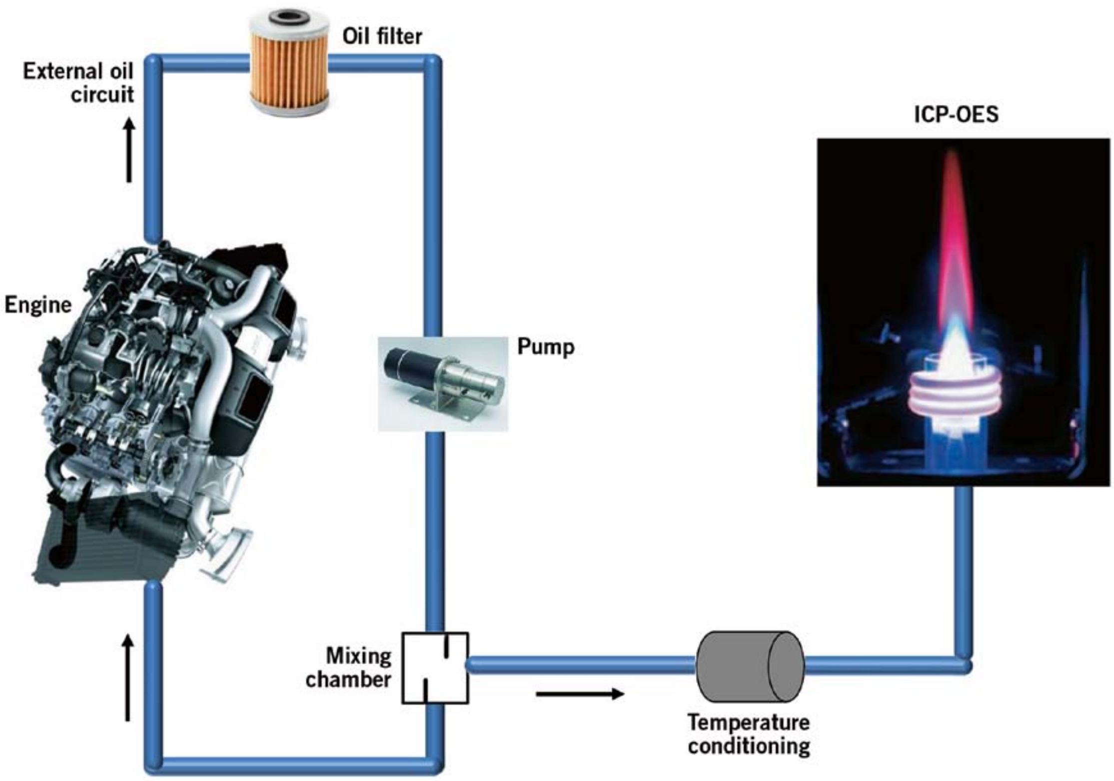

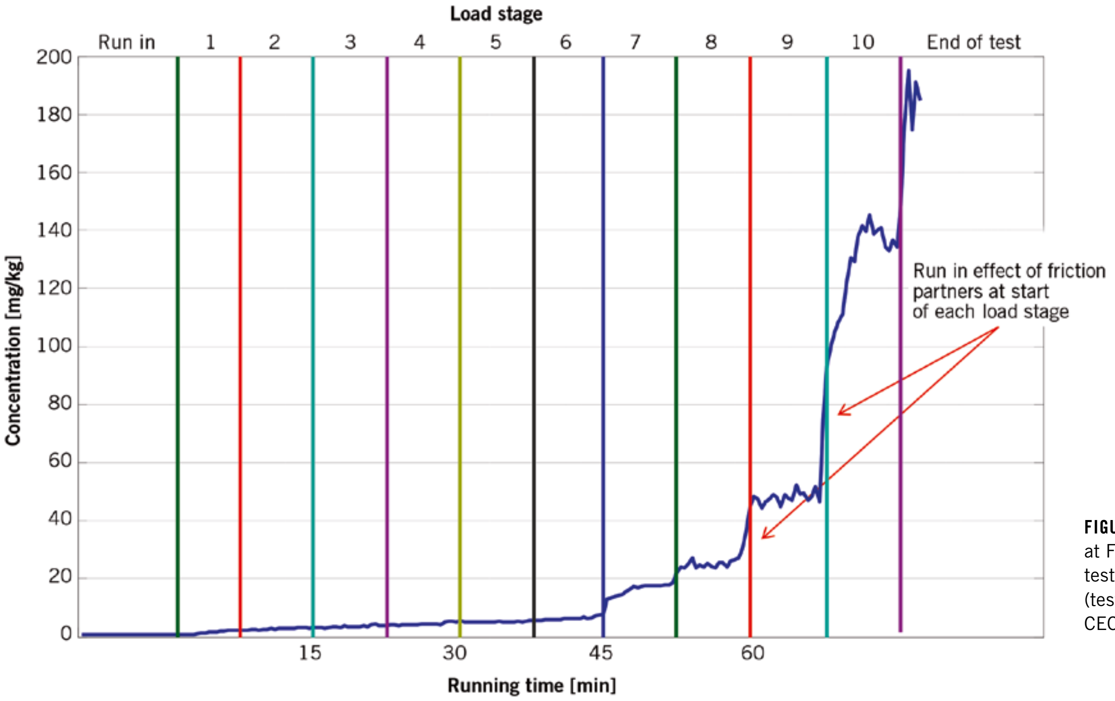

FIGURE 3 Iron-concentration at FZG testrig depending on test stages and running time (test procedure according to CEC L-84-02)

was reduced from 4 bar to lower than 1 bar. The element concentration in the lubricant was logged on the test-bed with the ICP OES-online system. In **FIGURE 4** the development of the concentrations of the wear elements across the duration of the online measurement is shown. An increase of the wear elements in the lubricant could be observed.

The concentrations of copper, iron, tin and aluminium increase by the factor 2 to 3, whilst the concentrations of molybdenum and manganese rise only pretty moderately. Because of the illustrated measurement results the progress of damages could be detected already in a very early stage by the increase of the wear element concentration. The systematically indicated high wear happened in the steady stage of the programme cycle at

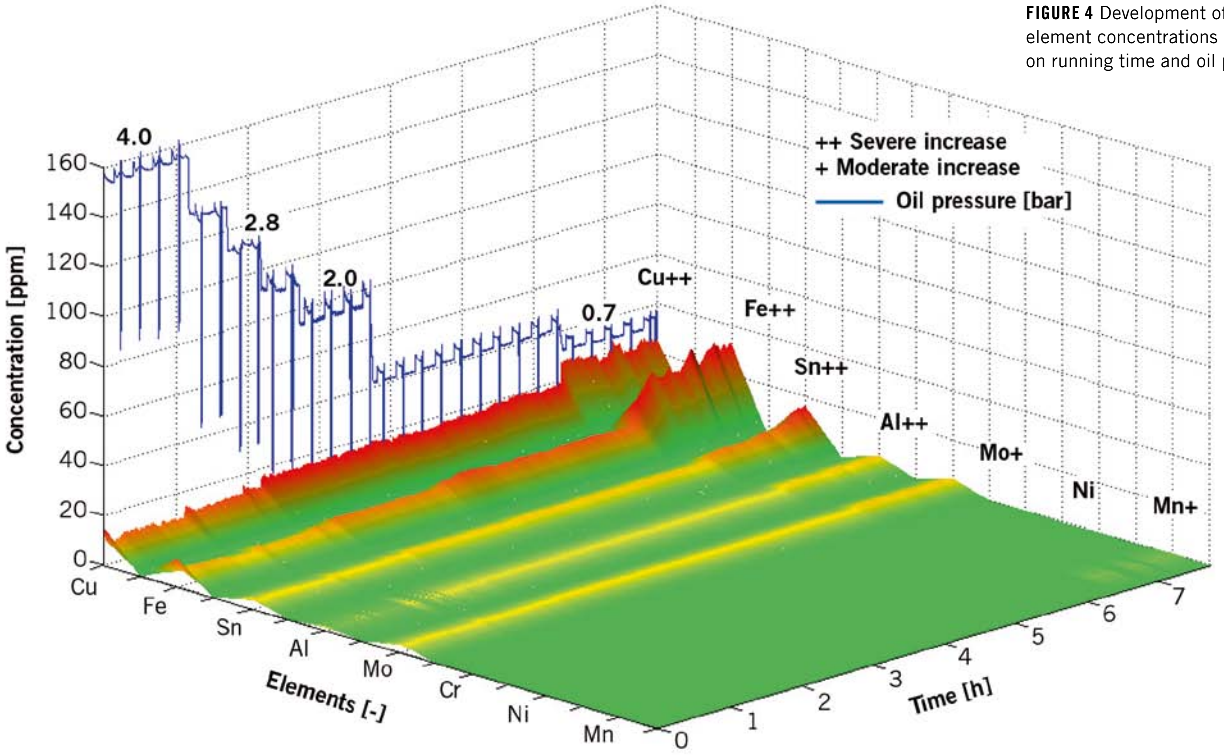

FIGURE 4 Development of selected element concentrations depending on running time and oil pressure

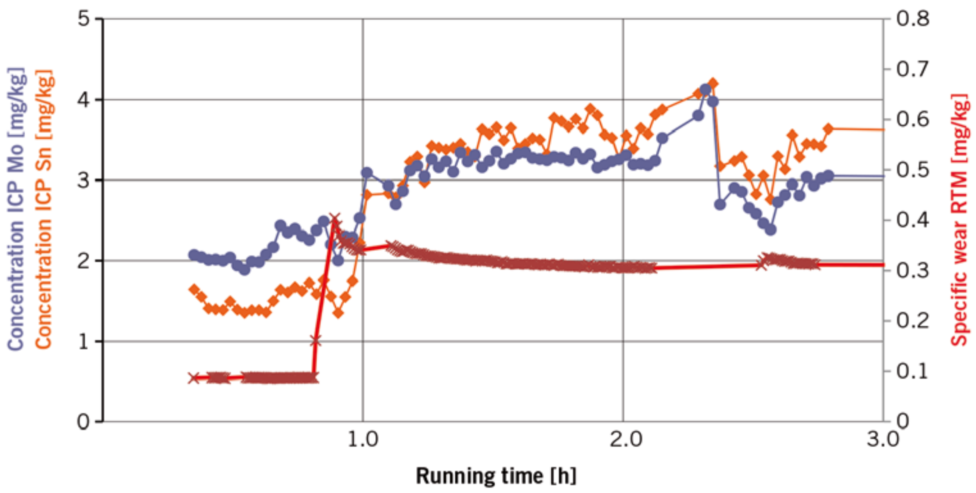

FIGURE 5 Development of selected element concentrations evaluated with ICP-online-technique and wear measured with RTM depending on running time

an engine speed of 6200 rpm and an oil pressure of 0.65 bar in the connecting rod bearing as well as on the corresponding crankshaft journal. The following inspection of the parts confirmed that with the reduced oil pressure the contact areas between crankshaft and conrod bearing could not be lubricated any more and the bearing layer out of an Al-Sn-Cu-alloy was worn out [5].

ADVANTAGES AND DISADVANTAGES OF THE ICP-ONLINE TECHNIQUE

To compare the ICP-online technique with the RTM-system on an engine testbed a premium aspirated DI gasoline engine was used (installation like **FIGURE 2**). By continuous reduction of the oil pressure with cyclic variation of the engine speed there was, along the line of the former investigations, a wear problem initiated.

FIGURE 5 shows a comparison of selected wear element concentrations with the wear detected via RTM. Molybdenum is part of the alloy of the main bearing and tin is part of the interlayer of the bearing shell. Both techniques show in a corresponding time window a significant increase of the wear behaviour.

At longer running times a reduction respectively heavy bouncing of the element concentration can be observed, detected with the ICP-online technique. The reasons for this bounce are multifaceted and mostly with different characteristic for all the elements. After a longer operation time a coking of the torch can be observed, which makes an adjustment of the Ar-plasma necessary. Bigger wear particles (>5 µm) cannot pass the nebuliser and are not detected. Also aging processes of the lubricant in a fired engine like soot and water input as well as oxidation cause a continuous variation of the physical properties of

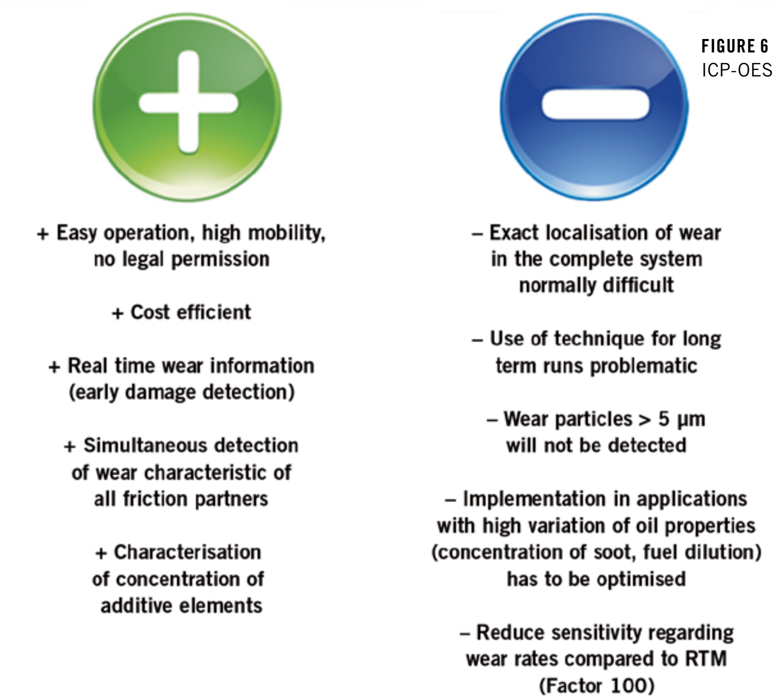

FIGURE 6 Advantages and disadvantages of the ICP-OES online technique compared with RTM

the oil. The changes in viscosity and the surface tension/wetting behaviour end up in a modification of the nebulising characteristics. Different droplet sizes and different droplet size distributions will be generated and finally different sizes and numbers of droplets will go into the Ar-plasma. So, a different light intensity will be detected which is not caused by an increase of the element concentration in the oil but by a modification of the total oil concentration in the plasma. One way to solve or at least to reduce the above problem is the use of an internal standard during the measurement. Shortly before the heating up/nebulising of the oil a defined multi-element-standard is added. This can be managed for example in using a suitable piezo-valve with defined dosage rate.

FIGURE 6 compares the potential of the ICP-technique for realtime investigation of wear behaviour with the challenges of this technique in comparison to established systems like RTM.

SUMMARY AND OUTLOOK

For the development and the optimisation of engines and their components, online methods for wear characterisation are absolutely necessary. It has been demonstrated, that the ICP-OES as a potential investigation tool offers additional possibilities. However, the use of it as investigation tool is in an initial phase and the identified weak points must be eliminated by additional development to enable the use of the entire potential of that system. Currently, ICP-OES as complement to RTM for special problems/trend analyses is already supposable.

REFERENCES

[1] Hadler, J.; Lensch-Franzen, C.; Kirsten, K.: Emissions- und CO_2-neutrale Energiekette – Fiktion oder Herausforderung? 9th MTZ conference “Der Antrieb von morgen“, Wolfsburg, 2014

[2] Müller, G.; Berlet, P.; Pöhlmann, K.; Stern, D.: Praxisnahe Alterung von Motorölen und Auswirkung auf tribologisch relevante Eigenschaften. Annual conference of Gesellschaft für Tribologie, Göttingen, 2013

[3] Berlet, P.; Dilbat, M.; Pöhlmann, K.; Kuse, S.: Reduzierung des Kraftstoffverbrauchs von Verbrennungsmotoren, Auswirkung auf Reibung und Verschleiß. Annual conference of Gesellschaft für Tribologie, Göttingen, 2013

[4] Nolte, J.: ICP-Emissionsspektroskopie für Praktiker: Grundlagen, Methodenentwicklung, Anwendungsbeispiele. Publisher Wiley, 2003

[5] Löprich, A.: Echtzeit-Schmierölanalytik an Verbrennungsmotoren. Thesis, Hamburg University of Technology, 2009

50 Years of ZF Automatic Transmissions

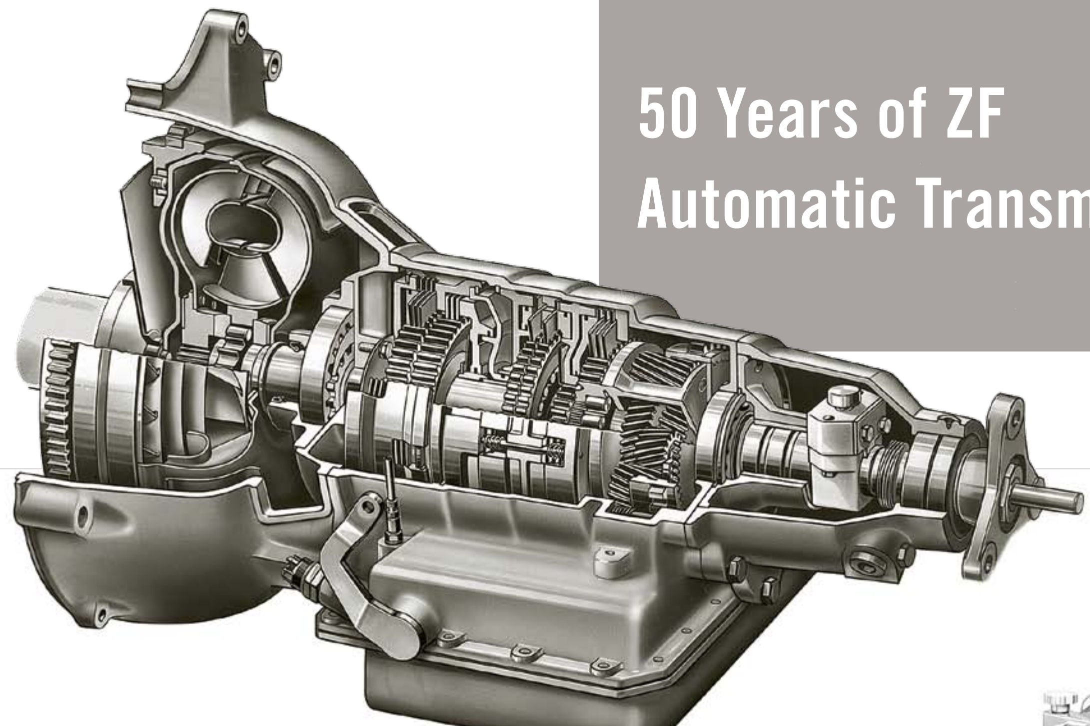

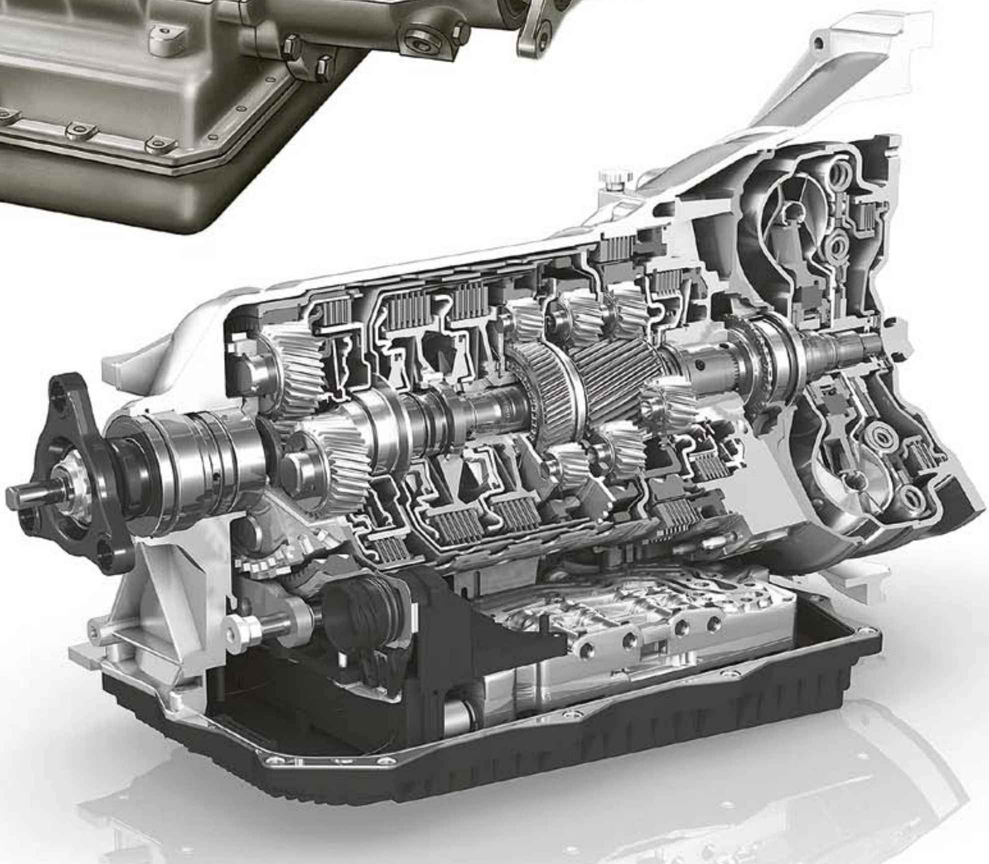

AUTHORS

Heribert Scherer
is Head of Testing at the Car Powertrain Technology Division of the ZF Friedrichshafen AG (Germany).

Ulrich Franzmann
is Head of Transmission Application Development at the Car Powertrain Technology Division of the ZF Friedrichshafen AG (Germany).

2015 is the 50th anniversary of the start of volume production of a ZF automatic transmission. The three-speed automatic transmission of which only limited quantities were produced at the time has today developed into a high-tech bestseller thanks to the 8HP and 9HP transmission model ranges. This can be attributed to a variety of innovations with which ZF has reworked almost all elements of a multi-ratio transmission from scratch.

GROWING ATTRACTIVENESS

Multi-ratio transmissions with a hydrodynamic torque converter as a starting element as well as a downstream transmission in a planetary design have been used in the field of automotive engineering since the end of the 1930s. The high level of shift comfort and the opportunity to shift without tractive force interruption in particular made this type of transmission increasingly attractive; initially in the USA and, later on, in Europe too. At the start of the 1960s,

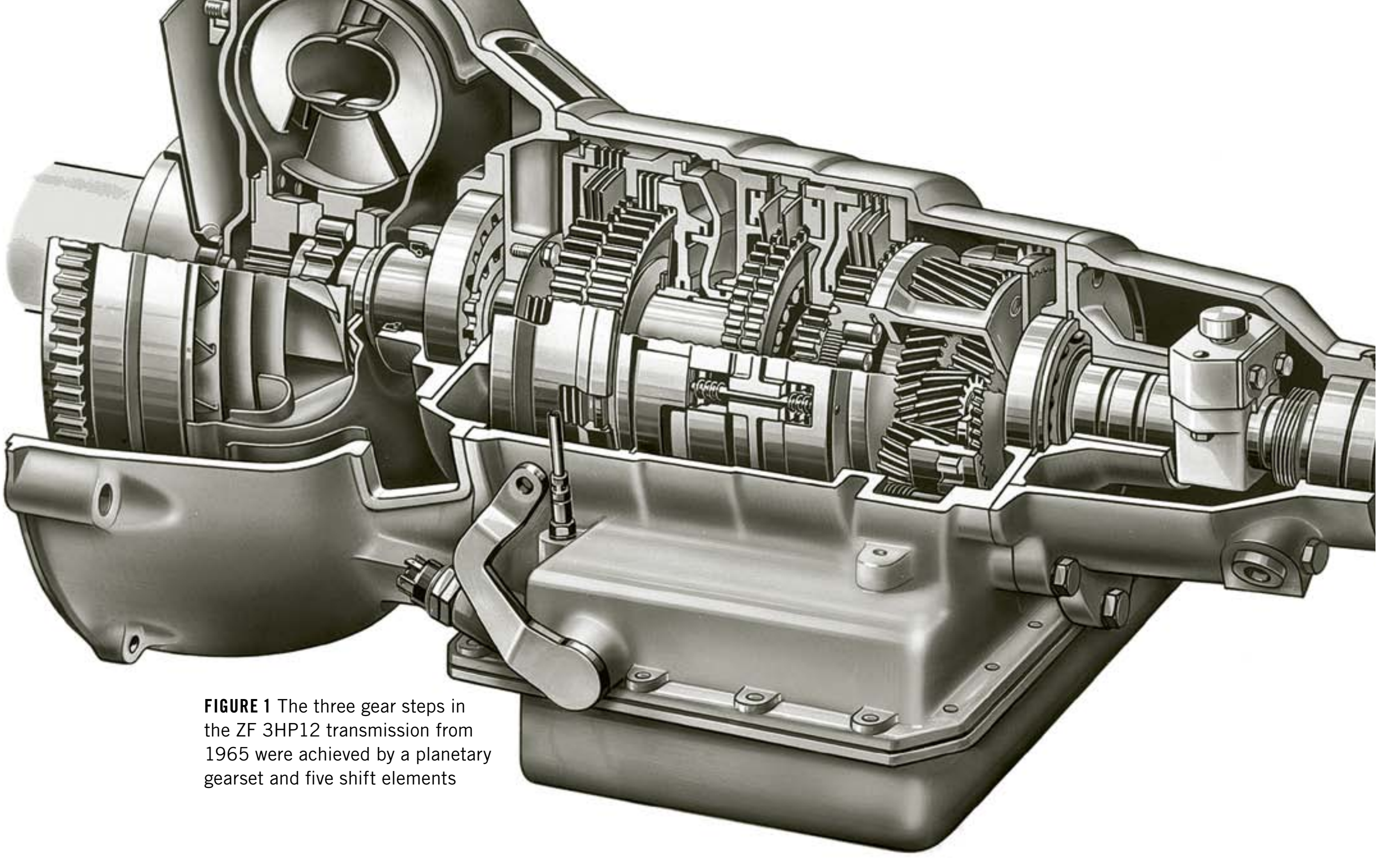

FIGURE 1 The three gear steps in the ZF 3HP12 transmission from 1965 were achieved by a planetary gearset and five shift elements

ZF Friedrichshafen AG therefore decided to introduce their own product to the market. The 3HP12 transmission entered volume production in 1965; the year of the company's 50th anniversary. Consequently, 2015 – the year of the company's centennial – is also the year of an important product anniversary: ZF has been offering automatic passenger car transmissions for 50 years. The new product from back then has developed into a major source of revenue for the international technology company.

THE BEGINNING 50 YEARS AGO: THE ZF 3HP12

The 3HP12 transmission, **FIGURE 1**, that was installed in a Peugeot 504 for the first time consisted of multiple assemblies: ZF procured a torque converter without lock-up clutch, for which the latest sheet metal forming technology of the time was utilised, from the Fichtel & Sachs company. The turbine wheels belonging to the torque converter transmitted up to 120 Nm of torque to the planetary assembly which consisted of a Simpson planetary gearset. Clutches and brakes with lined clutch disks were used as shift elements. The gear changes were performed in a purely hydraulic manner. An oil pump driven via the torque converter shell provided the oil volume, the oil pressure was generated in a hydraulic valve. The operating pressure was controlled via a further valve that was connected to the engine throttle cable via a wire rope hoist. The generated pressure was modulated in a speed-dependent manner by a centrifugal force governor located on the output shaft. This pressure then mechanically acted on the shift elements via a distribution system. Dampers that were only active during the shift itself and enabled a comfortable gear change were installed upstream of the shift elements.

A special feature of the 3HP transmission was the utilisation of three shift freewheels. They supported the shift quality as, when it came to pure hydraulic shift systems, it was difficult to synchronise a clutch-to-clutch shifting (simultaneous opening of one clutch and closing of another) and, without shift freewheels, noticeable shift jolting even occurred in multi-ratio transmissions with some gear changes at that time.

A two-speed automatic transmission (2HP14) which only made it to the prototype stage was developed at ZF prior to the volume production application of the 3HP. However, engineers who were involved at the time drew upon significant knowledge from the test ranges and applied it in the development of the 3HP12 transmission. Among other things, they decided in favor of three gear steps and realised the high significance of shift freewheels.

50 years of automotive history also mean enormous development leaps in the field of driveline technology. The multi-ratio transmission from back then has also significantly developed with each generation, new technical approaches and innovations have significantly increased driving dynamic characteristics as well as consumption and, ultimately, diversity in terms of operation. The multi-ratio transmission has preserved its place in the range of various transmission types and has, despite all pessimistic forecasts, even extended it. The engineering progress of certain elements of the multi-ratio transmission will be tracked and substantiated below through the development leaps of ZF products.

The starting point is a rough overview of over 50 years of automotive progress which highlights the commonalities and significant differences between a high-tech transmission, such as the current second-generation ZF 8HP, and the first multi-ratio transmission from 1965. If the multi-ratio transmission principle is looked at very generally, the constants come into view: The basic principle continues to be "hydrodynamic torque converter plus transmission with planetary gearsets" which is apparent at ZF by the "HP" identification code that the current transmissions also bear. Shafts continue to be responsible for the transmission of power inside the transmission, clutches and brakes today still function as shift

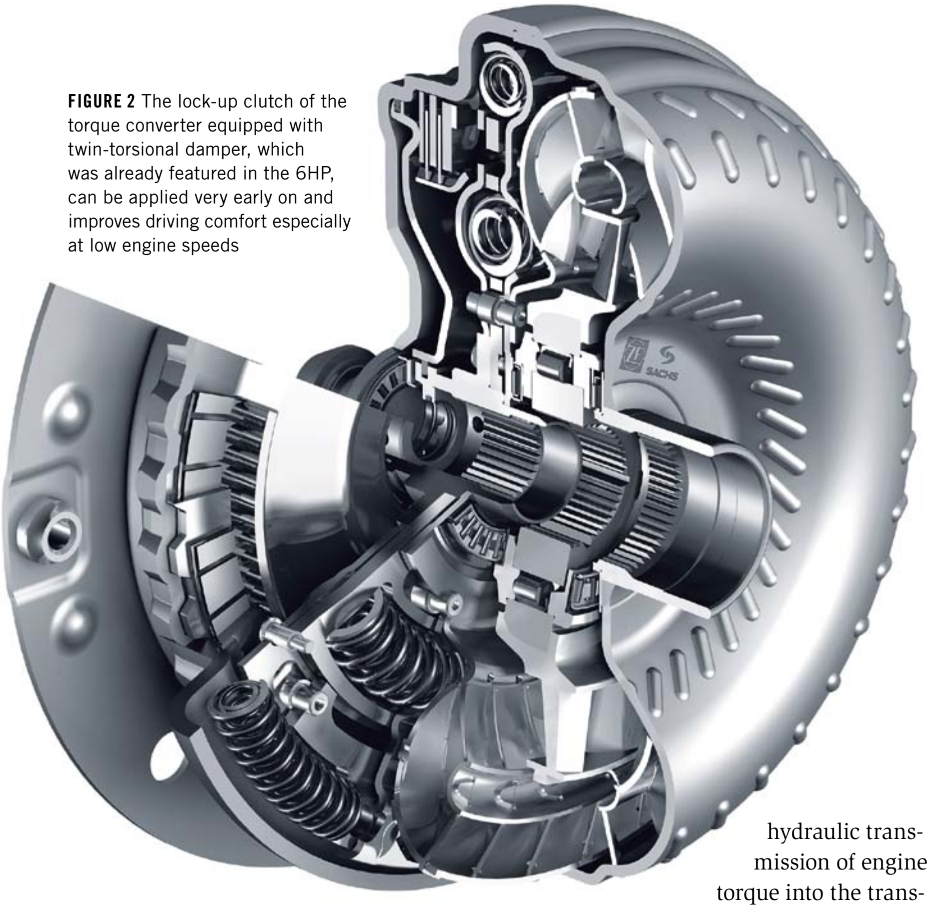

FIGURE 2 The lock-up clutch of the torque converter equipped with twin-torsional damper, which was already featured in the 6HP, can be applied very early on and improves driving comfort especially at low engine speeds

elements, gear changes are performed automatically and are triggered as well as controlled by means of hydraulics. However, if all of the named elements are looked at more closely, small technical revolutions have taken place almost everywhere.

TORQUE CONVERTER TECHNOLOGY

One of the main tasks of the torque converter is the decoupling of torsional vibrations. The torque converter which was still dominant 50 years ago and was part of the name continues to perform the hydraulic transmission of engine torque into the transmission but, in terms of the development expense, the technological know-how, and even the installation space volume in the torque converter, is now much more in the background. The so-called Trilok torque converter which was utilised in the 3HP12 50 transmission years ago did not yet boast a torque converter lock-up clutch. Consequently, the transmission of power into the transmission was always hydraulic. In doing so, a certain amount of slip occurred – a speed difference between the impeller and the turbine wheel – which resulted in efficiency losses. However, rotational irregularities of the engine are thereby virtually automatically neutralised. In order to limit the efficiency losses of a permanent converter slip, ZF utilised a torque converter lock-up clutch (unregulated) as early as the 4HP transmission – a multidisk clutch which connected the impeller and the turbine wheels in a force locking manner. When this component was closed, a rigid direct drive of the engine torque into the transmission occurred. However, there was no hydraulic damping of the engine rotational irregularities in this state meaning that it was necessary to develop and install mechanical dampers in the torque converter. On the 4HP transmission, comparatively simple spring systems prevented the engine rotational irregularities from being transmitted to the driveline and the entire vehicle in the form of uncomfortable vibrations from a certain speed range.

The next development step to the 5HP transmission in 1990 represented the entry of the regulated torque converter lock-up clutch into the field of automatic ZF transmissions. This transmission version even enabled the bridging of the converter slip in low engine speed ranges, even if the clutch was not fully closed in regulated mode. However, this solution which further reduced the consumption data also placed higher requirements on the torque converter lock-up clutch and the transmission oil. The result was further investments in the torsional damper technology of the torque converter. This trend continued with the six-speed automatic transmission. Alongside the torsional damper which had been available up to this point and (for more powerful engines) turbine torsional dampers, a combination of two independent spring systems in the form of the twin torsional damper (TWD) was utilised which was particularly suitable for the downsizing of gasoline and diesel engines and their extremely intense vibration characteristics at low speeds, **FIGURE 2**. The consequence: It was possible to move the operating point of the bridging even further forward, the clutch closed at extremely low engine speeds (without any noticeable restriction in comfort for the passengers) and, as a result, contributed to fuel savings.

With the latest generation of the 8HP transmission, ZF has moved a step closer to the objective of closing the torque converter lock-up clutch at ever-earlier operating points, i.e. lower engine speeds,

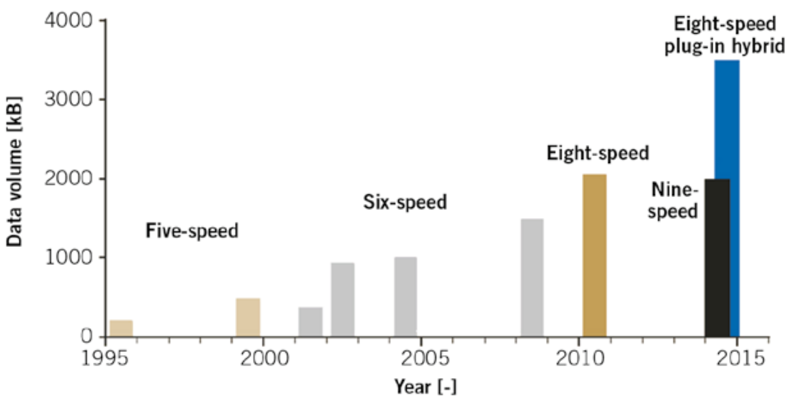

FIGURE 3 The amount of read-only memory (ROM) in ZF transmission control units has increased over the years and still could process more data and functions

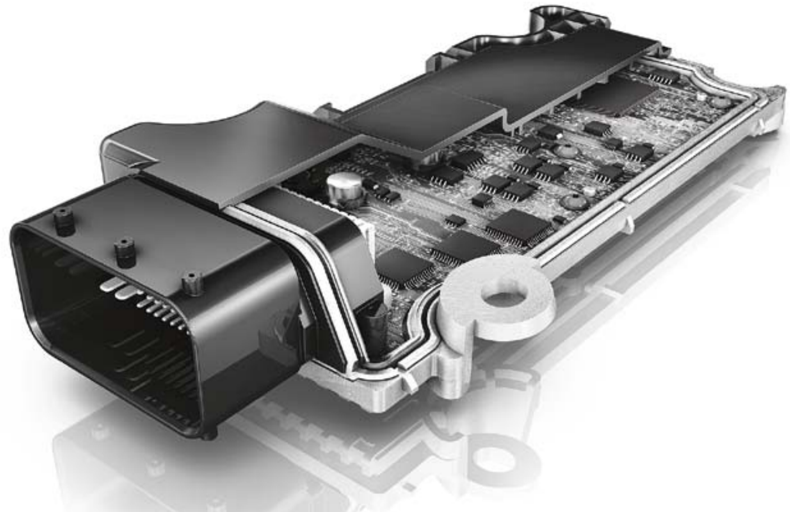

FIGURE 4 Electronic control unit 9HP

and enabling higher loads. One reason is the use of a triple-line converter which, via its own hydraulic line, is able to actuate the lock-up clutch and, consequently, enables more finely controlled bridging procedures. A further innovation, which was introduced with the second-generation of the 8HP transmission, is a torque converter with a speed-adaptive mass damper. In addition to the TWD spring damping system, a mass pendulum is used here which further increases the decoupling quality at specific operating points and, consequently, enables an even earlier bridging of the converter slip.

INCREASED USE OF ELECTRONICS

Today, it is generally acknowledged that transmission innovations are decisively determined by the integration of electrics, electronics, hydraulics, actuators, and sensors. In doing so, the system boundaries of the transmission have also recently been exceeded and functional growth has been achieved by means of networking in the overall vehicle. This development that has also significantly contributed towards efficiency gains in automatic ZF transmissions originated in 1987. Back then, the second-generation of the 4HP transmission was also optionally available with an electrohydraulic control unit. The necessary hydraulic controller for speed detection as well as a throttle cable for load detection were previously omitted on the respective transmissions. These functions were assumed by an (externally mounted) electronic control unit (ECU). This component with a size of a DIN A5 paperback book had a read-only memory (ROM) of 8 KB. The progress is clear to see when directly compared to the 8HP which boasts a CPU with the size of a stamp and can access a ROM of 2 MB, **FIGURE 3**.

Even the electrohydraulic control unit in the 4HP transmission communicated with the engine control. Consequently, it was possible to briefly reduce the engine torque during the gear changes by means of meshing in the ignition so that the gear change was even less noticeable for the driver and the loads of the shift clutches were reduced.

The electronics in the transmission rapidly gained importance up until the introduction of the 6HP in 2001. This became apparent as early as 1990 with the 5HP transmission where the use of electronics now permitted regulated and adaptive gear changes. Networking with the vehicle data allowed access to important influencing factors such as uphill gradient, load, or travelling with a trailer. The movements of the accelerator pedal were also evaluated via sensors and led to a driver type recognition and a respective adaption of the shifting characteristic.

The degree to which the electronic control unit now influenced the shifting quality can be seen in the use of the shift freewheels in the ZF transmissions. From the driver's point of view, these components permit a harmonious gear change as they facilitate the torque transfer in the synchronisation point. As it was not possible to implement a clutch-to-clutch shifting on a purely hydraulic basis, the engineers of the 3HP transmission also decided to support the torque during load shifts via a freewheel. Therefore, they decided to utilise three shift freewheels when designing the 3HP transmission. In the 6HP transmission, it was already possible to implement a pure clutch-to-clutch shifting via a fine dosing of the pressure regulators controlled by the electronics at the shift elements in the transmission. Here, the torque is transmitted from the opening to the closing clutch without detours. However, this electronically regulated transition requires the shift elements to be equipped with pressure regulators and also requires a powerful control software. In turn, the potential omission of the freewheels which is made possible by the electronics increases energy efficiency as the weight is reduced and installation space savings are achieved.

With the even more powerful electronic control unit that ZF also installed into the transmission oil sump in the 6HP transmission, a more sophisticated shifting strategy became possible which enabled economical, sporty, or extremely sporty driving. With the second-generation of the 6HP transmission in 2006, ZF performed changes to the hydraulics which permitted significantly shorter shifting times. This drastically changed the image of the multi-ratio transmission: The technology that was once considered to be comfortable yet fuel-intensive and less sporty has since (compared to the manual transmission) become measurably better in terms of economy and driving dynamics. Consequently, a variant of the 8HP transmission is being used as a racing transmission in mass motorsport. Although this 8HP racing transmission boasts specific control software, the transmission hardware actually corresponds to the status of volume production.

The electronics also played an important role with the nine-speed automatic transmission which ZF put into volume production in 2013 and with which ZF also extended the transmission portfolio of multi-ratio transmissions to vehicles with front-transverse motorisation for the first time since 1996 (SOP 4HP20), **FIGURE 4**. It permitted the use of dog clutches as two of the six shift elements of this transmission. The abrupt mechanical shifting characteristics of this clutch type which, however, boasted significant advantages in terms of drag losses and installation space, could be made comfortable and dynamic thanks to controlling interventions by the electronics.

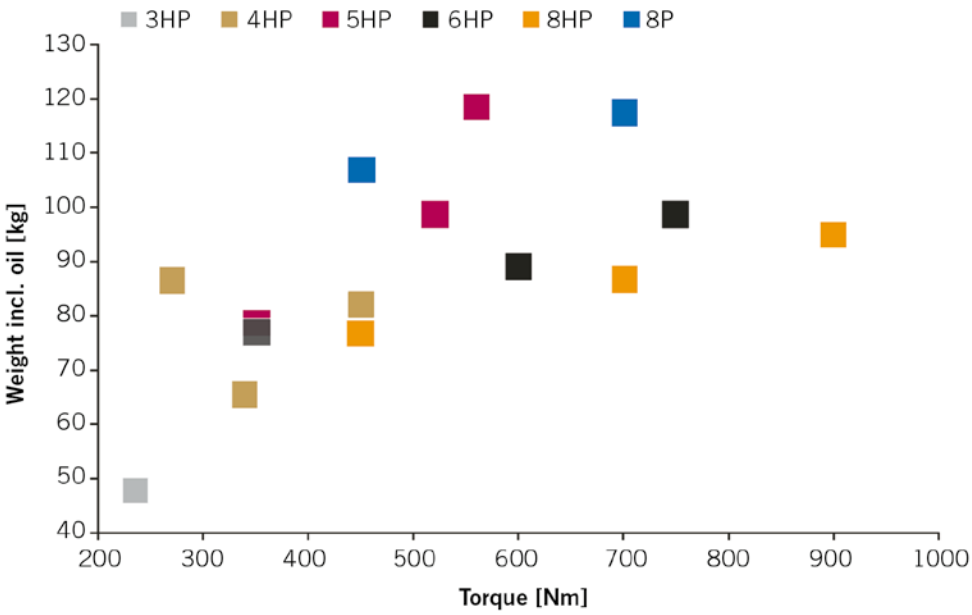

FIGURE 5 Comparison in the power-to-weight ratio of three-speed to eight-speed automatic transmissions with longitudinal drive

GEARSET COMBINATIONS

The layout of the three gear steps in the 3HP transmission was made possible by a planetary gearset and five shift elements. The increase in the number of gears and the pursuit of more energy efficiency which was also associated with this created a problem for the ZF engineers: More gears tended to require more gearsets and more shift elements. In addition to this, the engine performances also increased from 1965 onwards which meant that all components therefore had also to be dimensioned for high load peaks. This threatened to set a weight spiral in motion which can be seen in the development of ZF transmissions up to the 5HP: more gears, more performance, but also more weight, **FIGURE 5**. ZF put an end to this spiral in 2001 with the 6HP transmission: Even though the 6HP had similar performance figures compared to the predecessor, it not only boasted one gear step more, it was also 20 kg lighter. Thanks to the reduced number of components, it was also easier to assemble. A significant reason for these advantages was the gearset concept. With the 6HP, ZF used a Lepelletier gearset for the first time which made it possible to use gearset assemblies several times. Even though three gearsets and six clutch elements were required for a five-speed automatic transmission (without Lepelletier), a single and double gearset in conjunction with five clutch elements were sufficient for the six gears in the 6HP transmission. This alone enabled a weight saving of approximately 11 kg.

Four gearsets and six shift elements are used in the nine-speed automatic transmission for vehicles with front-transverse motorisation, a high nominal figure. However, the gearsets were nested in

FIGURE 6 The nested planetary gearsets in the 9HP use the limited installation space intelligently

FIGURE 7 Reduction of fuel consumption as a result of new automatic transmission generations (savings compared to the previous generation)

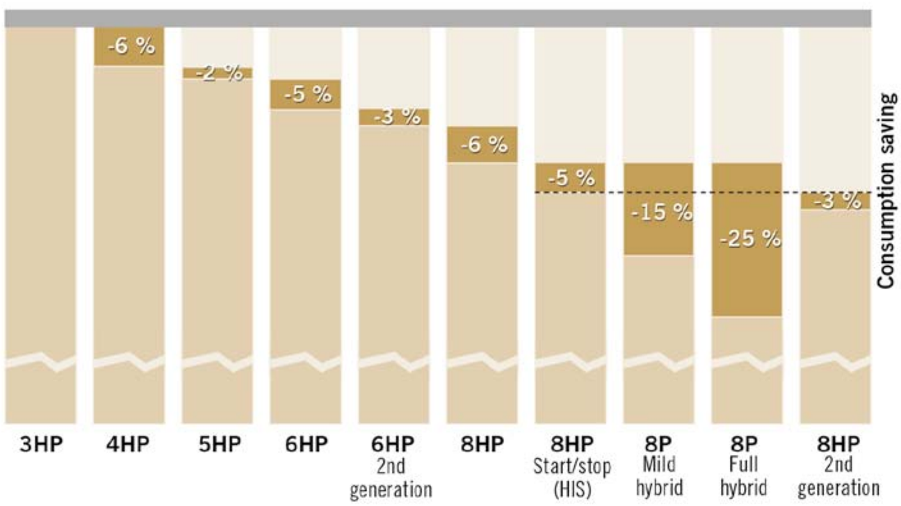

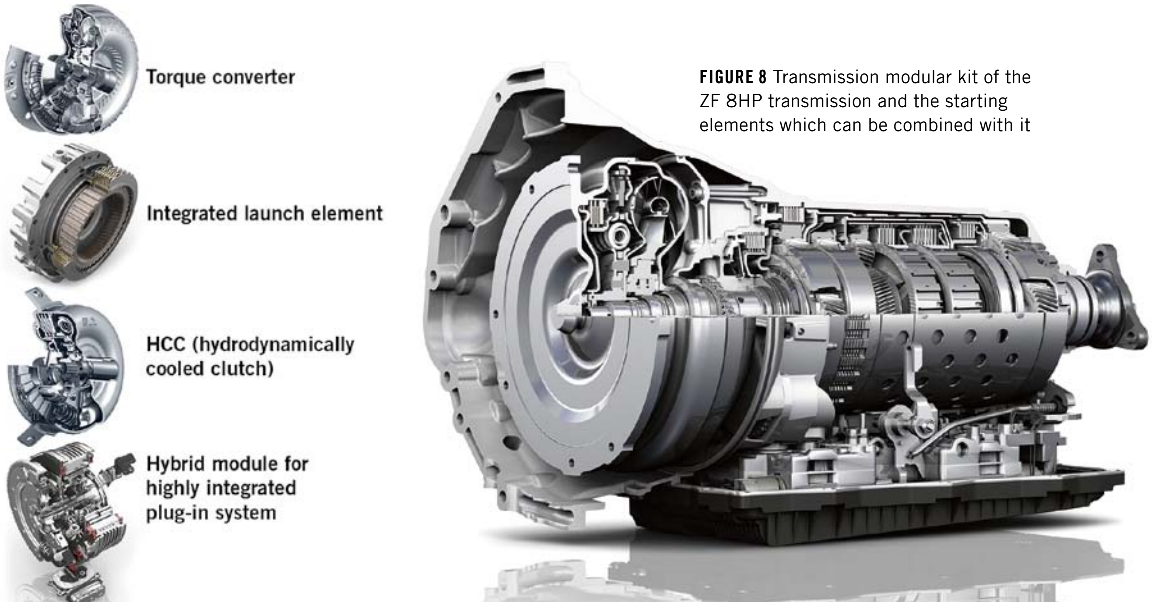

FIGURE 8 Transmission modular kit of the ZF 8HP transmission and the starting elements which can be combined with it

each other in such an intelligent manner that the tight installation space and weight provisions of a front-transverse transmission were not impaired, **FIGURE 6**. Furthermore, the first use of dog clutches in an automatic passenger car transmission was significant in terms of the compact installation space requirements of the 9HP transmission.

However, the number of gear steps or the transmission weight are not solely responsible for more fuel efficiency. Here, the drag losses inside the transmission represent a significant factor. The transmission oil, which ZF has constantly further developed with its transmissions, the hydraulic pump, and, once again, the gearset concept play a role here. For instance, if many of the multidisk clutches or brakes that rotate on the shaft in transmission oil are open, this leads to higher drag losses. When selecting a gearset concept for the eight-speed automatic transmission (with computer support), filtering among numerous possible gearset combinations also took place according to the criteria of drag losses. From five shift elements, only two shift elements are open in each gear. This concept makes a significant contribution to the energy efficiency of the current ZF automatic passenger car transmission which allows fuel savings of 6 % although it has more gearsets than the direct predecessor transmission, **FIGURE 7**.

MODULAR DESIGN

Over the course of time, ZF has increasingly made the modular concept in the field of transmission production a reality. While the 3HP22 transmission – which followed the 3HP12 debut transmission – was de facto a new design, the 4HP transmission already demonstrated approaches of a transmission family for various engine torques. To this very day, ZF follows this modular approach of adapting a basic transmission design for multiple torque classes by means of variously dimensioned components, especially gearsets and clutches. This modular approach was also transferred to the input and output components: Since the 4HP22 transmission in 1985, ZF has also offered its automatic transmissions with integrated transfer case for vehicles with four-wheel drive. The differentiation of the torque converter technologies for various motorisations had already been mentioned. The eight-speed automatic transmission was marketed as a "transmission modular kit" for the first time. This can be attributed to the fact that, with it, the same basic transmission can be equipped with various starting elements and four-wheel drive variants. This transmission modular kit represents consumption reductions, increases in dynamics and comfort, and flexibility: Besides vehicle segments, the 8HP modular kit, **FIGURE 8**, also enables plug-in hybrids, four-wheel drive configurations, motorsport applications, and can also be found in the field of highly-loaded LCV applications. In combination with an electric motor in place of the torque converter, all hybrid functions can be implemented from the mild hybrid to the plug-in hybrid. Even on the latter, the electric motor, separating clutch, torsional damper, and hydraulics are arranged in a space-saving manner that the eight-speed automatic transmission requires almost the same installation space as the conventional version with torque converter.

CONCLUSIONS AND OUTLOOK

Thanks to its high flexibility, the 8HP transmission modular kit covers all requirements across a wide range of vehicle segments and platforms that arise from current and forthcoming combustion engine technologies as well as the diversity required by OEMs and end customers. Alongside gains in dynamics and comfort, it focuses on the increase in passenger car efficiency. Thanks to optimised functions, increased efficiency, and operating point shifts, the second-generation 8HP basic transmission which was launched in June 2014 achieves a savings potential of up to 3 % compared to the predecessor transmission and is well suited for downsizing and downspeeding concepts. Furthermore, the 8HP transmission is a pioneer due to the fact that, via highly integrated hybrid modules, it enables relatively simple powerful plug-in systems and, consequently, a standard consumption reduction of over 70 %. In face of increasingly strict emission and consumption provisions, e.g. the EU-wide CO_2 fleet limit of 95 g/km planned from 2021 onwards as well as the forecast dominance of combustion engine-based drive concepts for at least a decade, the need for such flexible and advanced transmission technologies will increase further.

Condensing Venturi EGR Mixer

AUTHORS

David Roth
is Technical Specialist at Corporate Advanced R&D Organization of BorgWarner Inc. in Ithaca (USA).

Iago Gonzalez Tabares
is R&D Product Engineer at BorgWarner Emission Systems S.L. in Vigo (Spain).

Ángel Sotelo Álvarez
is R&D Product Engineer at BorgWarner Emission Systems S.L. in Vigo (Spain).

A significant hurdle to overcome in implementing low pressure loop EGR is dealing with condensation of water near the entrance of the turbocharger's compressor, which can damage the compressor wheel due to high-speed collision with water droplets. The team at BorgWarner has developed a low pressure loop EGR mixer that is effective at condensing and collecting the water droplets and routing the water around the compressor wheel.

LARGE NUMBER OF VARIABLES

In an engine equipped with a low pressure loop (LPL) EGR system, the junction upstream of the compressor wheel where the fresh air and exhaust gas mix, is the most favourable point in the system for condensation droplets because the exhaust gas in the EGR path is cooled as it travels through the EGR cooler and associated piping. A gasoline engine, and to a greater extent a natural gas engine, will encounter enough water condensation at some steady-state conditions to quickly damage the compressor wheel due to the

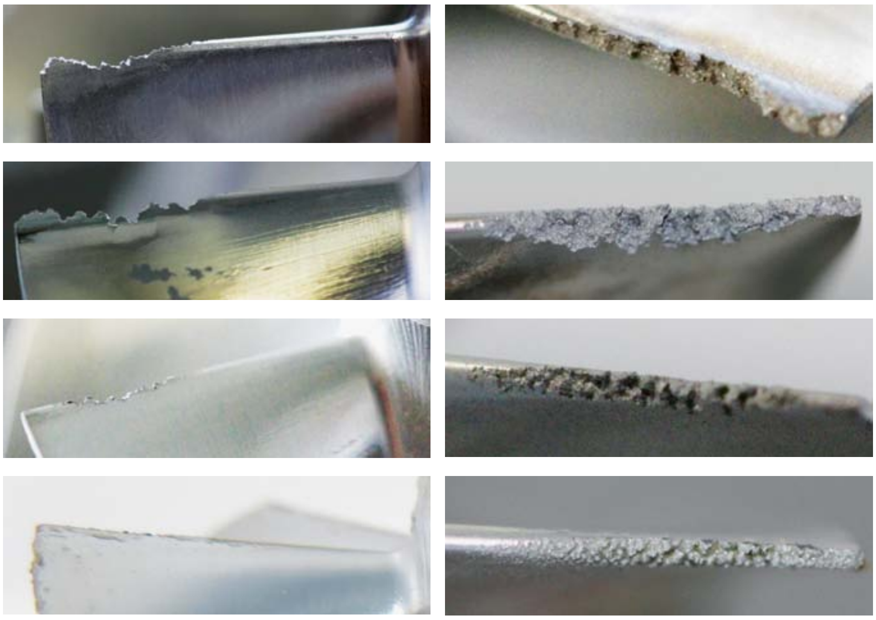

FIGURE 1 Compressor blade damage for different water injection parameters (from [1])

high-speed collision between the compressor blades and the water droplets [1]. These conditions are a function of ambient temperature and humidity as well as the engine speed and load, engine temperature, EGR rate and the vehicle under-hood airflow and thermal management. Due to the large number of variables that can effect condensation, a robust means of managing EGR condensate is needed.

A new condensing EGR mixer has been developed from BorgWarner as a compact module that mounts to, or can be incorporated into the turbocharger compressor housing and includes an integrated EGR valve. The mixer was developed from the known concept of utilising a mild venturi section to enhance EGR delivery and mixing. The system was designed to maximise condensation and separation of liquid water from the EGR stream. To manage the collected condensate BorgWarner has devised and tested an EGR/condensate "mid-pressure" path that is utilised to both purge the system of liquid water as, well as provide for an additional EGR route.

CONDENSATION MANAGEMENT

Depending on conditions, droplets may form anywhere in the EGR path and most-likely in the mixing junction, since the junction is cooled by the near-ambient temperature airflow coming from the aircleaner assembly. Compressor wheel damage from condensed droplets has been observed in the field in production diesel engines and studied on a test bench. Damage is a function of droplet size, quantity, location and turbocharger speed and can be catastrophic as seen in results from [1], **FIGURE 1**.

Prediction of condensation is greatly complicated by the fact that the heat transfer in the EGR path is not just a function of the characteristics of the EGR cooler and the EGR source temperature but also significantly affected by heat transfer from the EGR piping and the EGR valve itself, and this heat transfer is dependent on the underhood air temperatures and velocities, which in-turn are functions of:
– ambient air temperature
– vehicle speed
– ambient wind velocity and direction
– vehicle-to-vehicle variations in underhood airflow.

Therefore, any calibration strategy of avoiding the possibility of compressor damage from condensed water droplets by shutting off LPL EGR delivery, will require a significant safety factor beyond what might be determined based on steady-state and transient measurements on an engine dynamometer.

ESTIMATION OF LPL EGR CONDENSATION RANGE

To prepare for an evaluation of the new EGR mixer, tests to determine the approximate ranges for steady-state conditions of condensation on turbocharged 2-l GDI engine installed on an engine dynamometer at near-standard conditions of ambient temperature and humidity were performed.

For this series of tests, the engine was equipped with a prototype LPL EGR system comprised of stainless-steel tubing as well as an EGR valve and EGR cooler from BorgWarner. The EGR mixer was a stainless-steel fabricated "T" mixer. The test cell temperature was maintained at 21 °C, the engine coolant at 86 °C, and the combustion air was supplied at controlled temperature and humidity. Condensation was judged by observing a sight-glass installed at the entrance of the compressor, **FIGURE 2**, during a ten-minute steady-state run. Some observations about steady-state condensation limits are:
– As engine load rises, the likelihood of condensation reduces due to the increase of EGR source temperature and reduced temperature reduction through the EGR cooler and pipes.
– As EGR rate rises, the condensation likelihood reduces due to the reduced temperature drop through the EGR cooler and pipes.

Based on these near-standard condition tests, steady-state condensation can occur at engine loads up to 6 bar brake mean effective pressure (BMEP) and ambient conditions up to 25 °C at 50 % relative humidity.

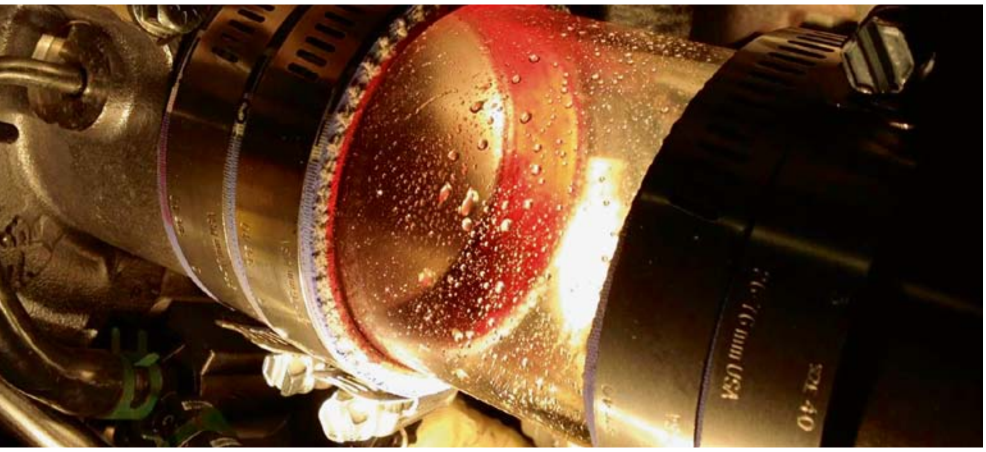

FIGURE 2 Observation of steady-state condensation on engine test bench

CONDENSING MIXER WITH MID-PRESSURE LOOP

In the early EGR tests the test team modified a natural-gas carburetor for use as an EGR-mixer and observed that the thin-wall aluminium venturi section provided an enhanced surface for condensation of water from the incoming EGR stream due to the large surface area of the venturi section being cooled by the incoming fresh air stream.

Since the outside surface of the venturi will tend to collect condensed water BorgWarner designed a prototype EGR mixer using a thin-wall aluminium venturi with the following enhancements:

- collection chamber with control valve
- cooling fins on the outside of the venturi to increase condensation rate
- integration of an EGR valve.

MIXER DESIGN

CFD was used to optimise the venturi pressure drop and the EGR holes (location, size and arrangement) in the throat of the prototype mixer design. The mixer assembly, **FIGURE 3**, consists of two housing components that creates a chamber that surrounds the venturi throat. One of the housings has the EGR connection and the condensate purge on it. The EGR valve is directly bolted to this mixer. Fins were incorporated on the external surface of venturi throat to enhance heat transfer (between hot EGR and cold air intake) to favour condensation of exhaust gas.

MID-PRESSURE PATH FOR CONDENSATE MANAGEMENT

While it is apparent that a venturi EGR mixer can offer some compressor protection due to the function of the small holes in the throat of the venturi acting to atomise water droplets in a fashion similar to that of a carburettor, a more robust solution would be to segregate the collected water and route it around the compressor. To this end, the possible dispositions of collected water were considered:

- compressor outlet
- charge-air-cooler outlet
- engine throttle (pre- or post-blade)
- environment
- turbine inlet or exit.

These choices, with the exception of post-blade throttle, would require a pump to purge the condensate reservoir. A better choice is to route the condensate drain to the intake manifold because there is a favourable pressure drop to purge the water collection reservoir whenever the throttle is not fully open. In addition, this path provides for the following advantages:

- Water spray may clean deposits from the intake ports and valves.
- Water spray may provide some knock relief.
- The path provides for another EGR path.

As shown in **FIGURE 4**, this additional path, a mid-pressure-loop (MPL) for EGR mixed with water droplets, is a result of this

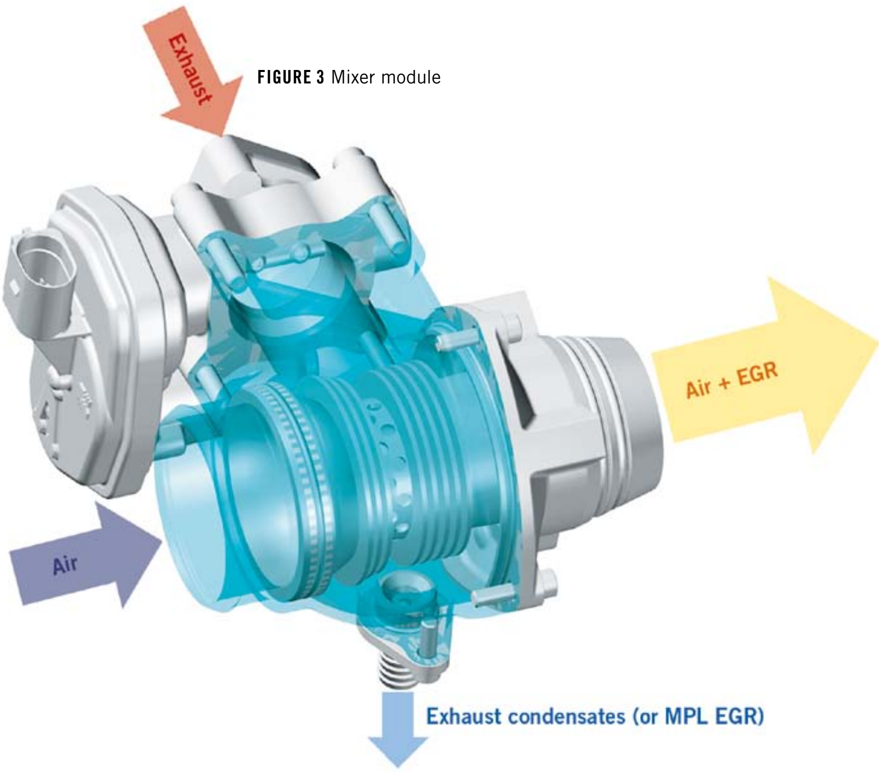

FIGURE 3 Mixer module

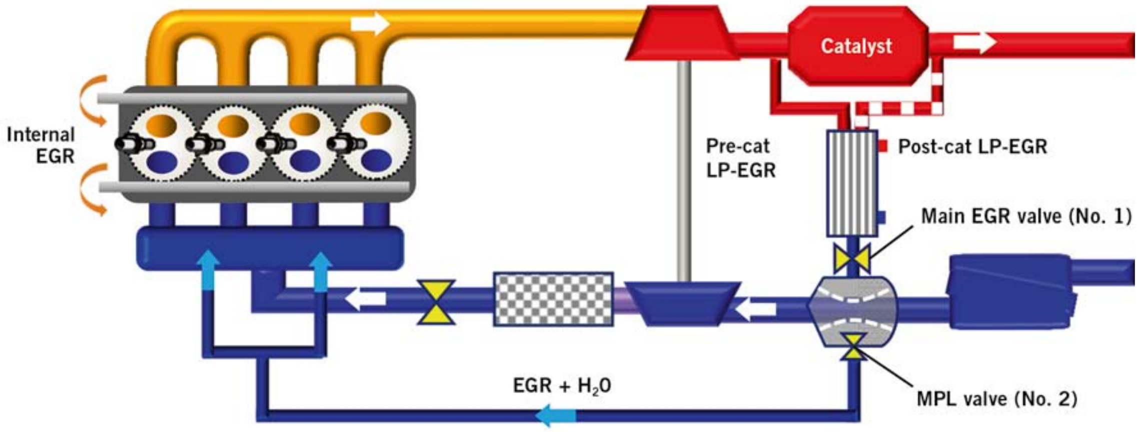

FIGURE 4 LPL venturi mixer with MPL

routing of the venturi chamber to the intake manifold. For a system as shown in **FIGURE 4**, the logic for operating the engine would be as described in **TABLE 1**, based on the main EGR valve being a normal proportional control valve and MPL valve being a simple on/off valve.

With this system design, the only engine operating condition where condensation can continuously collect is boost with the engine throttle fully-open. Fortunately, the likelihood of condensation reduces with power level, due to the temperature increases in the EGR path.

An alternative to active control of the condensate purge, is to adapt a positive crankcase ventilation (PCV) valve to the mixer drain in place of the on/off valve. A PCV valve combines the functions of a flow regulator and a check valve, and just as it functions in crankcase ventilation, it should provide continual purging of the condensate collection chamber. Evaluating this is a future planned activity. Whether purging the mixer is active or passive, the MPL path can eliminate the likelihood of water accumulation in the mixer and therefore minimise the possibility of water freezing in cold ambient conditions.

Another aspect of the MPL is that as an EGR path, it will tend to behave as a high-pressure-loop in terms of temperature of EGR delivered to the intake manifold, avoidance of fouling of the compressor and charge-air-cooler, and effect on pumping work. To evaluate these effects and confirm the effectiveness of the condensing EGR mixer with MPL to protect the compressor, BorgWarner tested the prototype on our 2.0-l turbo GDI engine.

CONDENSATE PROTECTION FROM MID-PRESSURE-LOOP OPERATION

To determine if operating the engine with the EGR coming through the MPL would protect the compressor from droplet damage, BorgWarner set the engine at a steady-state condition that had significant visible condensation at the compressor inlet. At an engine test condition of 2000 rpm, 6 bar BMEP, 10 % EGR, with 10 °C intake temperature and 50 % humidity combustion air fed from the test cell, steady-state condensation at the sight glass, was eliminated when we opened the MPL control valve and maintained the EGR rate equal to the pure LPL case.

MID-PRESSURE-LOOP EFFECT ON ENGINE EFFICIENCY

As has been reported in several publications, including [2], there may be significant pumping mean effective pressure (PMEP) improvements from use of HPL EGR compared to LPL due to changing the operating points of the turbocharger compressor and turbine and the engine throttle angle. To see if this effect held for the MPL, BorgWarner ran comparison tests at matched conditions with the MPL valve open vs. closed. In **FIGURE 5** the result at 2000 rpm, 6 bar engine load for a range of EGR rates during sweeps of intake cam phase is shown. The maximum PMEP reduction in at this engine condition was 4 %, which should yield a small (approximately 0.5 %) improvement in BSFC.

For the prototype mixer the target was to have no more than 5 kPa pressure-drop across the venturi at full-power. The maximum pressure drop across the prototype venturi mixer was

Engine condition	Valve No. 1	Valve No. 2	Logic
Boost	Modulating	Closed	Normal LPL EGR, condensate can accumulate, Venturi holes atomise droplets
Moderate load with intake vacuum	Modulating	Open	Lower PMEP, clearing out condensate, minimise deposits, minimise thermal load on coolers
Closed-throttle decel	Closed	Open	Clear-out condensation

TABLE 1 Logic for operating engine with MPL

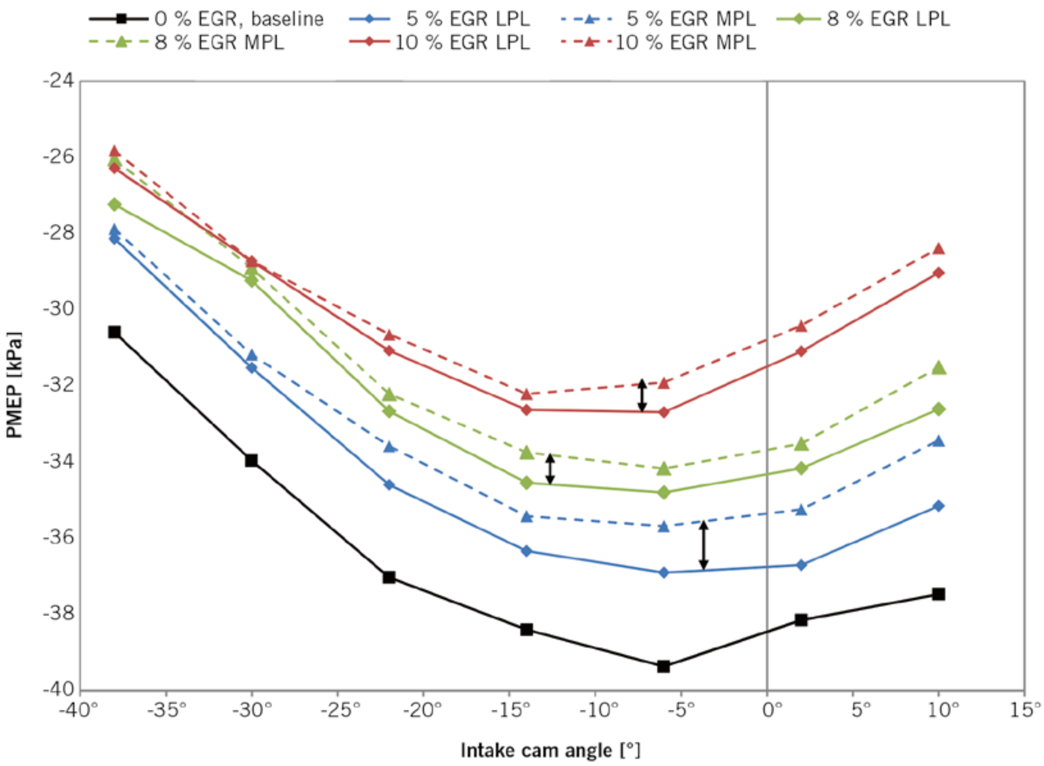

FIGURE 5 PMEP improvement from using MPL EGR at 2000 rpm, 6 bar (intake cam sweep)

3.5 kPa. This was within 1.5 kPa of the pressure drop of the simple "T" mixer. One of the advantages of a venturi is that the depression at the throat can be used to increase the pressure difference driving EGR and therefore enhance steady-state and transient EGR delivery. The maximum depression at the EGR port generated by this venturi mixer at full-load was 11 kPa. BorgWarner was not able to verify an increase in maximum EGR rate in these tests due to combustion quality limitations for both mixers.

SUMMARY

The new condensing EGR mixer was designed to both maximise condensation and separation of liquid water from the EGR stream, as well as manage its disposal through the engine in a manner that both avoids damage to the compressor and minimises liquid freezing potential in very low ambient conditions. The system architecture includes a mid-pressure path that is utilised to both purge the system of liquid water as, well as provide engine efficiency improvements at moderate load operation points. This mixer design when connected to an engine with a mid-pressure loop, will provide the following demonstrated advantages over a simple "T" mixer:

- management rather than avoidance of EGR condensation and protection of the compressor
- EGR steady-state and transient flow rate improvement
- small PMEP (and therefore engine efficiency) improvements.

In addition to the measured system benefits, the following are expected benefits that will be evaluated in future testing: engine intake noise attenuation, trapping of hard particles in EGR (such as pieces of catalyst substrate) and transient EGR control.

REFERENCES

[1] Karstadt, S.; Werner, J.; Münz, S.; Aymanns, R.: Effect of Water Droplets Caused by Low Pressure EGR on Spinning compressor Wheels. 19th Supercharging ConfereCce, Dresden, 2014

[2] Roth, D.; Zhang, R.; Sauerstein, R.; Becker, M.: New Aspects of Application of Hybrid EGR Systems to Turbocharged GDI Engines. 18th Aachen Colloquium Automobile and Engine Technology, 2009

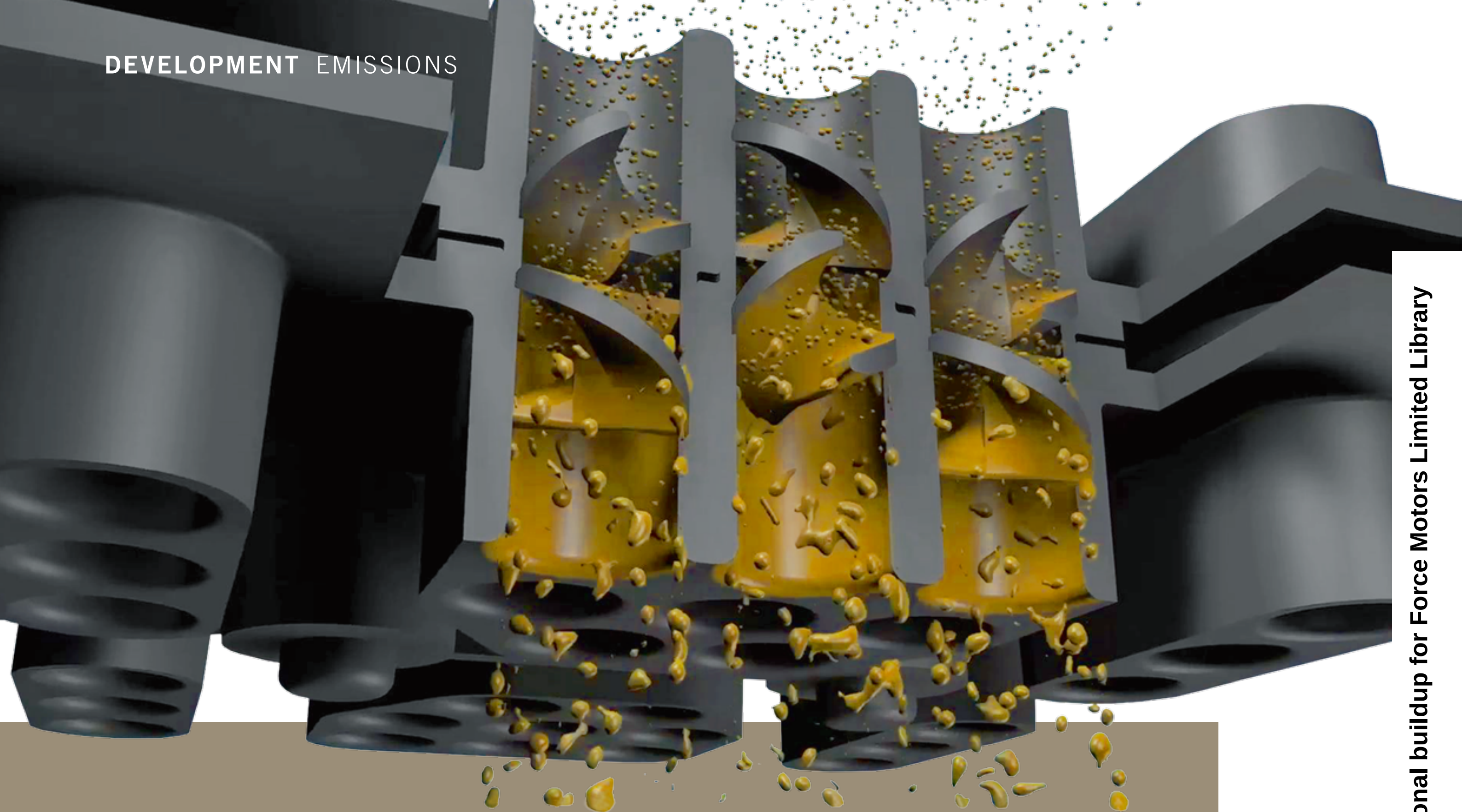

Adaptive Oil Separation for Efficient Crankcase Ventilation

The trend towards combustion engines with increasing mean pressures results in oil particles in the blow-by gas which are finer and finer. Oil separation systems separate these fine oil particles out of the blow-by gas, thus fulfilling an important function in the crankcase ventilation. With its new Multitwister technology, Reinz has expanded the oil separator by adding an adaptive solution which actively influences the pressure curve and increases its efficiency even further.

AUTHORS

Dipl.-Ing. (FH) Francesco Zitarosa is Director of the Global Crankcase Ventilation Application Technology Department at the Reinz-Dichtungs-GmbH in Neu-Ulm (Germany).

Philipp Zedelmair, B. Eng. works on Oil Separation Development at the Plastics Systems Division of the Reinz-Dichtungs-GmbH in Neu-Ulm (Germany).

Dipl.-Ing. (FH) Christoph Erdmann is Development Director at the Plastics Systems Division of the Reinz-Dichtungs-GmbH in Neu-Ulm (Germany).

Dr. Jürgen Schneider is the Director of the Product Development Europe Department at the Reinz-Dichatungs-GmbH in Neu-Ulm (Germany).

ONGOING CHALLENGES IN OIL SEPARATION

The general trend towards downsizing seems like it will never stop. However, this technology has a major drawback: finer oil particles in the blow-by gas. Due to the design, a mixture of these particles and combustion gas leaks past the piston and into the crankcase. The purpose of oil separation is to completely separate these oil particles from the blow-by gas in order to guarantee the best crankcase ventilation and cleanest exhaust gases possible. This is the only way to meet the demanding requirements of emissions legislation – which will only become more stringent in the future. What's more, efficient oil separation systems make for longer intervals between oil changes and protect components more effectively.

The smaller and smaller oil particles pose new challenges to developers. If the blow-by gas is sucked back out of the crankcase and fed into the combustion, the unseparated oil in the intake air will get into the intake tract. The possible consequences are deposits in the turbocharger and at the intake valves, as well as higher emissions. In addition, automobile and engine manufactures stipulate lower limit values for coarse and fine oil particles in the blow-by gas in the full load range – even over the entire engine characteristic map, as is the case with some manufacturers. About ten years ago, the permissible maximum was approximately 5.0 g/h, followed by a phase in which 1.0 g/h was considered the standard value. Nowadays, original equipment manufacturers demand specs no greater than 0.5 g/h in the oil discharge – and sometimes even 0.25 or less.

The combination of tiny oil particles and low limit values makes oil separation more and more complicated. Oil separators will have to become more efficient if future requirements are to be met dependably.

THE EVOLUTION OF OIL SEPARATION SYSTEMS

Multitwister technology from Reinz-Dichtungs-GmbH ranks among the smallest yet most effective oil separation systems for crankcase ventilation. The standard version of the injection-moulded part is made up of parallel-connected axial cyclones (boreholes/channels) with two 180° guide spirals with opposed rotation. As was previously the case, this configuration is achieved by connecting two identical "twister plates" to one another with the boreholes in a laterally inverted manner so that the opposing spirals converge. The blow-by gas, which is full of oil mist, is accelerated in a rotation while flowing through, causing the majority of the oil droplets to hit the outer walls, where they form a film. Turbulence caused by inversion of rotation within the Multitwister increases its performance even further. The end of the pipe now dependably discharges the even better separated quantity of oil, thus reintroducing the oil to the lubrication circuit in a highly environmentally friendly manner.

SYSTEM WITH ENHANCED EFFICIENCY

The most significant advancement of the Multitwister MT 2.0 is its increased efficiency, **FIGURE 1**. A decisive factor in the efficiency of an oil separator is how many of the coarse and fine oil particles it mixes out of the gas mixture flowing through it. This data describes the X50 value in relation to the number and quality of oil particles upstream of the oil separator. The newly developed system improved the Multitwister's performance, reducing the X50 value from 1.0 to 0.65 µm – at the same pressure loss. This improved value makes the system markedly more environmentally friendly: the more efficiently an oil separator works, the more oil can be fed back into the circuit.

The Multitwister MT 2.0 is robust, reliable, maintenance-free and is built into the valve bonnet and oil separator modules. It is highly flexible in volume regardless of its position, so that it can be installed at any location. Its 20 % increase in efficiency puts the Multitwister MT 2.0 in the top class of passive oil separation systems.

IMPROVED GEOMETRY

The main question in refining the Multitwister was: How can the design and efficiency be optimised without changing the size and shape? After all, the opportunities for changing the installation situation – and thus the valve bonnet – are marginal (if any), since the standardised outer contour of the Multitwister can only be inserted and welded in.

The development engineers pursued various innovative approaches with the same outside geometry, which they put into practice using CAD adaptations, flow simulations (CFD calculations), numeric and statistical methods and prototype analyses. The internal configuration of the Multitwister MT 2.0 presents the following optimisations:

- reduced wall thicknesses
- optimised twister diameters
- improved helix geometry within the individual channels
- efficient modular design for rapid serial production.

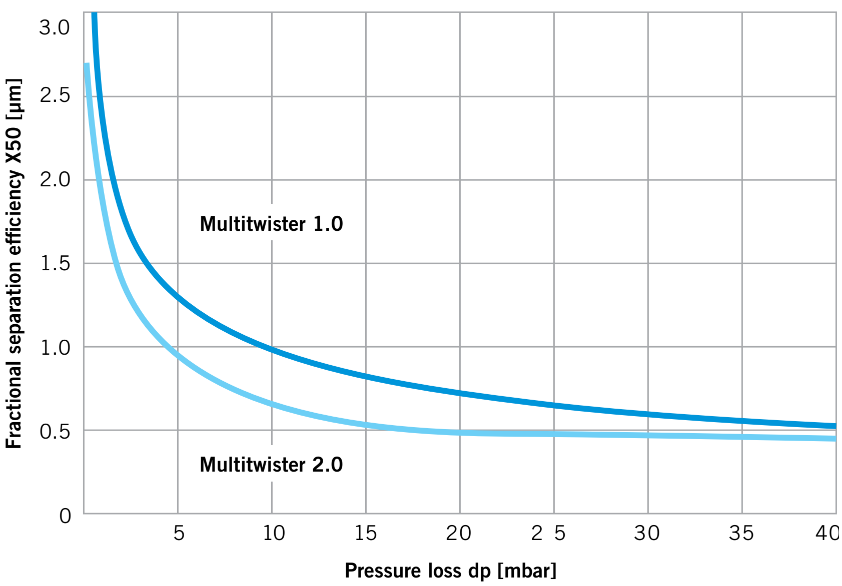

FIGURE 1 Increase in the Multitwister's efficiency from Version 1.0 to 2.0

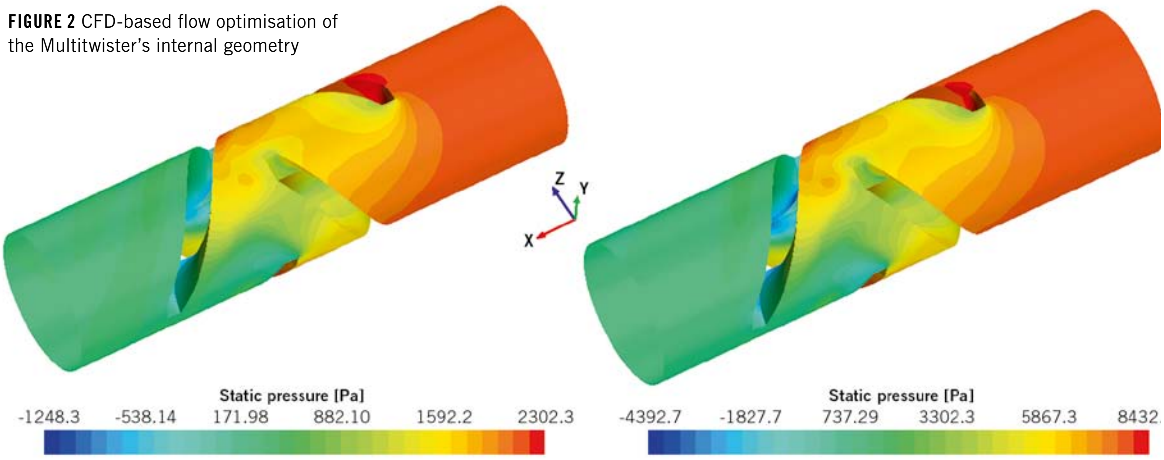

FIGURE 2 CFD-based flow optimisation of the Multitwister's internal geometry

The increased efficiency is especially the result of the improved helix geometry in conjunction with the optimised borehole diameter. The reduced flow resistance and the reduced pressure loss it entails markedly improve the efficiency of oil separation.

During the development phase, the engineers phased the "old" configuration of the Multitwister by modifying the helix geometry curve step-by-step. In order to reduce the flow resistance, the wall thickness was reduced from its original 0.9 to 0.15 mm and, in the final step, the borehole diameter was adapted to 2.0 mm. This makes for a lower flow resistance while keeping the deflection and acceleration of the oil particles the same and increasing the efficiency by 30 %.

All design modifications are based on flow simulations with subsequent prototype tests at the company's proprietary testing facilities. After all, the ratio of the aperture diameter to the wall thickness in the helix geometry had to be implemented in practice so the component could be reliably produced in serial production. Numeric calculation with CFD software played a decisive role in configuring the Multitwister, **FIGURE 2**. In order to make effective use of the flow simulations, the flow chambers were derived directly from a 3D CAD model and visualised with finite elements. The quotient of pressure loss and flow speed served as a guideline in this process. The goal was to keep pressure loss as low as possible and increase flow speed at the same time. The so-called radial speed determines the quality of oil separation. It also accelerates the particles towards the wall and enables the actual separation.

Over several test phases, the development team determined designs with various wall thicknesses and borehole diameters, which constituted a major advancement in efficiency. These specs were transferred to prototypes, measured in a laboratory and tested at our testing facilities. The Multitwister MT 2.0 and the adaptive Multitwister MT 3.0 described in the following are the results of a complete development chain with CAD, CFD, interpretation of the results, implementation in components as well as laboratory and testing facilities.

A twister plate with a wall thickness of 0.15 mm poses a special challenge for tool technology. The goal was to produce the complex component in a simple but reliable process. Reinz uses fibreglass-reinforced polyamide 6.6 for injection moulding – a highly resistant, antihydrolysis, standard-tested material for hot oil applications. This material has already proven itself in practice in valve bonnets and oil separator modules with resounding success.

The advantage of the Multitwister design over oil separation systems with non-woven solutions lies in its unlimited resistance to substances found in the blow-by gas. In contrast to non-woven materials, Multitwister shows no signs of sooting or aging processes. Multitwister even performed flawlessly in a test with extremely short drives in the winter time to check its behaviour in cold weather. Another benefit of Multitwister made of polyamide 6.6 is that it is free of residual

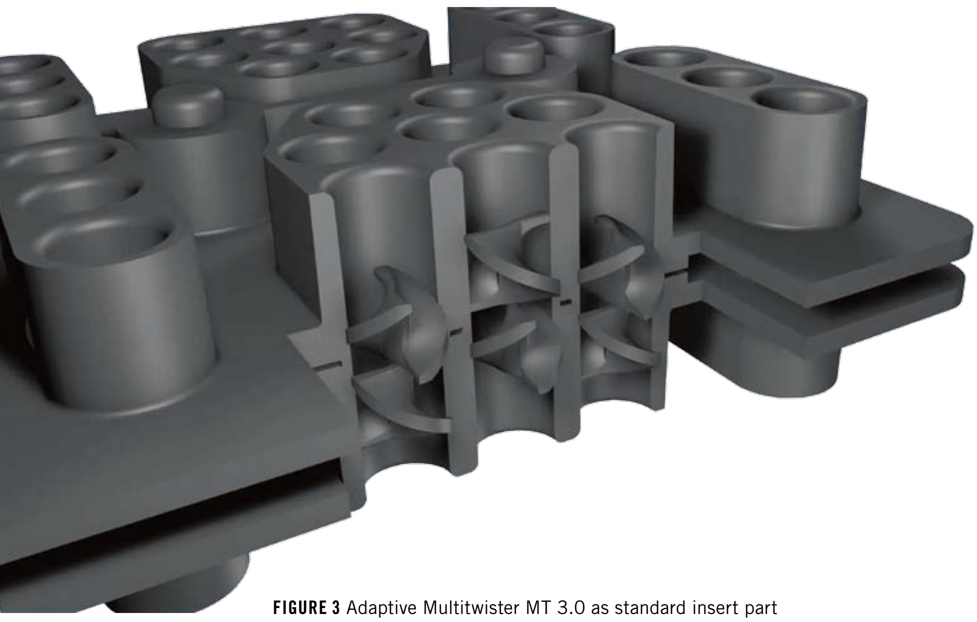

FIGURE 3 Adaptive Multitwister MT 3.0 as standard insert part

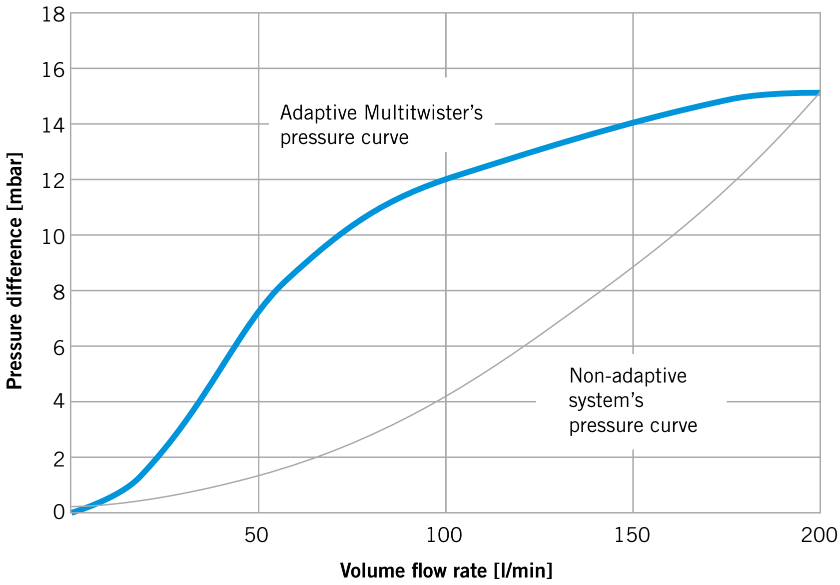

FIGURE 4 Comparison of pressure curves of adaptive and non-adaptive oil separation systems

dirt. While non-woven fibres can separate, Multitwister completely fulfils engine manufacturers' residual dirt requirements. Long-term results have shown that Multitwister is just as efficient after ten years of use as it does when new.

ADAPTIVE SYSTEM

The Reinz Multitwister MT 3.0, **FIGURE 3**, expands the spectrum of options by adding an adaptive version. A downstream, pre-tensioned valve plate opens and closes a defined number of Multitwister channels, thus optimising the pressure curve. The opening and closing action is controlled by the pressure of the volume flow. Fewer channels are open in areas where the volume flow is low. The higher the volume flow rate is, the more channels are released. Adjusting the volume flow rate makes the Multitwister more effective, especially at low volume flow rates – which clearly improves total oil separation over the entire characteristic map.

The developers had a special aspect to take into account when developing the adaptive technology based on the Multitwister MT 2.0: The CFD calculations required special simulation models due to the combination of flow and mechanics. These models first had to simulate the oncoming flow at the component, the resulting pressure loss, then the force on the switching device, and finally the renewed pressure drop when the switching device is opened. In addition, the pressure will vary depending on how far the gap between the switching device and component is set. **FIGURE 4** shows a comparison of pressure curves of adaptive and non-adaptive oil separation systems.

The oil separation is generally configured for the maximum or nominal volume flow rate specified by the OEM, and thus configured at a point. The static geometry did not optimise the oil separation, although the pressure conditions would permit this. The adaptive Multitwister MT 3.0 provides entirely new results in this respect. The Multitwister MT 3.0 is upgraded to a three-stage oil separation system in one variant: Only six of a total 22 channels are opened, and they separate oil quickly and efficiently when quantities of blow-by gas are low. If the volume flow rate reaches a defined level, eight more channels will be opened. The remaining eight channels are only opened once the maximum volume flow rate has been reached. The number of channels as well as the switching points are individually configurable.

SUMMARY AND OUTLOOK

Cost and weight reasons make passive oil separation systems remain the most efficient solution for car engines on the medium term. So the goal is to make these systems more efficient. The adaptive Multitwister MT 3.0 is an important step in this direction. Reinz is currently working on a new development which combines oil separation and pressure regulation in a single component. This system creates the conditions for using the maximum vacuum for oil separation at every load level. An integrated system like this is already being used in a preliminary development engine to regulate the crankcase pressure over the entire characteristic map, yielding results with considerably less oil discharge.

Measurements of Instantaneous Volume Flow Rates During Fuel Injections

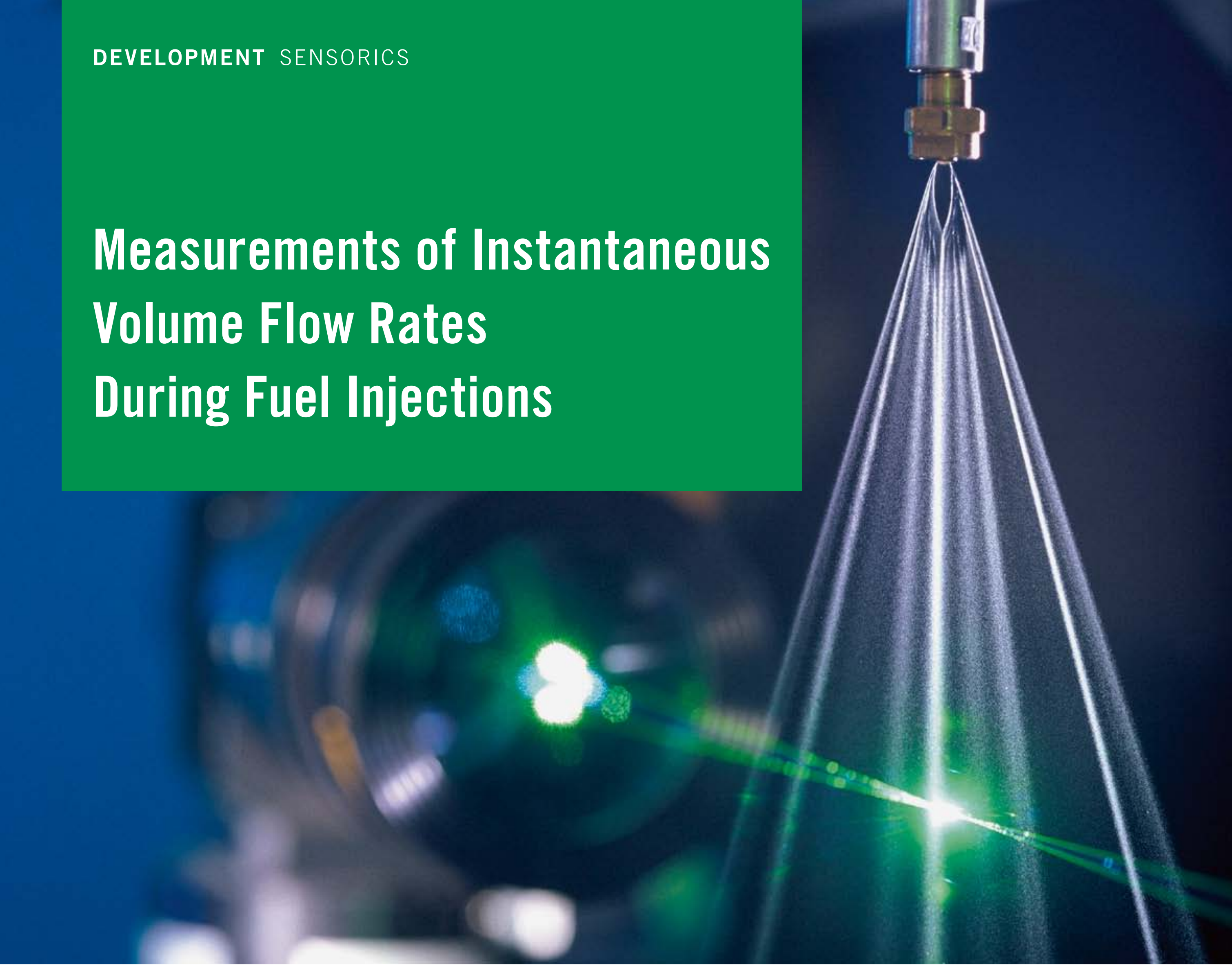

When fuel is injected into gasoline engines, pressure pulsations occur in the entire fuel injection system, such as common rail supply pipes or injectors. These pulsations prevent detailed information about the fuel injection from being deduced from the pressure signals detected in the system. But when dampers specially designed for these pressure pulsations are employed, pressure difference information, from signals at the front and at the end of the pulsation damper, can easily be utilised for instantaneous volume flow rate measurements. Furthermore, the inserted pressure pulsation dampers also allow the pressure reduction in the common rail, caused by the fuel injections, to be employed to measure the instantaneous fuel injection volume flow rates in running gasoline engines. In the following, FMP Technology reports the development and results of verification measurements.

AIMS OF THE WORK

To fulfill the stricter requirements of emission legislations and fuel economy, many new technologies have recently been developed to improve direct fuel injection systems. An important trend in current R&D work is precise control of the amount of fuel injected into the cylinders, as demanded by the engine load-dependent combustion processes. In modern DI systems, this is usually achieved by coordination of injection pressure and valve opening time. In this context, many new developments have emerged in the last few years, such as new magnetic/piezoelectric actuators with optimised opening and closing properties, optimisation of needle structure and improvements of injection orifice geometries. In spite of this, the control of fuel injection is still far from being perfect. Due to the rapid opening and closing of the injector

AUTHORS

Prof. Dr. Dr. h. c. Franz Durst
is CEO and Shareholder of
the FMP Technology GmbH
in Erlangen (Germany).

Yu Han, M. Sc.
is Project Engineer at
the FMP Technology GmbH
in Erlangen (Germany).

Hussain Abdul Hussain Ratlamwala, B. Sc.
is Master Student at
the FMP Technology GmbH
in Erlangen (Germany).

valves, pressure pulsations are produced and penetrate the entire injector system. Usually, such pressure pulsations propagate at the speed of sound and travel from one injector to another, passing the connecting pipes and also the common rail. The maximum amplitude of these pressure pulsations can reach up to ±30 % of the mean injection pressure. Since the flow rate through the injector nozzles is proportional to the pressure difference, pressure pulsations will cause different fuel flow rates through the individual injections into the cylinder. Hence, even though the opening time of the injector valves can be precisely controlled, the pressure pulsations distort the desired well-controlled fuel/air ratio adjustments for the combustion process. Pressure pulsation dampers are needed for better control of the fuel injection into the cylinders of gasoline engines.

Numerous pressure pulsation dampers have been described in the literature and also in numerous patents (e.g. [1, 2, 3, 4, 5, 6, 7, 8, 9, 10]). Most of these dampers work on the principle of detuning of a resonator section in an injector, producing a basic frequency of:

Eq. 1	$f_B = \frac{c}{4\,L_{CN}}$

where c is the velocity of sound for gasoline and L_{CN} is the length of the considered injector from the common rail to the nozzle exit. Placing an orifice at the common rail exit detunes the resonator and, for a frequency of $c/2L_{CN}$, damping of the basic frequency in Eq. 1 occurs. Pressure pulsation dampers of this type are available for gasoline engines.

Other damping mechanisms are nowadays available for injector systems in gasoline engines, and the reader is referred to the literature for the different pressure pulsation dampers employed in internal combustion engines. For the present work, the damping employed in [11] is of particular interest since it employs the same pressure damping mechanism as used here, which utilises the viscous damping of the pressure pulsations:

Eq. 2	$E_{diss} = (\tilde{\dot{V}} + \dot{V}_{pul})\ \Delta P$

and the fact that $\dot{V}_{pul}$-pulses move with sonic velocity, i.e. about ten times faster than the fluid pulse. Being reflected at the end of the ring type damper, the $\dot{V}_{pul}$-pulses penetrate the energy dissipation section several times in the time the fluid flow pulse penetrates it only once. Hence the dissipations, per sound wave penetration, are as follows:

Eq. 3	$(E_{diss})_{\tilde{V}} = \frac{8\mu\,\tilde{\dot{V}}\,L}{\pi r4}$

and thus

Eq. 4	$(E_{diss})_{\dot{V}pul} = \frac{N\,8\mu\,\dot{V}_{pul}L}{\pi r4}\ (N \approx 10)$

All this is described in the patent applications DE 10 2012 212 745 A1 and PCT/EP2013/065318. A sketch of the ring slot damper applied is shown in **FIGURE 1**.

THEORY OF THE INSTANTANEOUS FLOW RATE MEASUREMENTS

FIGURE 2 shows an example of pressure distributions measured in the injection system without a damper (left) compared with that with a damper (right). It is clear that, with a pressure pulsation damper, the temporal pressure distributions at different positions are almost linearly parallel to each other. The start

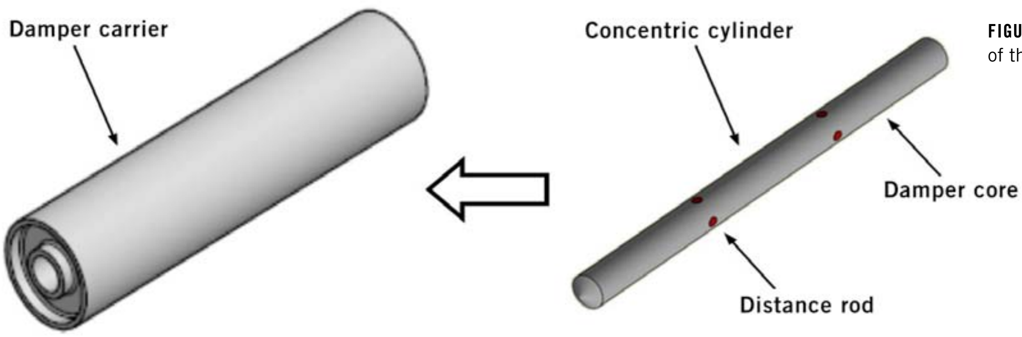

FIGURE 1 Sketch of the components of the ring slot damper

of injection (SOI) and end of injection (EOI) can be easily determined from the intersections of the pressure curves. The pressure drops before and after the damper can be modelled as linear functions of injection time. The well-defined pressure curve and valve opening time provide all necessary information for calculation of the instantaneous injection volume rate.

Based on the temporal pressure distributions, the instantaneous flow rate during injection can be obtained using the following equation:

Eq. 5	$\dot{V}(t) = \frac{\pi D_{in} \delta^3}{12 \mu L} \Delta P_{CI}(t)$

where ΔP_{CI} *(t)* is the pressure difference before and after the damper, **FIGURE 3**, D_{in} is the inner diameter of the ring slot, δ is the slot width with $\delta \ll D_{in}$, μ is the dynamic viscosity of the fuel and L is the effective length of the ring slot. The theoretical modelling is based on the volume flow rate through a small rectangular channel. Detailed information can be found in [11, 12, 13]. The instantaneous flow rate can be used for investigations of the needle action, the pressure change and the actual injection time etc. during injection.

In theory, the total amount of fuel injected is dependent only on the pressure loss in the common rail if one neglects the influence of the fuel pump. When introducing a ring slot damper in the measurements, the pressure distribution in the common rail is almost a straight line during injection. Hence, the total amount of injected fuel can be easily modelled as:

Eq. 6	$M_{inj} = \rho_f \int_0^{t_{end}} c_s \Delta P_{CR}(t)\, dt$

where M_{inj} is the total mass injected, ρ_f is the fuel density, c_s is a system-dependent constant and ΔP_{CR} *(t)* is the time-varying pressure drop in the common rail. Thus, by integrating the pressure loss in the common rail during the valve opening time, the total mass supplied by one injection can be obtained through Eq. 6. Hence, two ways can be adopted to measure the instantaneous flow rates from the pressure signal detected from the pressure difference over the employed pulsation dampers or deduced from the pressure in the common rail.

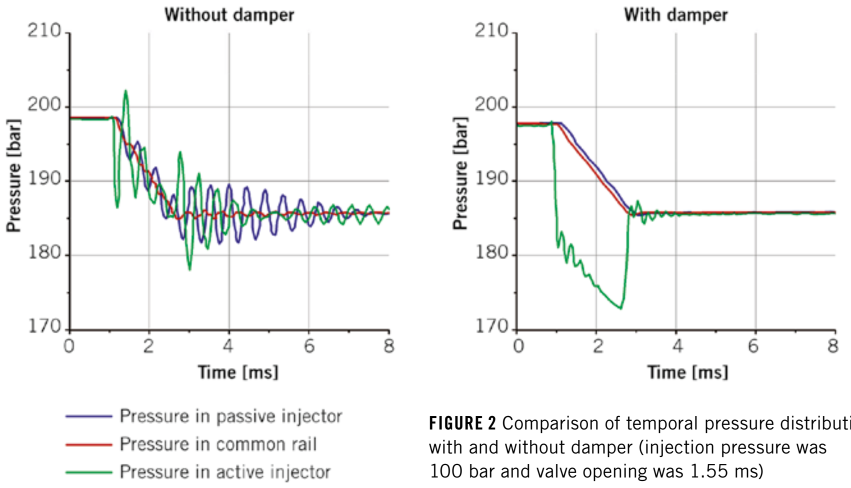

FIGURE 2 Comparison of temporal pressure distribution with and without damper (injection pressure was 100 bar and valve opening was 1.55 ms)

TEST RIG AND MEASURING PROCEDURE

As shown in **FIGURE 4**, the experimental setup consists of a fluid supplying system, a high-pressure pump, a common rail injection system and an electric control unit. A rail pressure up to 220 bar could be produced by adjusting the rotation speed of the pump. A valve was placed between the common rail and the fuel pump to exclude the influence of the pump in the system during the flow rate measurements. A pressure sensor was mounted on the common rail to record the temporal pressure distribution during the injection. Commercial injectors of the type Bosch HDEV 5.2, with an electromagnetic valve, were applied to make the injections. The injection-controlling signal was generated with a signal generator driven by the programme Labview that was employed to control the start and the duration of the injection. A ring slot pulsation damper was applied in the damper carrier between the common rail and the injector to determine the injected mass flow rate.

A detailed description of the carriers of the pressure pulsation dampers is shown in **FIGURE 5**. Two pressure sensors were mounted on the damper housings (the blue parts in **FIGURE 5**), in order to measure the pressure at the front and end of the dampers. The instantaneous pressure was measured as a voltage signal by the sensors and then transformed into digital signals by the data acquisition system. These digital signals were exported to the programme Matlab where they were processed to calculate the actual injector valve opening time (this is because of the inability of the magnetic valves to respond rapidly to the pulse signal) and the pressure drop in common rail. Through this pressure drop and valve opening time

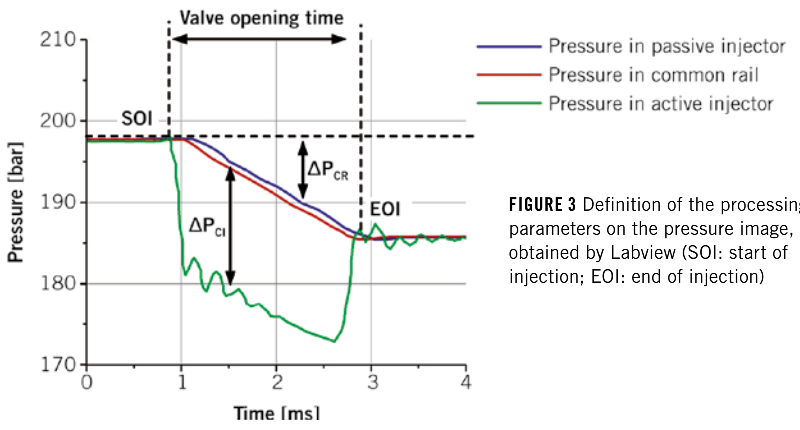

FIGURE 3 Definition of the processing parameters on the pressure image, obtained by Labview (SOI: start of injection; EOI: end of injection)

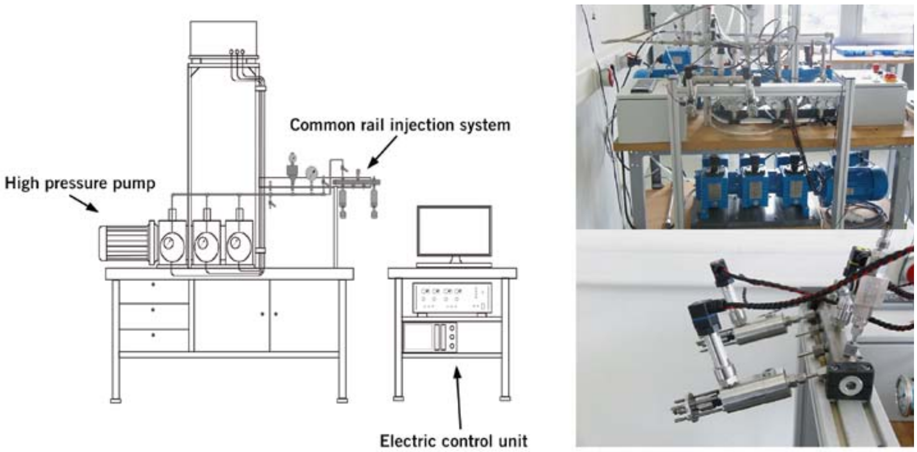

FIGURE 4 Sketch and photograph of the test rig

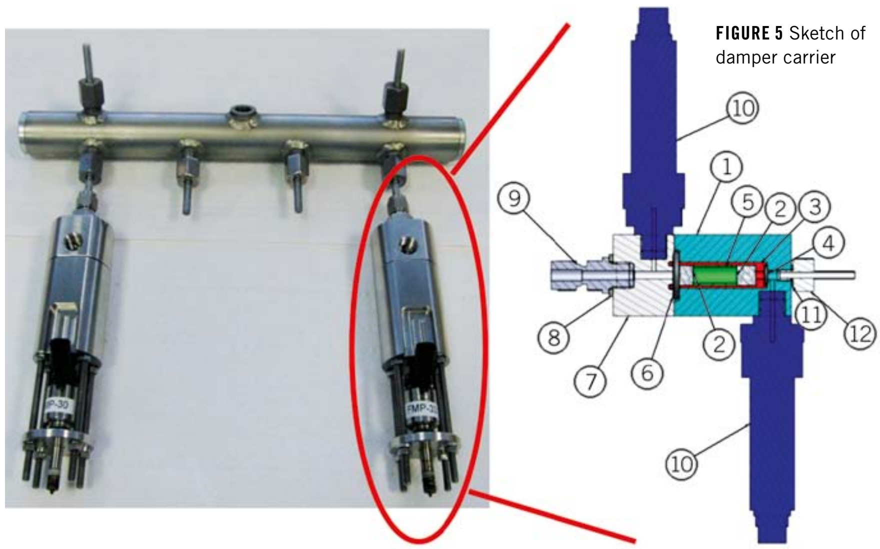

FIGURE 5 Sketch of damper carrier

1) Receptacle for damping unit
2) Damping elements
3) Carrier sleeve
4) O-ring 6x2 Viton
5) Distance sleeve
6) O-ring 18x3 Viton
7) Closure of damping unit
8) Sealing ring G14
9) Swagelok connection 1/4 inch
10) Pressure transmitter
11) Sealing disc CU6,0 10,0
12) Pipe nipple

FIGURE 6 Temporal pressure distributions during the injections with pulse widths of 1.5 ms (left) and 2.0 ms (right)

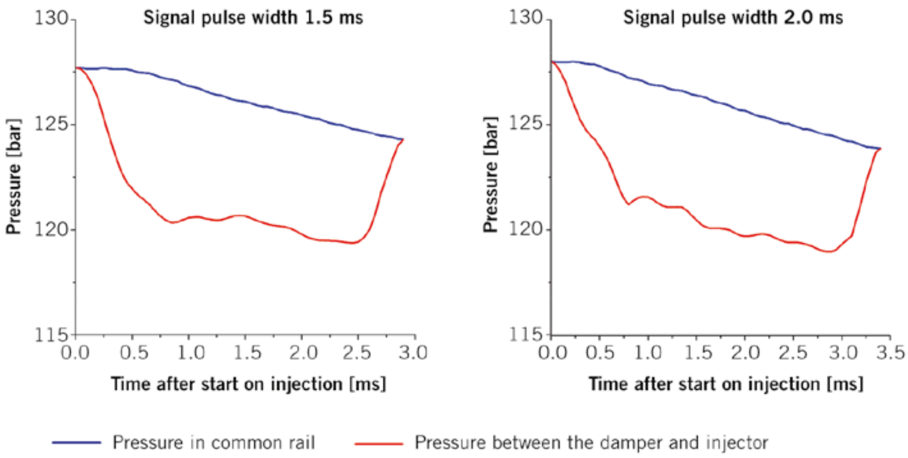

the injected volumetric flow rate can be calculated.

Note that the pressure oscillations induced by the fuel pump were excluded by closing the valve between the pump and the common rail during the injection. The pressure pulsations generated by the fuel pump contribute are very small compared with the pressure pulsation caused by the opening and closing of the injector valve. Therefore, in order to provide a detailed understanding of the valve-induced pressure pulsations, the individual injections were carried out at constant common rail pressure.

RESULTS AND DISCUSSION

The injection time and pressure distributions during the valve opening were extracted on the basis of the two intersection points of the pressure curves in the common rail and the injector, **FIGURE 3**. Two examples obtained with rail pressures of about 127 bar and signal pulse widths of 1.5 and 2.0 ms are shown in **FIGURE 6**. All other measurements with different injection parameters provided very similar results so only the example in **FIGURE 6** is shown here.

The instantaneous flow rate of the injection can be determined using Eq. 5. **FIGURE 7** shows the measured instantaneous pressure drop (left) and the flow rates obtained (right) during the injections with the pulse width of 1.5 ms.

The results show clearly that the instantaneous flow rate during one injection consists of three phases, namely the building-up phase for the injection flow rate, the actual injection phase and the closing-down phase. From these diagrams, the times of needle lift-up, main injection and needle shut-down can be quantitatively defined and the outlet velocity at the orifice exit can be easily obtained by the ratio of the volume flow rate to the cross-sectional area of the orifice. For example, with an injection time of 1.5 ms, the valve reaction time was about 0.6 ms and the actual valve opening time was about 2.8 ms. The volume flow rate of the main spray was approximately 5 cm³/s, but reaction with the injection time. It can also be clearly seen that the distribution of the pressure drop is very close to that of the volume flow rate. Using these signals, the mean flow rate of one injection can be easily determined, and showed very good agreement with the measurement.

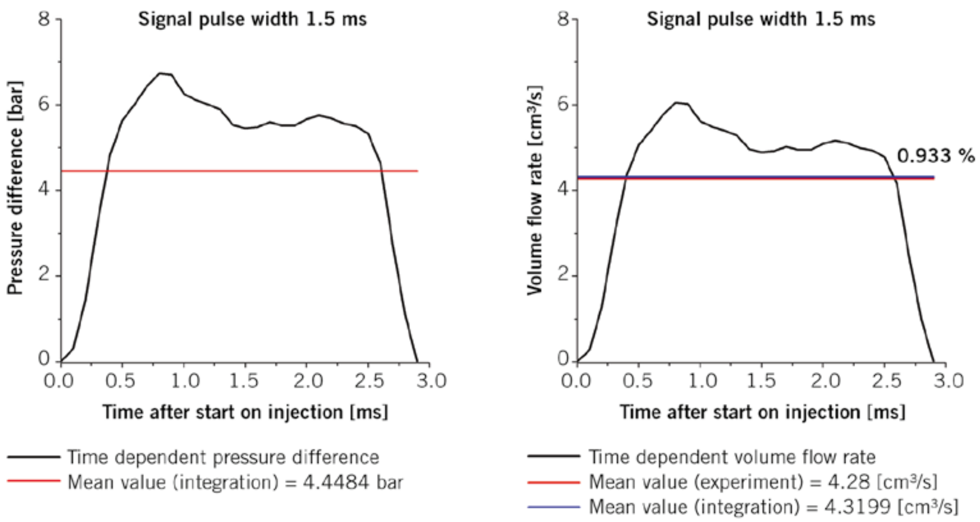

FIGURE 7 Plot of the measured instantaneous pressure drop (left) and the obtained flow rates (right) during the injections with a pulse width of 1.5 ms

In order to verify this method, further measurements were carried out under different conditions. The results of the method are compared with the experimental measurements in **FIGURE 8**, which clearly indicates that the developed method shows very good agreement with the total mass weight method for different injection times. The maximum standard deviation between the two methods is approximately 3 %.

Furthermore, because the valve between the fuel pump and the common rail was closed during this set of experiments, the pressure loss of the common rail during the injection is due solely to its volume loss. Hence, the total injected mass can also be determined by the temporal pressure distribution in the common rail. The points in **FIGURE 9** indicate the relation between the measured injected mass and the maximal pressure drop $\Delta P_{\mathrm{CR,max}}$ in the common rail. A linear distribution is obtained, between the total mass injected and the maximal pressure drop in the common rail over a wide range of signal time. This indicates that the amount of fuel injected can be easily determined from the pressure signal in the common rail. The measurement results give a simple correlation for the prediction of the total mass injected:

Eq. 7 $$M_{inj} = \frac{CD\delta^3\rho_f}{\mu L}\,\Delta P_{CR,max}$$

where C is an empirical constant depending on the system set-up.

CONCLUSIONS AND FINAL REMARKS

At present, fuel injection flow rates into gasoline engines can only be measured under laboratory conditions, using the HAD Moehwald or IAV system ([14, 15]), both employing the same measurement method. They employ fluid in jection into filled chambers and, if the compressibility of the injected fuel is known, the instantaneous pressure changes in the chamber can be used to measure the instantaneous flow rate of the employed injector.

There have been other attempts to measure instantaneous flow rates in strongly time-dependent flows. Such attempts are described in [16,

FIGURE 8 Comparison of the measured mass per injection obtained by weighing with that obtained by pressure damping

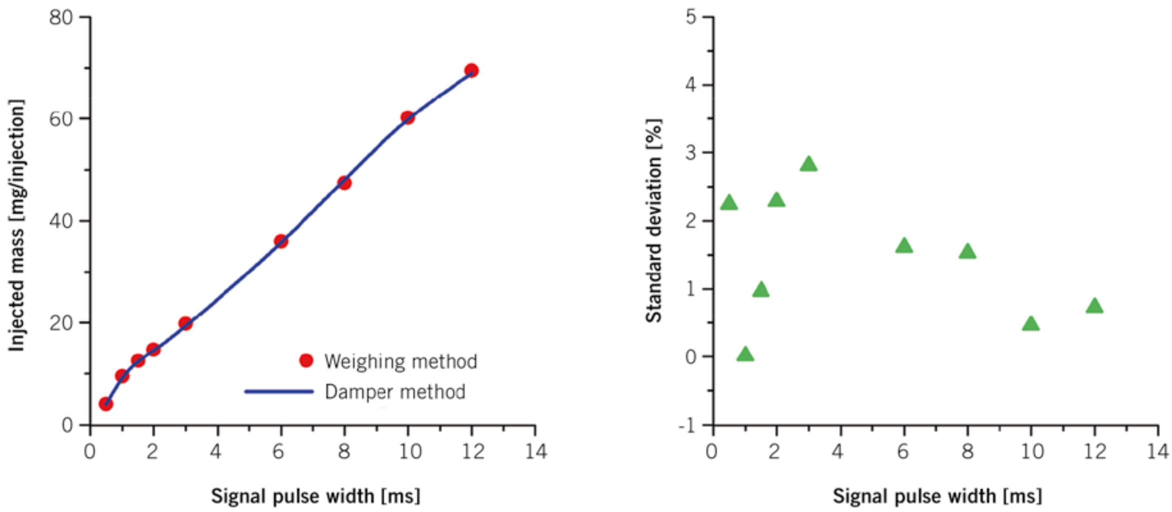

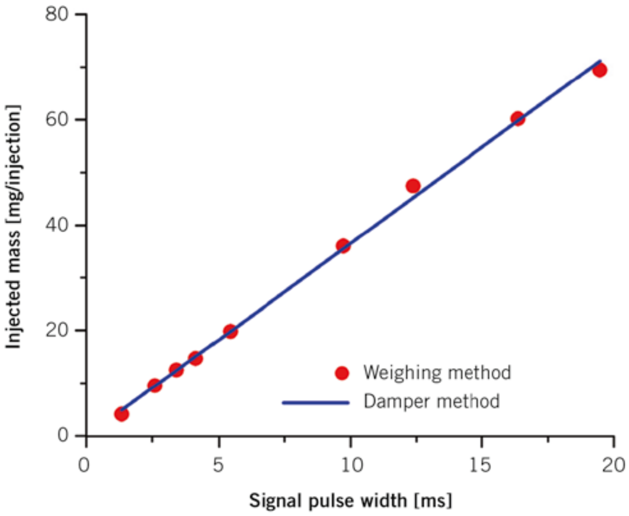

FIGURE 9 Relation between the total injected mass and the maximum pressure drop in the common rail

17, 18] and are based on centerline velocity measurements in pipes, yielding the specific information needed to deduce the entire velocity profile at a certain time. With this profile, the instantaneous flow rate through the pipe could be obtained by integration over the computed velocity profile.

All the above-mentioned methods have the disadvantage that they are very expensive and require considerable space for the instrumentation. Because of this, there is no practically applicable method available to measure injection flow rates in gasoline engines that are running in automobiles. To remedy this situation, the authors carried out the development work described in this paper, which resulted in a measuring technique that utilises inexpensive components that could be incorporated in the injection systems of automobiles driven by gasoline engines in order to permit instantaneous volume flow rates to be measured utilising the pressure difference signals over a pulsation damper and/or the pressure reduction in the corresponding common rail.

REFERENCES

[1] Niles, A.B.: Filtering and dampening apparatus. US patent 4 356 091, 1982
[2] Pfingst, J.; Jacob, M.: Hydraulischer Pulsationsdämpfer. Patent DE 10 2006 016 937 A1, 2007
[3] Kino, H.; Oshima, T.: Fuel pressure pulsation damper. Japan patent 08261100 A, 1995
[4] Schreurer, H.-P.: Kraftstoffeinspritzungssystem für eine Brennkraftmaschine mit druckschwingungsgedämpfter Kraftstoffrücklaufleitung. Patent DE 10 2006 054 178 A1, 2008
[5] Fath, A.: Accumulator injection system for damping pressure waves, especially in a common rail injection system. Patent PCT/DE2003/002868 WO2004/036029, 2004
[6] Hiller, M.: Verfahren zum Verringern von Druckpulsationen. Patent DE 103 51 089 A1, 2005
[7] Li, J.Z.; Treusch, C.; Honel, B.; Neyrat, S.: Simulation of pressure pulsations in a gasoline injection system and development of an effective damping technology. SAE Technical Paper, 2005
[8] Ghidaoui, M.S.; Zhao, M.; McInnis, D.A.; Axworthy, D.H.: A review of water hammer theory and practice. In: Applied Mechanics Reviews 58 (2005), No. 1, pp. 49-76
[9] Handtmann, A.; Haspel, D.; Schilling, L.: Druckpulsationsdämpfer für Injektoren. In: MTZ 73 (2012), No. 11, pp. 870-876
[10] Durst, F.: Fluid mechanics: an introduction to the theory of fluid flows. Springer, 2008
[11] Durst, F.: Kraftstoffeinspritzsystem. Patent DE 10 2012 202 745 A1, 2014
[12] Durst, F.; Haspel, D.; Unsal, B.; Resch, R.: Fast-operating injection valves with virtually pressure wave-free supply lines. In: MTZ worldwide 68 (2007), No. 10, pp. 21-23
[13] Durst, F.; Ray, S.; Unsal, B.; Bayoumi, O.A.: The development lengths of laminar pipe and channel flows. In: Journal of Fluids Engineering 127 (2005), No. 6, pp. 1154-1160
[14] Moehwald, Bosch Group: Einspritzmengen- und -ratenverlaufmessgerät
[15] Kwast, T.; Marohn, R.; Rölle, T.: Verfahren und Vorrichtung zur Einspritzraten- und/oder Einspritzmassenbestimmung. Patent DE 10 2005 040 768 A1, 2007
[16] Bosch, W.: The fuel rate indicator: a new measuring instrument for display of the characteristics of individual injection. SAE Technical Paper, 1966
[17] Durst, F.; Melling, A.; Trimis, D.; Volkholz, P.: Development of a flowmeter for instantaneous flow rate measurements of anaesthetic liquids. In: Flow Measurement and Instrumentation, 7 (1996), No. 3, pp. 215-221
[18] Unsal, B.; Trimis, D. ; Durst, F.: Instantaneous mass flowrate measurements through fuel injection nozzles. In: International Journal of Engine Research 7 (2006), No. 5, pp. 371-380

IMPRINT

MTZ

WORLDWIDE

www.MTZonline.com

Founded 1939 by Prof. Dr.-Ing. E. h. Heinrich Buschmann and
Dr.-Ing. E. h. Prosper L'Orange

Organ of the Fachverband Motoren und Systeme im VDMA, Verband Deutscher Maschinen- und Anlagenbau e.V., Frankfurt/Main, for the areas combustion engines and gas turbines
Organ of the Forschungsvereinigung Verbrennungskraftmaschinen e.V. (FVV)
Organ of the Wissenschaftliche Gesellschaft für Kraftfahrzeug- und Motorentechnik e.V. (WKM)
Organ of the Österreichischer Verein für Kraftfahrzeugtechnik (ÖVK)
Cooperation with the STG, Schiffbautechnische Gesellschaft e.V., Hamburg, in the area of ship drives by combustion engine

06|2015 _ Volume 76

Springer Vieweg | Springer Fachmedien Wiesbaden GmbH
P. O. Box 15 46 · 65173 Wiesbaden · Germany | Abraham-Lincoln-Straße 46 · 65189 Wiesbaden · Germany

Amtsgericht Wiesbaden, HRB 9754, USt-IdNr. DE811148419
Managing Directors Armin Gross, Joachim Krieger, Dr. Niels Peter Thomas

Managing Director Marketing & Sales Armin Gross | **Director Magazines** Stefanie Burgmaier | **Director Production** Dr. Olga Chiarcos

EDITORS IN CHARGE
Dr. Johannes Liebl, Wolfgang Siebenpfeiffer

EDITOR IN CHIEF
Dr. Alexander Heintzel
phone +49 611 7878-342 · fax +49 611 7878-462
alexander.heintzel@springer.com

VICE EDITOR IN CHIEF
Dipl.-Ing. (FH) Richard Backhaus
phone +49 611 5045-982 · fax +49 611 5045-983
richard.backhaus@rb-communications.de

MANAGING EDITOR
Kirsten Beckmann M. A.
phone +49 611 7878-343 · fax +49 611 7878-462
kirsten.beckmann@springer.com

EDITORIAL STAFF
Dipl.-Ing. (FH) Andreas Fuchs
phone +49 6146 837-056 · fax +49 6146 837-058
fuchs@fachjournalist-fuchs.de
Angelina Hofacker
phone +49 611 7878-121 · fax +49 611 7878-462
angelina.hofacker@springer.com
Dipl.-Ing. Michael Reichenbach
phone +49 611 7878-341 · fax +49 611 7878-462
michael.reichenbach@springer.com
Stefan Schlott
phone +49 8726 9675-972
redaktion_schlott@gmx.net
Markus Schöttle
phone +49 611 7878-257 · fax +49 611 7878-462
markus.schoettle@springer.com
Martina Schraad
phone +49 611 7878-276 · fax +49 611 7878-462
martina.schraad@springer.com

PERMANENT CONTRIBUTORS
Andreas Burkert, Prof. Dr.-Ing. Stefan Breuer, Hartmut Hammer, Detlef Krehl, Dipl.-Ing. Ulrich Knorra, Roland Schedel

ENGLISH LANGUAGE CONSULTANT
Paul Willin

ONLINE | ELECTRONIC MEDIA
Portal Manager Automotive
Christiane Brünglinghaus
phone +49 611 7878-136 · fax +49 611 7878-462
christiane.bruenglinghaus@springer.com
Editorial Staff
Katrin Pudenz M. A.
phone +49 6172 301-288 · fax +49 6172 301-299
redaktion@kpz-publishing.com

SPECIAL PROJECTS
Managing Editorial Journalist
Markus Bereszewski
phone +49 611 7878-122 · fax +49 611 7878-462
markus.bereszewski@springer.com
Editorial Staff | Coordination
Dipl.-Reg.-Wiss. Caroline Behle
phone +49 611 7878-393 · fax +49 611 7878-462
caroline.behle@springer.com
Christiane Imhof M. A.
phone +49 611 7878-154 · fax +49 611 7878-462
christiane.imhof@springer.com

PROJECT MANAGEMENT | ASSISTANCE
Yeliz Konar
phone +49 611 7878-180 · fax +49 611 7878-462
yeliz.konar@springer.com

ADDRESS
Abraham-Lincoln-Straße 46 · 65189 Wiesbaden
P. O. Box 1546 · 65173 Wiesbaden, Germany
redaktion@ATZonline.de

ADVERTISING

SALES MANAGEMENT
Volker Hesedenz
phone +49 611 7878-269 · fax +49 611 7878-78269
volker.hesedenz@best-ad-media.de

MEDIA SALES
Frank Nagel
phone +49 611 7878-395 · fax +49 611 7878-78395
frank.nagel@best-ad-media.de

KEY ACCOUNT MANAGEMENT
Rouwen Bastian
phone +49 611 7878-399 · fax +49 611 7878-78399
rouwen.bastian@best-ad-media.de

DISPLAY AD MANAGER
Nicole Brzank
tel +49 611 7878-616 · fax +49 611 7878-78164
nicole.brzank@best-ad-media.de

AD PRICES
Advertising ratecard from October 2014.

MARKETING | OFFPRINTS

HEAD OF MARKETING MAGAZINES + EVENTS
Jens Fischer

PRODUCT MANAGEMENT AUTOMOTIVE MEDIA
Jens Fischer
phone +49 611 7878-340 · fax +49 611 7878-407
jens.fischer@springer.com

OFFPRINTS
Martin Leopold
phone +49 2642 907-596 · fax +49 2642 907-597
leopold@medien-kontor.de

PRODUCTION | LAYOUT
Heiko Köllner
phone +49 611 7878-177 · fax +49 611 7878-78177
heiko.koellner@springer.com

SUBSCRIPTIONS
Springer Customer Service Center GmbH
Haberstraße 7 · 69126 Heidelberg · Germany
phone +49 6221 3454-303 · fax +49 6221 3454-229
Monday to Friday, 8 a.m. to 6 p.m.
springervieweg-service@springer.com
www.my-specialized-knowledge.com/automotive

SUBSCRIPTION CONDITIONS
The eMagazine appears 11 times a year at an annual subscription rate 199 € for private persons and 333 € for companies. Special rate for students on proof of status in the form of current registration certificate 98 €. Special rate for VDI/ÖVK members on proof of status in the form of current member certificate 172 €. Special rate for studying VDI members on proof of status in the form of current registration and member certificate 71 €. Annual subscription rate for combination MTZworldwide (eMagazine) and MTZ (print) 399 €. All prices include VAT at 7%. Every subscription comes with access to the online archive. However, access is only available for the individual subscription holder. To obtain access for your entire company/library/organisation, please contact sales@springerprofessionals.de or phone +49 611 7878-686. The subscription can be cancelled in written form at any time with effect from the next available issue.

YOUR HOTLINE TO MTZ

Editorial Staff
☎ +49 611 5045982
Customer Service
☎ +49 6221 3454-303
Advertising
☎ +49 611 7878-395

HINTS FOR AUTHORS
All manuscripts should be sent directly to the editors. By submitting photographs and drawings the sender releases the publishers from claims by third parties. Only works not yet published in Germany or abroad can generally be accepted for publication. The manuscripts must not be offered for publication to other journals simultaneously. In accepting the manuscript the publisher acquires the right to produce royalty-free offprints. The journal and all articles and figures are protected by copyright. Any utilisation beyond the strict limits of the copyright law without permission of the publisher is illegal. This applies particularly to duplications, translations, microfilming and storage and processing in electronic systems.

PEER REVIEW

Peer Review Process for Research Articles in ATZ, MTZ and ATZelektronik

STEERING COMMITTEE

Prof. Dr.-Ing. Lutz Eckstein	RWTH Aachen University	Institut für Kraftfahrzeuge Aachen
Prof. Dipl.-Des. Wolfgang Kraus	HAW Hamburg	Department Fahrzeugtechnik und Flugzeugbau
Prof. Dr.-Ing. Ferit Küçükay	Technische Universität Braunschweig	Institut für Fahrzeugtechnik
Prof. Dr.-Ing. Stefan Pischinger	RWTH Aachen University	Lehrstuhl für Verbrennungskraftmaschinen
Prof. Dr.-Ing. Hans-Christian Reuss	Universität Stuttgart	Institut für Verbrennungsmotoren und Kraftfahrwesen
Prof. Dr.-Ing. Ulrich Spicher	MOT	
Prof. Dr.-Ing. Hans Zellbeck	Technische Universität Dresden	Lehrstuhl für Verbrennungsmotoren

ADVISORY BOARD

Prof. Dr.-Ing. Klaus Augsburg
Prof. Dr.-Ing. Michael Bargende
Prof. Dipl.-Ing. Dr. techn. Christian Beidl
Prof. Dr. sc. techn. Konstantinos Boulouchos
Prof. Dr. Dr. h.c. Manfred Broy
Prof. Dr.-Ing. Ralph Bruder
Dr. Gerhard Bruner
Prof. Dr. rer. nat. Heiner Bubb
Prof. Dr. rer. nat. habil. Olaf Deutschmann
Prof. Dr.-Ing. Klaus Dietmayer
Dr. techn. Arno Eichberger
Prof. Dr. techn. Helmut Eichlseder
Prof. Dr. Wilfried Eichlseder
Dr.-Ing. Gerald Eifler
Prof. Dr.-Ing. Wolfgang Eifler
Prof. Dr. rer. nat. Frank Gauterin
Prof. Dr. techn. Bernhard Geringer
Prof. Dr.-Ing. Uwe Dieter Grebe
Dr. mont. Christoph Guster
Prof. Dr.-Ing. Holger Hanselka
Prof. Dr.-Ing. Horst Harndorf
Prof. Dr. techn. Wolfgang Hirschberg
Prof. Dr. techn. Peter Hofmann
Prof. Dr. rer. nat. Peter Holstein
Prof. Dr.-Ing. Volker von Holt
Prof. Dr.-Ing. habil. Werner Hufenbach
Prof. Dr.-Ing. Armin Huß
Dr. techn. Heidelinde Jetzinger
Prof. Dr.-Ing. Roland Kasper
Prof. Dr.-Ing. Prof. E. h. mult. Rudolf Kawalla
Prof. Dr.-Ing. Tran Quoc Khanh
Dr. Philip Köhn
Prof. Dr.-Ing. Ulrich Konigorski
Prof. Dr. Oliver Kröcher
Prof. Dr.-Ing. Peter Krug
Dr. Christian Krüger
Prof. Dr. techn. Thomas Lauer
Prof. Dr. rer. nat. Uli Lemmer
Dr. Malte Lewerenz
Prof. Dr.-Ing. Markus Lienkamp
Prof. Dr. rer. nat. habil. Ulrich Maas
Prof. Dr.-Ing. Markus Maurer
Prof. Dr.-Ing. Martin Meywerk
Ao. Univ.-Prof. Dr. Gregor Mori
Prof. Dr.-Ing. Klaus D. Müller-Glaser
Dr. techn. Reinhard Mundl
Prof. Dr. rer. nat. Peter Neugebauer
Prof. Dr. rer. nat. Cornelius Neumann
Prof. Dr.-Ing. Nejila Parspour
Prof. Dr.-Ing. Peter Pelz
Prof. Dr. techn. Ernst Pucher
Dr. Jochen Rauh
Prof. Dr.-Ing. Konrad Reif
Prof. Dr.-Ing. Stephan Rinderknecht
Prof. Dr.-Ing. Jörg Roth-Stielow
Dr.-Ing. Swen Schaub
Prof. Dr. sc. nat. Christoph Schierz
Prof. Dr. rer. nat. Christof Schulz
Prof. Dr. rer. nat. Andy Schürr
Prof. Dr.-Ing. Ulrich Seiffert
Prof. Dr.-Ing. Hermann J. Stadtfeld
Prof. Dr.-Ing. Karsten Stahl
Prof. Dr. techn. Hermann Steffan
Prof. Dr.-Ing. Wolfgang Steiger
Prof. Dr.-Ing. Peter Steinberg
Dr.-Ing. Peter Stommel
Dr.-Ing. Ralph Sundermeier
Prof. Dr.-Ing. Wolfgang Thiemann
Prof. Dr.-Ing. Dr. h.c. Helmut Tschöke
Prof. Dr.-Ing. Georg Wachtmeister
Prof. Dr.-Ing. Jochen Wiedemann
Prof. Dr. rer. nat. Gerhard Wiegleb
Prof. Dr. techn. Andreas Wimmer
Prof. Dr. rer. nat. Hermann Winner
Prof. Dr. med. habil. Hartmut Witte
Dr.-Ing. Michael Wittler

Scientific articles of universities in ATZ Automobiltechnische Zeitschrift, MTZ Motortechnische Zeitschrift and ATZelektronik are subject to a proofing method, the so-called peer review process. Articles accepted by the editors are reviewed by experts from research and industry before publication. For the reader, the peer review process further enhances the quality of the magazines‘ content on a national and international level. For authors in the institutes, it provides a scientifically recognised publication platform.

In the Peer Review Process, once the editors has received an article, it is reviewed by two experts from the Advisory Board. If these experts do not reach a unanimous agreement, a member of the Steering Committee acts as an arbitrator. Following the experts’ recommended corrections and subsequent editing by the author, the article is accepted.

In 2008, the peer review process utilised by ATZ and MTZ was presented by the WKM (Wissenschaftliche Gesellschaft für Kraftfahrzeug- und Motorentechnik e. V./German Professional Association for Automotive and Motor Engineering) to the DFG (Deutsche Forschungsgemeinschaft/German Research Foundation) for official recognition. ATZelektronik participates in the Peer Review since 2011.

Mistuning and Damping of Turbine Impellers

AUTHORS

Dipl.-Ing. Thomas Maywald is Research Assistant at the Institute for Transport Engineering, Chair of Structural Mechanics and Vehicle Vibrational Technology of the Brandenburg University of Technology (Germany).

PD Dr.-Ing. habil. Bernd Beirow is Senior Research Assistant at the Institute for Transport Engineering, Chair of Structural Mechanics and Vehicle Vibrational Technology of the Brandenburg University of Technology (Germany).

Prof. Dr.-Ing. Arnold Kühhorn is Head of the Chair of Structural Mechanics and Vehicle Vibrational Technology at the Institute for Transport Engineering of the Brandenburg University of Technology (Germany).

Modern combustion engines have to comply with a permanently growing requirement profile with respect to economy, power and environmental acceptability. In this regard, the turbocharging technology became more significant. Primarily, casted radial impellers are deployed in small and medium sized turbochargers with wheel diameters ranging between 30 and 250 mm. The impact of operational parameters on structural dynamic characteristics of such radial impellers has been analysed at the Institute of Transport Engineering of the Brandenburg University of Technology at Cottbus within the framework of an FVV research project.

THE SEAL OF APPROVAL FOR SCIENTIFIC ARTICLES IN MTZ.
MTZ
PEER REVIEW
RECEIVED 2014-09-29
REVIEWED 2014-11-16
ACCEPTED 2015-03-02
REVIEWED BY EXPERTS FROM RESEARCH AND INDUSTRY.

1 MOTIVATION

The operation of exhaust turbochargers yields an increase of engine efficiency and a decrease of exhaust emissions. Turbochargers applied in Diesel engines of small and medium size are mainly crafted by casting. These commonly integrally manufactured impellers are denoted as blade integrated disks (Blisks). The mechanical damping of such wheels is reduced to the magnitude of material damping due to the lack of join patches as being present in separated blade-disk constructions [1]. However, despite of intensive efforts in manufacturing it is not possible to craft geometrically and materially identical blades [2]. Both deviations of blade geometry from the desired contour and material inhomogeneities occur in consequence of the casting process. These deviations from the ideal design intention known as mistuning are connected with a number of particularities with respect to structural dynamic characteristics, which have to be considered in terms of a reliable design. Among others mistuning can affect localised operational deflection shapes yielding a concentration of vibration energy on one or a few of blades, respectively [2]. Blades being concerned can be faced to higher magnitudes of vibration compared to the tuned design intention and the regular character of mode shapes gets lost. Hence blades are confronted with the danger of crack initiations causing blade failure in the worst case. Aiming for a save operation of the turbocharger, more advanced endurance predictions of casted turbine impellers are required considering mistuning. For this reason numerical models of the impeller being close to reality are needed. These models are derived updating originally ideal design models based on measured data of vibration tests. Analyses presented below refer to the research project 'Mistuning and Damping, Part II [3, 4] which has been initiated by the Research Association Combustion Engines (FVV). Different ambient pressure and temperature conditions as well as centrifugal forces affecting the forced response are explained by means of comprehensive experimental work in combination with numerical analyses.

2 DAMPING CONTRIBUTION OF AMBIENT FLUID

A reliable prediction of vibration levels expected while operation of a turbine impeller requires a substantial knowledge about damping characteristics. Due to the lack of join patches as well the extremely low mechanical damping of casted turbine impellers the main damping contribution results from the impact of the ambient air. Experimental investigations carried out considering at an impeller at rest within a pressure chamber, **FIGURE 1**, will explain the correlation between ambient pressure and damping contribution of the ambient fluid. An impeller MTU ZR 265 type bas been provided for this purpose.

Starting at 1013 mbar the ambient pressure is gradually decreased down to technical vacuum at 1 mbar within the first part of the test series. Subsequently, a second test series covers operationally relevant pressures ranging between 1000 and 6000 mbar. Electrodynamic shaker excitation of the impeller is employed inside the test facility, whereas the vibration response is measured at the blade tip close to the trailing edge (turbine outlet, **FIGURE 1**) via a Laser-Doppler scanning device. Aiming at a quantification of the ambient pressure's effect on damping according to the research objectives formulated before, exclusively the internal pressure is varied. All other test parameters (e.g. ambient temperature) are kept constant.

By means of multi degree of freedom (MDOF) fitting evaluations of all resonances ranging between frequencies of 4800 and 15,000 Hz yield the dependencies of modal damping ratios on ambient pressure given in **FIGURE 2**. The normalisation of all damping ratios refers to a mean damping ratio at normal conditions (p = 1013 mbar, ϑ = 20 °C). In detail a clear drop of the damping ratios with decreasing ambient pressure becomes apparent. This proves that the damping being measured at the impeller at rest mostly results from the ambient fluid. In particular those modes of vibration are affected which are characterised by large-scale displacements of the blade and with that by a large transfer or energy into the fluid. Comparable results could be found within investigations at similar impellers [5, 6]. From the physical point

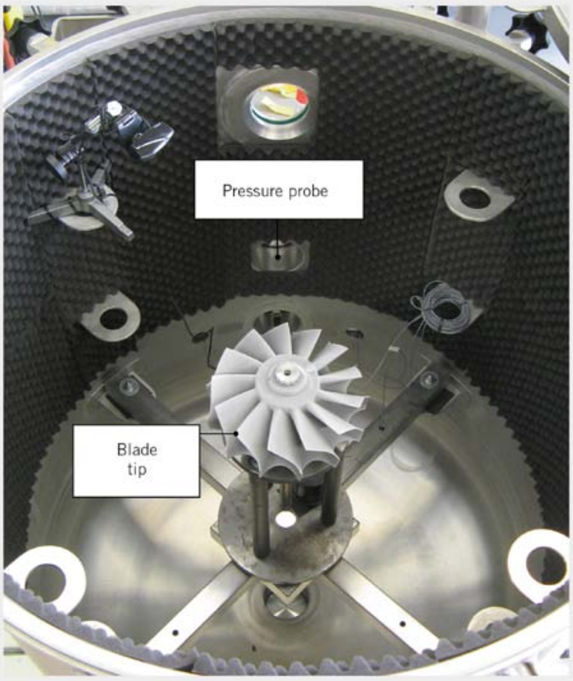

FIGURE 1 Pressure chamber with impeller MTU ZR 265

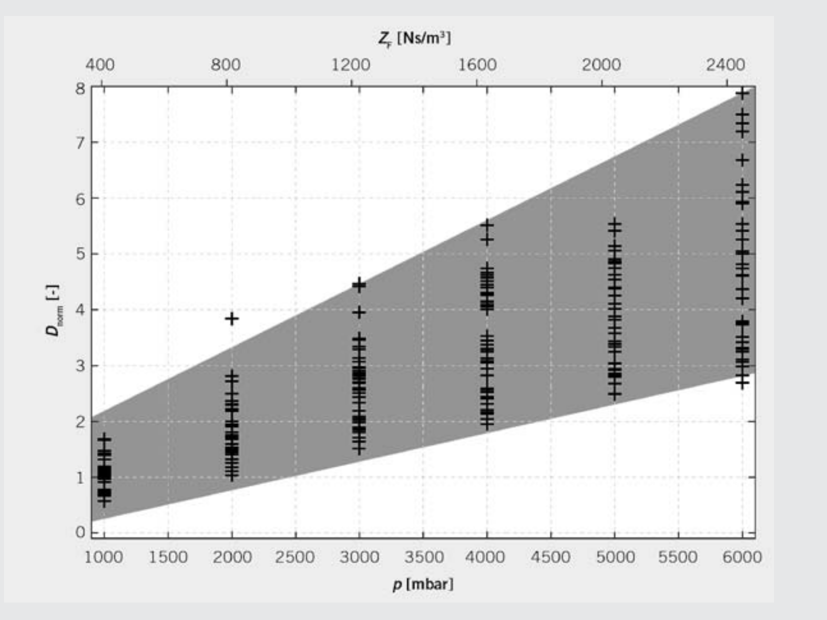

FIGURE 2 Modal damping ratios of all resonances between 4.8 and 15 kHz at rest (ϑ = 20 °C, p = 1 to 6000 mbar) normalised on mean damping ratio at ϑ = 20 °C and p = 1013 mbar)

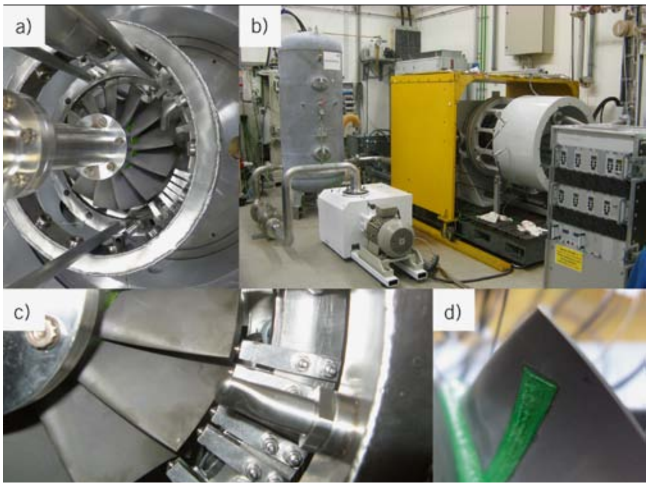

FIGURE 3 Horizontal spin test stand with impeller MTU ZR 265 (a, b) and positions of BTT probes (c) and strain gauges (d)

of view the reduced fluid damping at lower pressures can be explained with the reduced wave impedance in this case. The noise radiation in the open area can be quantified with the aeroacoustic impedance, which is defined by the product of fluid density and acoustic velocity [7, 8]. A decreasing ambient pressure level at constant temperature affects a reduction of the fluid density as well which finally yields a reduced wave impedance or a reduced fluid damping, respectively.

3 MODAL PARAMETERS OF ROTATING IMPELLER

Subsequently centrifugal forces are considered in order to contribute to a more advanced structural mechanical understanding of rotating impellers. In detail the tests aim at a clarification of centrifugal forces on mistuning and damping, the horizontal test facility used for this purpose is shown in **FIGURE 3** (a, b). The forced response is measured synchronously via 13 identical strain gauges positioned on each blade as well as via blade tip-timing (BTT). The positioning of the strain gauges is chosen in a way that blade dominated modes with up to four nodal lines could be detected at sufficiently high signal level, **FIGURE 3** (d). BTT signals are gathered at the blade tip (turbine outlet, **FIGURE 3** (c). This position enables to measure blade dominated modes of vibration featuring one, two or four nodal lines on the blade.

The test stand provides a speed range between 10,000 and 19,000 rpm (166 to 316 Hz). Targeted variations of rotation speed shall identify the dependence of modal parameters on the speed. Using only one air jets enables the excitation of speed synchronised operational vibrations in numerous engine orders. In order to keep transient effects as small as possible the lowest feasible speed ramp of 0.5 Hz/s has been chosen corresponding to the technical limit of the test stand.

The dependence of natural frequencies on rotational speed is shown in **FIGURE 4** for a margin limited by 4800 and 4950 Hz. As expected increasing rotational speeds effect increasing natural frequencies. The measuring methods, strain gauges and BTT both yield identical results. Hence, the effect of stiffening due to centrifugal forces causing the rise of natural frequencies could be proved. A sole exception could be found close to a comparatively high rotary frequency of about 300 Hz where a drop of natural frequencies appears. This can be explained by a simultaneous but not avoidable heating of the impeller. In this case the temperature caused drop of Youngs's Modulus results in lower natural frequencies. This illustrates that all operational parameters have to be considered for a prediction of vibration characteristics. If the stiffening impact due to centrifugal forces also effects the mistuning, the distance between adjacent resonance peaks would change. However, such a behaviour could not be proved by the measurement data. Hence it can be concluded that rotational speeds rang-

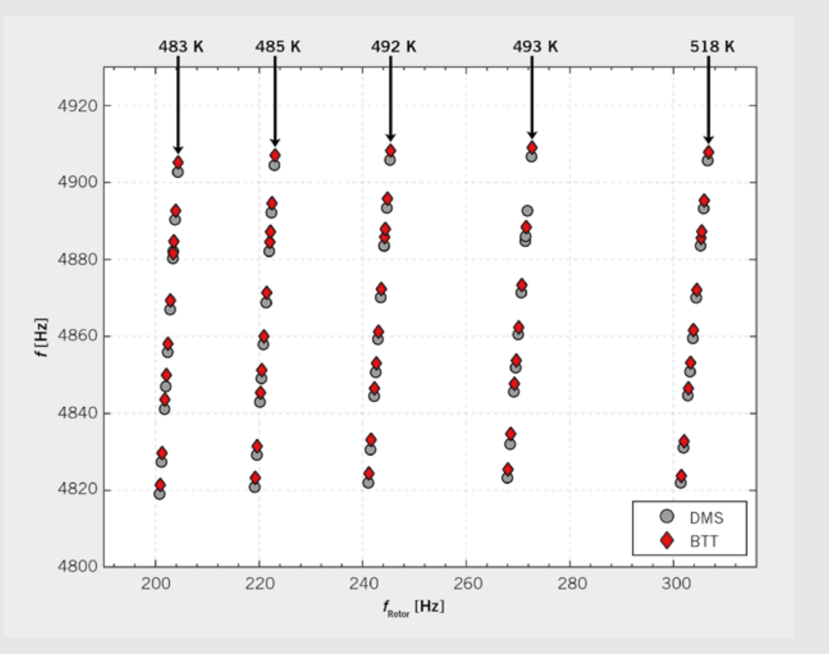

FIGURE 4 Natural frequencies in dependence on rotary speed (strain gauges and BTT)

ing from 10,000 to 19,000 rpm do not cause any change of impeller mistuning.

In derogation from the dependence of natural frequencies on rotational speed no clear correlation could be found considering the distribution of modal damping ratios in the whole speed range. Instead it is apparent that a comparison of damping ratios obtained from rotational testing and those measured at rest at coarse vacuum (1 to 360 mbar, Section 2) approximately yield identical results, **FIGURE 5**. According to Eq. 1 the original pressure dependence of damping ratios measured at rest has to be specified in dependence on the impedance. With this a direct comparison of measurement data gathered at different pressures and temperatures at rest as well as under rotation becomes possible.

Eq. 1 $$Z_F = \rho \cdot c = \frac{p}{R_s \cdot T} \cdot \sqrt{\kappa \cdot R_s \cdot T}$$

Here are ZF the acoustic impedance, ρ the fluid density, c the speed of sound, p the fluid pressure, R_S the specific gas constant, T the fluid total temperature und κ the isentropic exponent.

Based on the analyses shown before, the dependence of natural frequencies on rotary speed could be confirmedwhereas no cor-

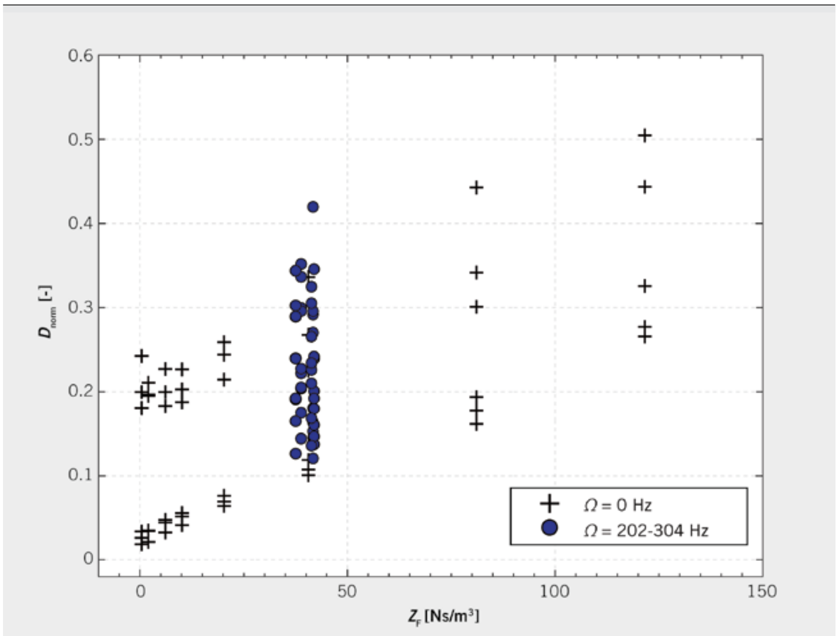

FIGURE 5 Modal damping ratios measuered at rest and under rotation (4850 to 4950 Hz) in dependence on acoustic impedance of ambient fluid

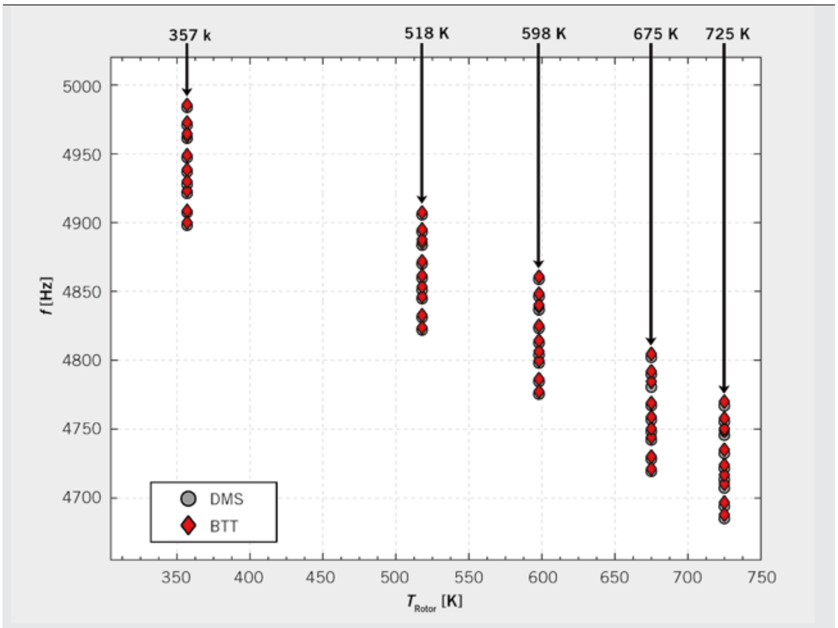

FIGURE 6 Natural frequencies (S/G, BTT) in dependence on impeller temperature

relation has been found with respect to modal damping ratios. Adjusted to the specific operational conditions damping ratios measured at rest and those measured under rotation demonstrate a match of high degree.

4 EFFECT OF IMPELLER TEMPERATURE ON MISTUNING AND DAMPING

Investigations of this section aim at a targeted heating of the impeller to high temperature level instead of moderate variations of impeller temperature caused by operation shown before. The experimental set-up as well as the test runs largely remain unchanged and correspond to the description given in Section 3. Further impeller temperatures of 357 K, 598 K, 675 K and 725 K are provided. Results of all test-runs showing the dependence of natural frequencies and impeller temperature are shown in **FIGURE 6** for frequencies between 4650 and 5000 Hz. Increasing temperatures yield a continuous drop of resonance frequencies at the rotating impeller. Again the results measured with strain gauges and those measured via BTT are in close correlation. Besides the absolute drop of natural frequencies the distances between adjacent resonance peaks remain unchanged, similar to findings within the test-runs at varying speeds. In spite of significant variations of temperature the scatter band of pos-

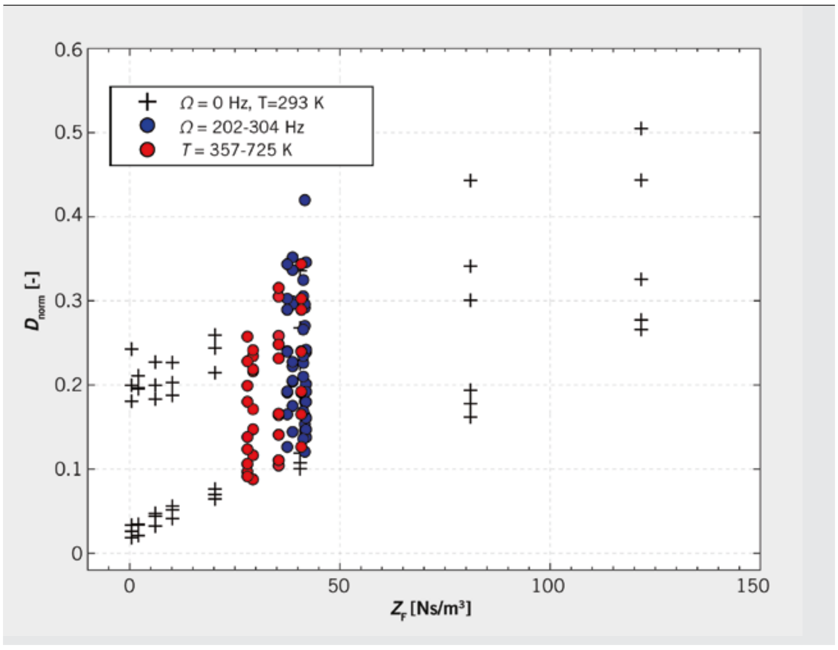

FIGURE 7 Damping ratios obtained at hot rotating operational conditions versus ambient normal conditions at rest (ϑ = 20 °C and p = 1013 mbar)

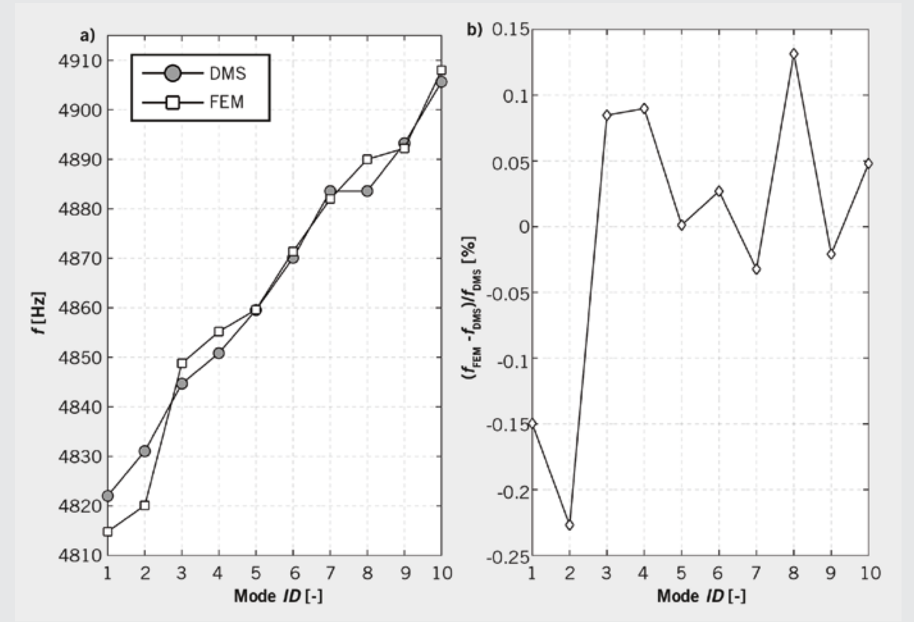

FIGURE 8 Measured versus calculated natural frequencies absolute a) and relative error b)

sible resonances due to mistuning at each engine order excitation does not change.

Aiming at close to reality predictions of the forced response during impeller operation, the quantification of the damping as accurate as possible is a necessary condition. In agreement with Eq. 1 the dependence of modal damping ratios on the acoustic impedance of the fluid is given in **FIGURE 7**. It is assumed that the fluid temperature corresponds to the blade temperature at striking distance. It is confirmed that the damping ratios are decreased with decreasing acoustic impedance.

5 SIMULATION OF ROTATING IMPELLERS AT HIGH TEMPERATURES

It is addressed how far the FE Model updated according to [9] is suited for reliable forced response computations of rotating impellers at high temperatures. Within linear, dynamic simulation gravitational and centrifugal forces as well as the impeller's temperature have to be considered. **FIGURE 8** shows a comparison of numerically and experimentally determined natural frequencies between 4800 and 4950 Hz at a rotary speed of 303 Hz (18,200 rpm)

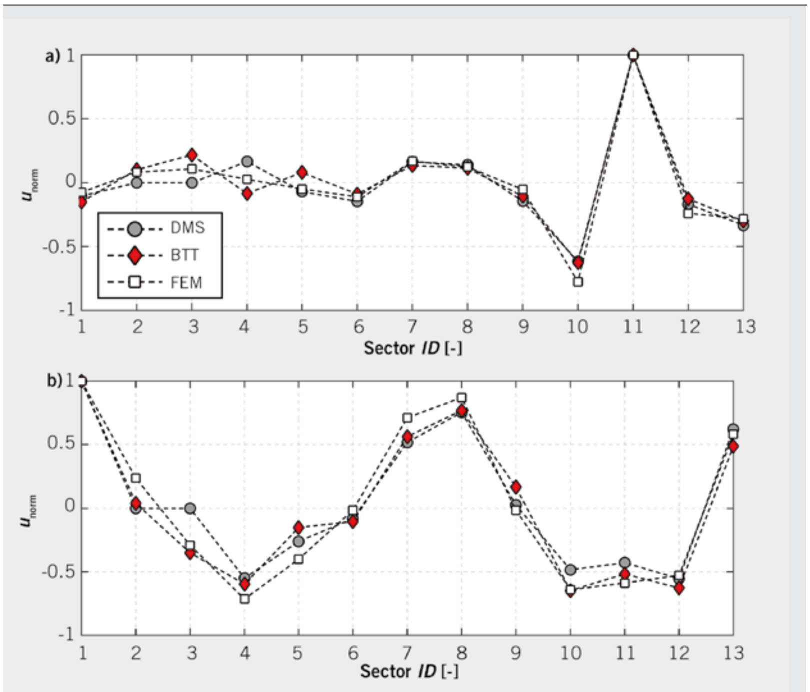

FIGURE 9 Eigenmode transactions of the hot rotating impeller MTU ZR 265 (n = 18,200/min, ϑ = 518 K, p = 122 mbar) – compare between S/G (S/G 2 and 3 defective), BTT and updated FE-model

and an average impeller temperature of 518 K (244.85 °C). A good match is found with respect to the predicted band of resonances and results measured by the strain gauges.

Operational deflection shapes obtained from simulation, strain gauge and BTT-measurement are compared in **FIGURE 9** each normalised with respect to blade tip deflections. Apart from the failure of the strain gauges positioned at Blades 2 and 3, wherefore zero values are dedicated to these blades, comparable BTT and strain gauge results are obvious. In addition, the good match of numerical and experimental results proves the validity of the model updated before. Considering all results it can be concluded that FE-models adjusted for laboratory conditions at rest [9] are well suited to predict the forced response of a real turbine impeller at arbitrary operational conditions in terms of pressure, temperature and rotational effects.

6 SUMMARY AND OUTLOOK

The effect of pressure, temperature and centrifugal forces on mistuning and damping of a radial impeller could be quantified by means of comprehensive test series. According to this gas pressure and gas temperature or acoustic impedance, respectively significantly affect the damping contribution of the fluid. This is of primary importance since damping measurements at room conditions have shown that the overall damping is mainly contributed from fluid structure interactions.

Natural frequencies of the impeller clearly change in case varying structural temperatures due to the material law's dependence on temperature. In addition, centrifugal forces yield blade stiffening explaining the rise of natural frequencies with increasing rotary speed. However, mistuning remains unchanged. Furthermore it could be shown that FE-models updated with measurement data obtained at room conditions [9] are well suited to compute forced response analyses at rotation, modified pressure or increased temperatures close to reality. Hence, these FE-models enable the user to consider local amplifications of stress due to mistuning under hot operating conditions.

Future research aims at the consideration of further fluid parameters such as viscosity and their effect on damping characteristics. Up to now the impact of operational wear has not been taken account. It is expected that both, particle erosion and fowling of blade surface significantly affect mistuning as well as damping.

REFERENCES

[1] Beirow, B.: Grundlegende Untersuchungen zum Schwingungsverhalten von Verdichterlaufrädern in Integralbauweise. Aachen: Shaker Verlag, 2009
[2] Klauke, T.: Schaufelschwingungen realer integraler Verdichterräder im Hinblick auf Verstimmung und Loaklisierung. Cottbus: Der Andere Verlag, 2008
[3] Maywald, T.; Beirow, B.; Kühhorn, A.: Mistuning und Dämpfung II. FVV-Abschlussbericht, FVV 2014, Issue 1047
[4] Maywald,T.; Beirow, B.; Kühhorn, A.: Mistuning und Dämpfung II. FVV-Informationstagung Turbomaschinen, FVV 2014, Issue R569
[5] Kammerer, A.; Abhari, R. S.: Experimental study on impeller blade vibration during resonance part 2: Blade damping. In: Proceedings of the ASME Turbo Expo 2008, Paper GT2008-50467
[6] Gibert, C. et al.: Modal tests and analysis of a radial impeller at rest: influence of surrounding air on damping. In: Proceedings of ASME Turbo Expo 2012, Paper GT2012-69577
[7] Henn, H.; Sinambari, G. R.; Fallen, M.: Ingenieurakustik. Wiesbaden: Vieweg+Teubner, 2008
[8] Günther, B.; Hansen, K. H.; Veit, I.: Technische Akustik – Ausgewählte Kapitel. Renningen: Expert Verlag, 2008
[9] Kühhorn, A.; Beirow, B.: Verfahren zur Ermittlung der Schaufelverstimmung bei Laufrädern in Integralbauweise. EP 1988391A2 Europa, 03. März 2008

THANKS

The work presented herein has been supported by the Research Association Combustion Engines (FVV). The independent investigations contribute to the research project 'Mistuning and Damping of Radial Turbine Impellers II (AIF-Nr.17451 BR)' with a funding by the German Federal Ministry of Economics and Technology (BMWi/AiF). The authors thank for this commitment. Further thanks are given to the working group of industrial representatives and the chairman Thomas Winter.

Control Strategy for a Parallel Hybrid Drive

By measuring the real driving emissions, the pressure to meet the CO_2 targets has been further increased. CO_2 and pollutant emissions can already be improved considerably through partial electrification (hybridisation) of the conventional drivetrain. Hybridisation requires a suitable control strategy, which ideally takes the different types of emissions, such as CO_2, NO_x and soot emissions, and customer use into account. At the Institute of Automotive Engineering at the TU Braunschweig, a research project was carried out, which was awarded with the Hermann Appel Prize 2014 of the IAV.

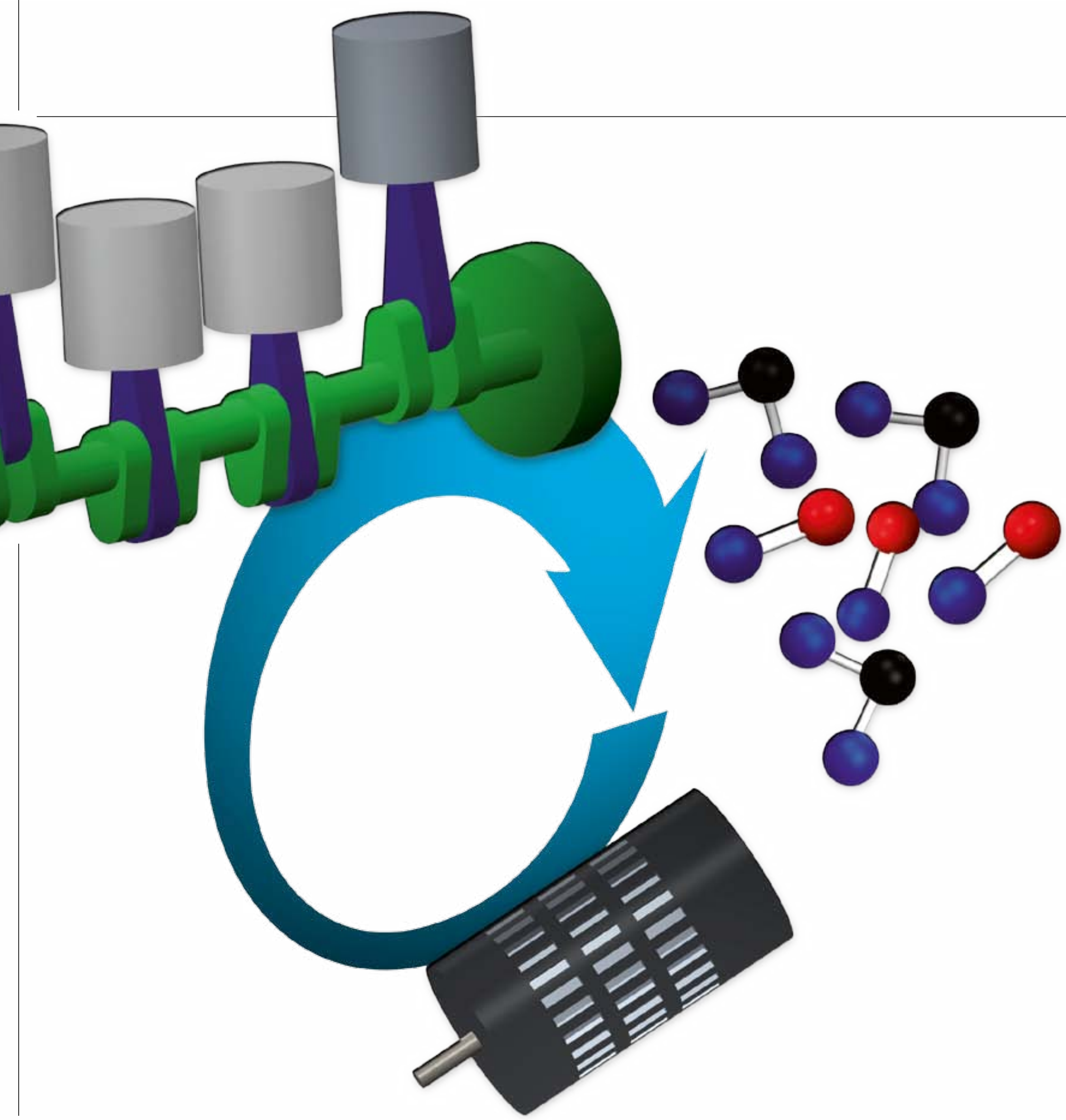

AUTHOR

Mark Schudeleit, M. Sc. studied at the Technical University of Braunschweig Mechanical and Automotive Engineering and works now as Research Assistant at the Institute of Automotive Engineering at the TU Braunschweig (Germany).

1 MOTIVATION

Increasing political pressure to reduce fuel consumption, CO_2 and pollutant emissions (e.g. soot and NO_x) from the vehicle fleets forces the automotive industry to develop alternative vehicles. In addition to electric cars, with infrastructure and range problems still not being solved, hybrid vehicles currently play a particularly important role. The New European Driving Cycle (NEDC) is used as a standard of comparison for the efficiency of vehicles [1, 2]. The emissions in the legislated driving cycles are less relevant for the customers and in view of planned measurements of the real driving emissions (RDE). In fact, the emission performance in individual customer use is important, which comprises different driving styles and vehicles loads on urban and extra-urban roads and on freeway. Therefore, an approach to design the control strategy of a hybrid vehicle was developed, which takes the driving cycle and customer use as well as the combined emissions into account and minimises them.

2 VEHICLE MODEL

FIGURE 1 shows the structure of the simulation model for driving cycle and customer simulation. The driving requirements in customer use, such as the target speed (also referred to as orientation speed profile or OSP), and speed changes are generated by statistics generators, which are based on real measured data. The statistical real-world driver tries to reach the specified speed by using the foot pedals. This is characterised by a specific behaviour with different accelerator gradients and positions that varies according to driven vehicle, driving style and driving environment [3]. In the cycle simulation, the driver and driving environment models are replaced by a speed controller, which keeps the vehicle exactly at the specified speed.

3 VEHICLE

The modelled vehicle is a parallel, full hybrid (full HEV) with torque addition. In addition to the conventional internal combustion engine (ICE) and a dual-clutch transmission (DCT), there is a second shaft between ICE and transmission, which can be separated by two clutches (K0 and K1). The electric motor (EM) is located on this shaft.

The control strategy of the hybrid vehicle is represented in **FIGURE 2**. It selects the operating mode based on the state of charge (SOC) of the battery and propulsion power P. Recuperation, purely electric driving, purely combustion-engine operation and load point shifting are possible hybrid functions. In load point shifting an intelligent fuzzy control is used to control the torque distribution between ICE and EM based on several rules. Finally, hysteresis is implemented to prevent an alternating change between the operating modes.

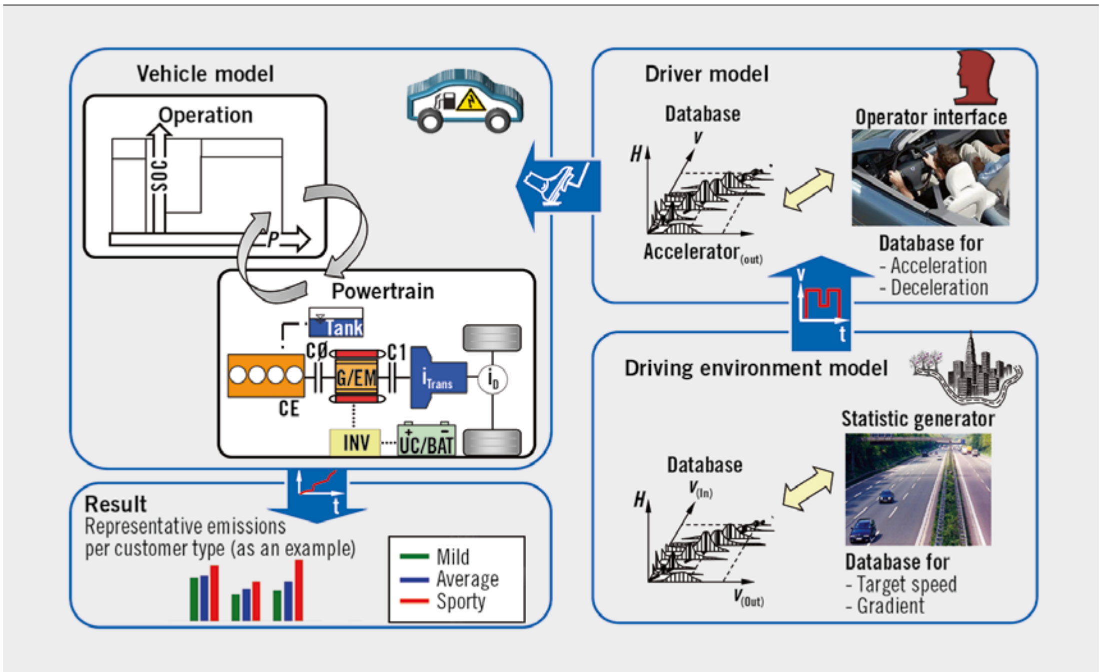

FIGURE 1 Structure of the simulation model for driving cycle and customer simulation based on Matlab/Simulink

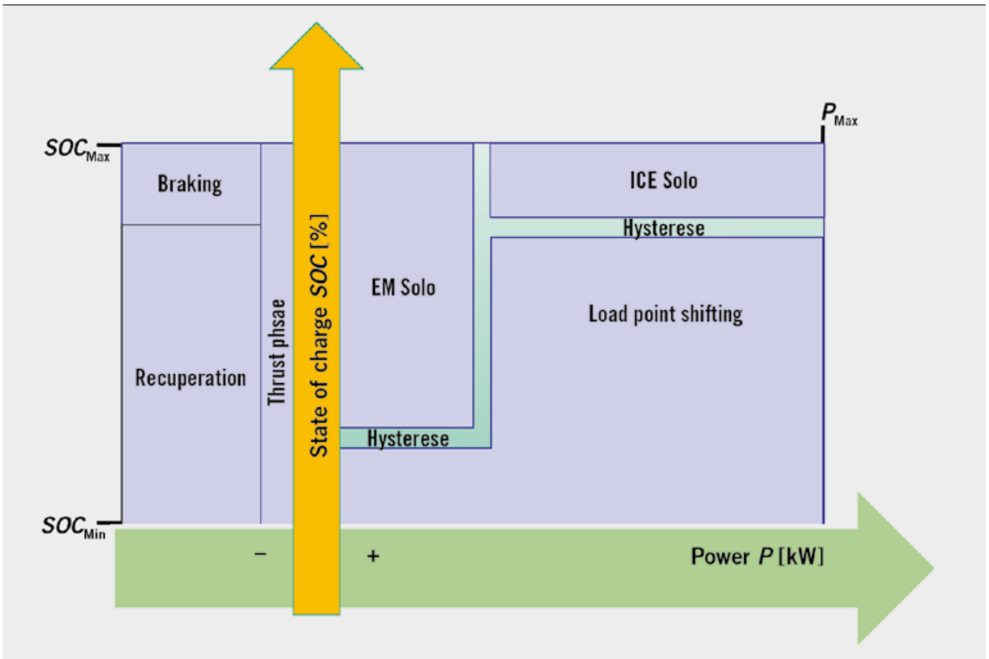

FIGURE 2 SOC-propulsion-power-based control strategy of a parallel hybrid drive with intelligent fuzzy control in load point shifting operating mode

4 DYNAMIC EMISSION MODELLING

Suitable emission models are required for the layout of the control strategy to reduce emissions. Simulations showed that the frequently used static emission maps (based on the input signals torque and rotational speed) can lead to deviations in comparison with dynamic test rig measurements. In customer use, the emissions between simulation and measurement differ significantly from each other. Better accuracy can be achieved by considering a transient or dynamic input signal [4].

Since synthetic driving cycles, such as the NEDC, include less dynamic driving manoeuvres and only a limited number of different operating points (due to the periods of constant driving), the engine emission behaviour can be represented by a simple empirical meta model. Thus, neural networks are developed for the NEDC in accordance with the measured data of rotational speed, torque and the respective type of emissions. **FIGURE 3** shows a comparison of the simulated time curves of the dynamic emissions CO_2, NO_x and soot and the emission measurements for a conventional vehicle in the NEDC. The dynamic emission models lead to emission values similar to the emissions measured in the cycles. The accumulated values show a deviation of less than 1 %. For NO_x emissions, there are only slight deviations in the first 200 s (cold start phase). The soot emissions are also close to the measurements.

In order to model dynamic emissions in customer use, a more complex approach is required since the correlations between real driving manoeuvres and emissions are also more complex. For this reason, a semi-empirical approach was chosen, which is presented in [5]. Representative driving manoeuvres are used as input data; the respective emissions were determined on an engine test rig. Modelling resulted in meta models, which are based on T-varying first and second order transfer functions. Input variables of the transfer functions include emissions from static maps and transient time constants, which are represented by a neural network. The time constants vary depending on rotational speed, torque and torque gradient. Experience has shown that real emissions in customer use can be calculated more precisely using this model approach.

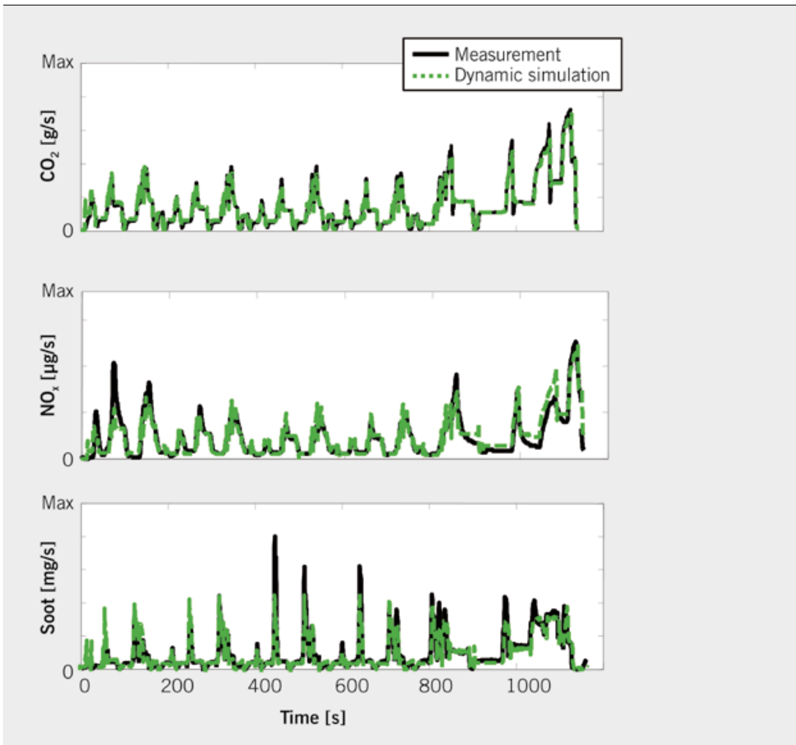

FIGURE 3 Comparison of measurement and dynamic simulation of CO_2, NO_x and soot emissions in the NEDC, conventional vehicle (neural networks with rotational speed, torque and torque gradient as input variables are used for the simulation)

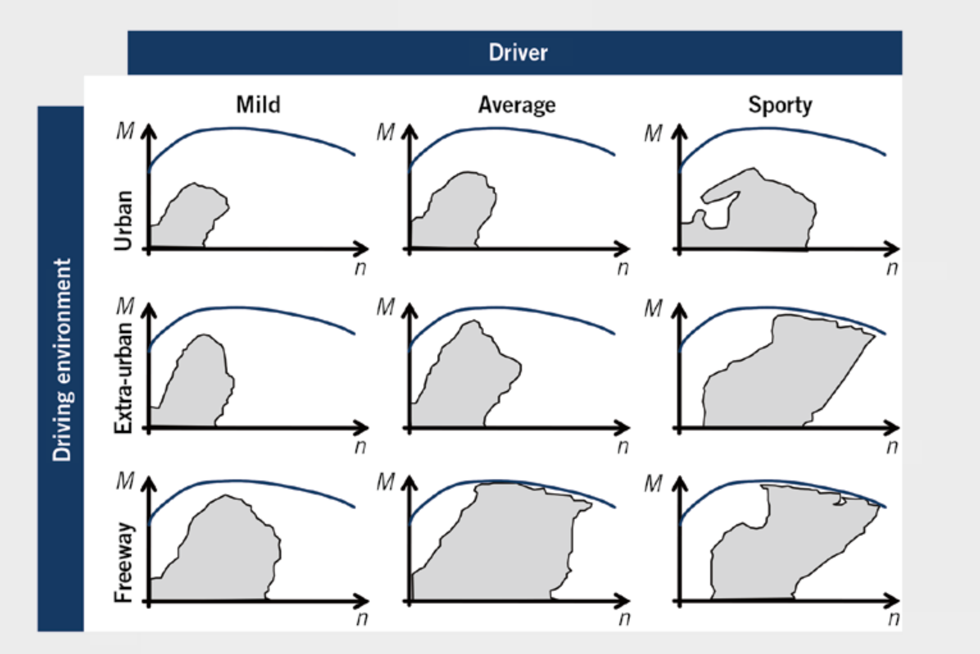

FIGURE 4 Operating ranges in torque/rotational speed diagrams for different customers

5 IDENTIFICATION OF A ROBUST CONTROL STRATEGY IN THE NEDC

FIGURE 4 shows the operating ranges in a torque/rotational speed diagram of an ICE for different customers (variation of driving style and driving environment). In urban traffic, the ICE is mainly operated at low rotational speeds and torques. On extra-urban roads and freeway, however, considerably higher torques and rotational speeds are required. The driving style also has significant influence on the operating points and therefore also on the resulting emissions and fuel consumption in customer use. This emphasises that it is not sufficient to only consider the operation area represented in driving cycles when developing the control strategy for real driving.

A control strategy needs to be found that on the one hand reduces the combined emissions and, on the other, leads to similarly low emissions for different driving conditions. It can thus be said that influences – or basic parameters – have a low sensitivity for changes in fuel consumption or emissions, that is to say they have to be robust. In order to meet these requirements, the limits of the control strategy were varied using a Sobol DoE with approximate 2000 combinations, the emission values were combined as one target function and a robust control strategy parameter set was identified [6-8]. The objective parameters (raw emission values) are normalised and then combined as one target function, Eq. 1. Furthermore, the normalised objective parameters are weighted according to their priority.

Eq. 1

$$z = g_1 \cdot CO_2 + g_2 \cdot NO_x + g_3 \cdot soot + \ldots$$

With g_1, ..., g_n as the weighting factors and n as the number of objective parameters.

In order to determine the robust control strategy, not only the minimum values of the target function, but also results similar to the minimum value (5 % tolerance) are used, **FIGURE 5** (left). Based on a frequency distribution (derived from classifying the values according to Sturges' rule [9]) the robust optimum can be identified. The robust optimum is located in a flat area surrounded by a high number of minimum-similar results. Hence, conclusions can be drawn about the robustness of the control strategy.

Since the parameters of the robust control strategy deviate from the optimum NEDC control strategy due to the optimum compromise for different driving styles, they are tested in customer use to illustrate the advantages of the stable character of the robust control strategy. The results of the CO_2, NO_x and soot emissions are represented in **FIGURE 6** for different customers. The CO_2 emissions of the robust control strategy are at least as low as those resulting from the optimum NEDC control strategy. An exception is the sensible urban driver. In terms of NO_x emissions, the robust control strategy is superior in customer use as well. The robust control strategy also leads to a reduction of soot emissions. Higher soot emissions (in the raw emissions) are only expected for the sporty urban driver.

6 RESULTS DRIVING CYCLE AND CUSTOMER SIMULATION

A comparison of the emissions in customer use and in legislated driving cycles shows that the lowest emissions occur in the NEDC, **FIGURE 7**, which can be explained by the low dynamics in the cycle. Despite the lower average speed, the results of the FTP75 are slightly above those of the NEDC due to the higher accelerations. The highest emissions occur in the WLTP, owing to the highest speeds and the highest requirements in terms of longitudinal dynamics.

As expected, the emissions occurring in customer simulation deviate from those in the driving cycles. While the NEDC leads to slightly lower CO_2 values, the FTP75 simulation generates values that are similar to those generated by some customers. The results for NO_x revealed the following: the emissions in the NEDC and FTP75 are similar to those occurring with sensible and some aver-

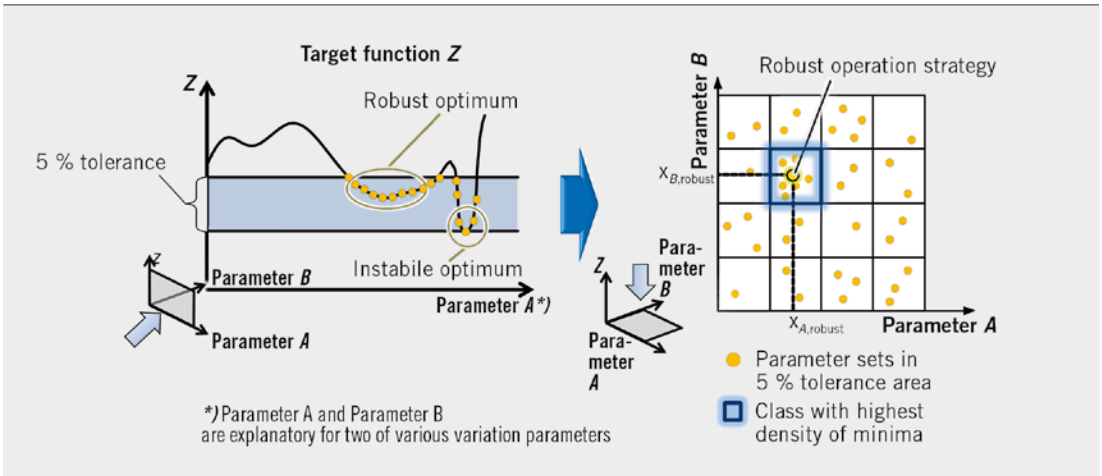

FIGURE 5 Identification of parameter sets with solutions similar to minimum value (5 % tolerance, left) and classification of the minimum 5 % of the target values for identification of the robust control strategy, which is in the class with the highest frequency (exemplary representation, right)

age drivers while a sporty driving style leads to considerably higher NO_x emissions.

Compared to customer use, the soot emissions in driving cycles tend to be higher. The emissions generated by sensible and average drivers in urban traffic and on extra-urban roads are similar to those in the NEDC and FTP75 cycles.

7 SUMMARY

The control strategy of a hybrid vehicle can be modified in order to reduce CO_2 and pollutant emissions (through engine operation optimisation). Due to the current emissions legislation, the focus here is on the NEDC. The customer use also has to be taken into account when developing the control strategy since the real driving emissions will be measured in the future for legislation. A robust control strategy is therefore required, which leads to similar and at the same time low combined emissions independent of the type of use.

Based on a DoE and a subsequent evaluation of the target function values, which consists of the normalised and weighted raw emission values of CO_2, NO_x and soot, different control strategy configurations could be rated in terms of robustness and emission reduction potential. For this, a minimum of a target function was identified, which is located in a flat area surrounded

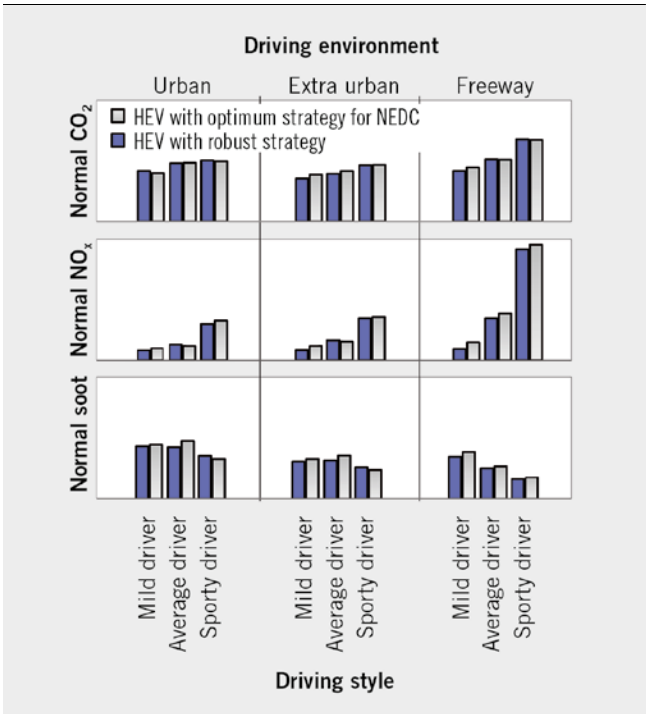

FIGURE 6 CO_2, NO_x and soot emissions of two control strategy configurations of a hybrid vehicle (left: robust control strategy, right: optimum NEDC control strategy)

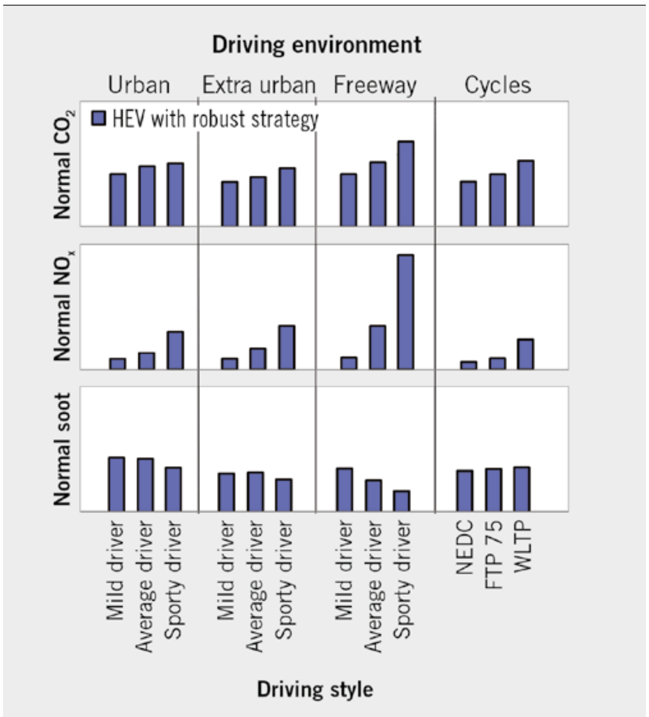

FIGURE 7 CO_2, NO_x and soot emissions of the robust control strategy compared to the emissions in NEDC, FTP75 and WLTP

by a high quantity of similar values. Compared to an optimum NEDC – but not robust – control strategy, the identified robust control strategy leads to slightly higher emissions in the NEDC. In customer use, however, it reduces the CO_2, NO_x and soot values considerably.

Due to their driving style specific customers, such as the sporty one, lead to higher NO_x emissions than in the considered legislated driving cycles (NEDC, FTP75 and WLTP) for any control strategy configuration. The CO_2 and soot emission values of the full hybrid with robust control strategy, however, are similar in customer use and driving cycles.

REFERENCES

[1] Barsali, S. et al.: A control strategy to minimize fuel consumption of series hybrid electric vehicles. IEEE Transactions on Energy Conversion, 2004, volume 19

[2] N. N.: Regulation (EC) No. 661/2009 of the European Parliament and of the Council. Official Journal of the European Union, 2009

[3] Müller-Kose, J. P.: Repräsentative Lastkollektive für Fahrzeuggetriebe. Shaker Verlag, 2002

[4] Nüesch, T. et al.: Optimal energy management for a diesel hybrid electric vehicle considering transient PM and quasi-static NO_x emissions. Control Engineering Practice, 2014

[5] Schudeleit, M.; Schober, F.: Optimized operation of HEV in customer use in consideration of dynamic emissions. Proceedings of the 8th International CTI-Symposium Automotive Transmissions, HEV and EV Drives, USA, 2014

[6] Röpke, K.: Design of Experiments (DoE) in Engine Development III. expert Verlag, 2007

[7] Siebertz, K. et al.: Statistische Versuchsplanung. Design of Experiments (DoE). Springer Verlag, 2010

[8] Bratley, P.; Fox, B. L.: Algorithm 659: Implementing Sobol's quasirandom sequence generator. ACM Transactions on Mathematical Software (1988), volume 1, pp. 88-100

[9] Sturges, H. A: The choice of a class interval. In: Journal of the American Statistical Association (1926), No. 153, pp. 65-66